

ELECTRON PARAMAGNETIC RESONANCE INVESTIGATIONS  
OF ADDUCTS OF HUMAN HEMOGLOBIN

by

David Earl Schwab

A dissertation submitted in partial fulfillment  
of the requirements for the degree

of

Doctor of Philosophy

in

Chemistry

MONTANA STATE UNIVERSITY  
Bozeman, Montana

February 2010

©COPYRIGHT

by

David Earl Schwab

2010

All Rights Reserved

APPROVAL

of a dissertation submitted by

David Earl Schwab

This dissertation has been read by each member of the dissertation committee and has been found to be satisfactory regarding content, English usage, format, citation, bibliographic style, and consistency, and is ready for submission to the Division of Graduate Education.

Dr. David J. Singel, Chair of Committee

Approved for the Department Chemistry and Biochemistry

Dr. David J. Singel, Department Head

Approved for the Division of Graduate Education

Dr. Carl A. Fox

## STATEMENT OF PERMISSION TO USE

In presenting this dissertation in partial fulfillment of the requirements for a doctoral degree at Montana State University, I agree that the Library shall make it available to borrowers under rules of the Library. I further agree that copying of this dissertation is allowable only for scholarly purposes, consistent with "fair use" as prescribed in the U.S. Copyright Law. Requests for extensive copying or reproduction of this dissertation should be referred to ProQuest Information and Learning, 300 North Zeeb Road, Ann Arbor, Michigan 48106, to whom I have granted "the exclusive right to reproduce and distribute my dissertation in and from microform along with the non-exclusive right to reproduce and distribute my abstract in any format in whole or in part."

David Earl Schwab

February 2010

## ACKNOWLEDGEMENTS

I would like to thank David Singel for his help and guidance during the years I was a student under his care. I am grateful for the education he has provided me from his wealth of knowledge— including in matters unrelated to the field of chemistry.

I would also like to thank former members of the Singel research group: Karl Sebby and Lisa Mellmann for their assistance in the preparation of this dissertation; and Ben Luchsinger for insightful discussions relating to hemoglobin.

I thank the staff of the Department of Chemistry and Biochemistry for handling all the details that arose along the way. Their assistance has been invaluable.

I thank my lovely wife, Tanya, for her love, patience, encouragement and understanding over the past months while I completed this work.

I thank my parents for their love and support during my time of study.

I also thank Edward Robson for his faithful, weekly encouragement during the writing process.

Most of all, I am grateful to God, my Redeemer, for allowing me a glimpse into one aspect of his glorious creation.

Isaiah 44:24: Thus says the LORD, your Redeemer, and He who formed you from the womb: I am the LORD, who makes all things, who stretches out the heavens all alone, who spreads abroad the earth by Myself.

## TABLE OF CONTENTS

1. INTRODUCTION.....	1
General Introduction.....	1
Background and Significance.....	1
Hemoglobin and Allostery.....	1
Blood Flow and Nitric Oxide.....	4
Hemoglobin Interaction with NO.....	5
SNO-Hemoglobin.....	6
Methemoglobin.....	7
Reactions of Nitrite and Hemoglobin.....	8
Summary.....	10
2. EPR SPECTROSCOPY OF METHEMOGLOBIN:NITRITE.....	11
Introduction.....	11
Materials and Methods.....	13
Hemoglobin.....	13
Fe(II)NO/Fe(III)NO <sub>2</sub> <sup>-</sup> -Hb hybrids.....	13
SNO-Hb.....	14
D <sub>2</sub> O Solutions.....	14
EPR Spectroscopy.....	15
UV-Vis Spectroscopy.....	15
Results.....	16
Doublet Structure.....	16
pH Dependence.....	20
Variable Temperature EPR.....	22
Hb Hybrids.....	25
Affinity.....	28
Discussion.....	31
Conclusion.....	36
3. ELECTRONIC STRUCTURE OF METHEMOGLOBIN:NITRITE.....	37
Introduction.....	37
Materials and Methods.....	38
Low-Spin d <sup>5</sup> Hole Theory.....	38
Results and Discussion.....	43
Conclusion.....	49
4. X-BAND EPR INVESTIGATION OF METHEMOGLOBIN: TEMPERATURE AND BUFFER DEPENDENCE.....	50
Introduction.....	50
Materials and Methods.....	51

## TABLE OF CONTENTS - CONTINUED

Hemoglobin.....	51
EPR Spectroscopy.....	52
EPR Spectra Simulations.....	52
Results.....	52
Buffer Dependence at 10 K.....	52
Temperature Dependence.....	55
Discussion.....	58
Bis-histidine Hemichromes.....	58
Hb(NO) <sub>4</sub> .....	61
Conclusion.....	61
5. TEMPERATURE DEPENDENCE OF THE W-BAND EPR SPECTRUM OF HB(NO) <sub>4</sub> .....	63
Introduction.....	63
Materials and Methods.....	64
Hemoglobin.....	64
EPR Spectroscopy.....	65
EPR Spectra Simulation.....	65
Results.....	66
General Observations.....	66
Spectral Simulation.....	69
Trends with Temperature.....	73
Discussion.....	76
Subunit Differences.....	79
Axial to Rhombic Ratio.....	81
Low Temperature Species.....	83
Comparison to Met-Hb:NO <sub>2</sub> <sup>-</sup> and Met-Hb.....	84
Conclusion.....	85
6. INVESTIGATION OF MIXED-VALENCE, PARTIALLY NITROSYLATED HEMOGLOBIN TETRAMERS AS SNO-PRECURSORS.....	87
Introduction.....	87
Methods and Materials.....	88
Hemoglobin.....	88
EPR Spectroscopy.....	89
UV-Vis Spectroscopy.....	89
Results.....	89
Hb[α(NO) <sub>2</sub> β(Fe(II)) <sub>2</sub> ].....	89
Deoxy-Hb + Hb(NO) <sub>4</sub> .....	92
Deoxy-Hb + DEANO.....	93
Discussion.....	94

## TABLE OF CONTENTS - CONTINUED

Conclusions.....	96
7. CONCLUSION.....	97
REFERENCES CITED.....	100
APPENDICES.....	113
APPENDIX A: Sulfur K-Edge X-Ray Absorption Spectroscopy as an Experimental Probe for S-Nitroso Proteins.....	114
APPENDIX B: Supplementary Met-Hb:NO <sub>2</sub> <sup>-</sup> Plots.....	120
APPENDIX C: Supplementary Variable Temperature Met-Hb Plots.....	124
APPENDIX D: Supplementary Variable Temperature Hb(NO) <sub>4</sub> Plots.....	127
APPENDIX E: Supplementary Hybrid Nitrosyl-Hb Plots.....	129

## LIST OF TABLES

Table	Page
3-1: The ground state wave function coefficients and the tetragonal and rhombic distortions for various Met-Hb adducts.....	47

## LIST OF FIGURES

Figure	Page
1-1: Oxygen saturation curves for hemoglobin and myoglobin as a function of $pO_2$ .....	2
1-2: Crystal structures of T-state deoxy-Hb and R-state SNO-Hb(NO) <sub>4</sub> .....	3
2-1: X-Band EPR spectra of solutions of Met-Hb:NO <sub>2</sub> <sup>-</sup> in HEPES and PBS buffers at 20 K.....	17
2-2: EPR spectra of solutions of Met-Hb:NO <sub>2</sub> <sup>-</sup> in H <sub>2</sub> O and D <sub>2</sub> O.....	18
2-3: S-Band EPR spectrum of solutions of Met-Hb:NO <sub>2</sub> <sup>-</sup> .....	19
2-4: pH dependence of EPR spectra of Met-Hb:NO <sub>2</sub> <sup>-</sup> .....	21
2-5: Relative concentrations of MetHb species as a function of pH.....	22
2-6: Variable temperature (22-97 K) EPR spectra of solutions of Met-Hb:NO <sub>2</sub> <sup>-</sup> in HEPES buffer at pH 7.4.....	23
2-7: Variable Temperature (100-175 K) EPR spectra of solutions of Met-Hb:NO <sub>2</sub> <sup>-</sup> in HEPES buffer at pH 7.4.....	25
2-8: EPR spectra of Fe(II)NO/Fe(III)NO <sub>2</sub> <sup>-</sup> hybrids and related hemoglobins.....	27
2-9: Fe(II)NO EPR spectra of Fe(II)NO/Fe(III)NO <sub>2</sub> <sup>-</sup> hybrids.....	28
2-10: Exemplary Hill plot summarizing the titration of Met-Hb with NaNO <sub>2</sub> .....	29
2-11: Scheme depicting the reactions of MetHb:NO <sub>2</sub> <sup>-</sup> , MetHb:H <sub>2</sub> O and MetHb:OH <sup>-</sup> .....	30
3-1: Splitting of the 3d orbitals as a function of ligand environment.....	39
3-2: Splitting of the t <sub>2g</sub> orbitals as viewed according to the hole model.....	40
3-3: X-Band EPR spectrum of Met-Hb:NO <sub>2</sub> <sup>-</sup> .....	44
3-4: The abbreviated structures of $\alpha$ -Met-Hb:NO <sub>2</sub> <sup>-</sup> and $\beta$ -Met-Hb:NO <sub>2</sub> <sup>-</sup> .....	46

## LIST OF FIGURES - CONTINUED

Figure	Page
3-5: Plot of the squares of the orbital mixing coefficients of ground state wavefunction as a function of g-anisotropy.....	48
4-1: X-Band EPR spectra of Met-Hb in aqueous HEPES and PBS buffers.....	54
4-2: X-Band EPR spectra of Met-Hb in aqueous PBS buffer at various temperatures (10-80 K).....	56
4-3: X-Band EPR spectra of Met-Hb in aqueous HEPES buffer at various temperatures (10-95 K).....	57
4-4: Relative percentages of Met-heme species as a function of temperature.....	58
5-1: W-Band EPR spectra of Hb(NO) <sub>4</sub> in aqueous solution at various temperatures (10K-200 K).....	68
5-2: Simulated W-Band EPR spectra of Hb(NO) <sub>4</sub> at various temperatures (10K-200 K).....	69
5-3: Exemplary experimental and simulated Hb(NO) <sub>4</sub> spectra, with component spectra, at 10K, 76K and 200K.....	71
5-4: Plot of rhombic percentage vs. temperature and plot of fraction of axial/rhombic species vs. inverse temperature.....	74
5-5: Simulated EPR spectra of Rhombic A at various temperatures (10-200 K).....	75
5-6: X-Band EPR spectrum of Hb(NO) <sub>4</sub> and its derivatives.....	77
6-1: UV-Vis spectra tracking the oxidation of Hb(NO) <sub>4</sub> .....	90
6-2: EPR spectra of Hb(NO) <sub>4</sub> and various hybrid derivatives.....	91
6-3: EPR spectra of a 3:1 mixture of deoxy-Hb and Hb(NO) <sub>4</sub> .....	92
6-4: EPR spectra of aqueous solutions of deoxy-Hb and DEANO in a 10:1 heme to NO ratio.....	93

## LIST OF FIGURES - CONTINUED

Figure	Page
B-1: UV-Vis absorbance spectrum of Met-Hb and its derivative spectrum with best fit.....	121
B-2: Exemplary experimental EPR spectra with best fits of Met-Hb:NO <sub>2</sub> <sup>-</sup> .....	122
B-3: Exemplary EPR basis spectra employed in fitting of Met-Hb:NO <sub>2</sub> <sup>-</sup> experimental spectra.....	123
B-4: Exemplary Hill plot.....	123
C-1: Exemplary experimental and best fit EPR spectra of neat Met-Hb.....	125
C-2: Exemplary EPR basis spectra employed in fitting neat Met-Hb experimental spectra.....	126
D-1: W-Band EPR experimental and best fit spectra of Hb(NO) <sub>4</sub> .....	128
E-1: Exemplary experimental and best fit EPR spectra of a 3:1 mixture of deoxy-Hb and Hb(NO) <sub>4</sub> .....	130
E-2: Exemplary experimental and best fit EPR spectra of deoxy-Hb and DEANO, in a 10:1 ratio.....	131
E-3: Exemplary experimental and best fit EPR spectra of Hb(NO) <sub>4</sub> and a deoxy/nitrosyl-hybrid Hb.....	132

## ABSTRACT

Hemoglobin transports oxygen to the tissues of the body. The delivery of oxygen to tissues by hemoglobin is dependent on blood flow, which is determined by vessel tension regulated by local oxygen gradients. Dilation of the blood vessels in the microcirculation of tissues under high metabolic demand is induced by the endothelium-derived relaxation factor, nitric oxide, in a process known as hypoxic vasodilation. Although the means of nitric oxide bioactivity preservation and transportation in the blood are disputed, it is clear that S-nitrosohemoglobin, a nitrosylated variant of hemoglobin, plays a pivotal role. The details surrounding S-nitrosohemoglobin formation *in vivo*, however, remain uncertain.

Using electron paramagnetic resonance (EPR) spectroscopy, in conjunction with detailed spectral simulation and least-squares fitting, various hemoglobin species which possibly participate in the formation of S-nitrosohemoglobin were characterized. The EPR spectrum of methemoglobin-nitrite, a purported precursor to S-nitrosohemoglobin formation, was determined to be a composite spectrum arising from the presence of two species, the origin of which is proposed to lie in the differences between the distal heme pockets and histidine residues of the  $\alpha$ - and  $\beta$ -subunits of hemoglobin. By direct measurement of methemoglobin-nitrite by EPR spectroscopy, the weak affinity of methemoglobin for nitrite was confirmed, precluding nitrite-methemoglobin from having a direct role in physiological hypoxic vasodilation. Furthermore, the temperature dependence of the EPR spectra of the various species of neat methemoglobin was determined, as was the temperature dependence of the nitrosyl-hemoglobin ( $\text{Hb}(\text{NO})_4$ ) spectrum at high frequency. The high frequency spectrum of  $\text{Hb}(\text{NO})_4$  provided additional resolution of the axial and rhombic components of the spectrum, but revealed no evidence of distinct subunit spectra. Finally, synthetic routes to generate  $\text{Fe}(\text{II})\text{NO}/\text{Fe}(\text{III})\text{-Hb}$  hybrids have been presented, which, among other things, demonstrated that bolus addition of nitric oxide can produce similar results as the addition of time and condition dependent nitric oxide donors. Overall, this work expands the understanding of hemoglobin, specifically with regard to hemoglobin species with possible involvement in S-nitrosohemoglobin formation.

## CHAPTER 1

### INTRODUCTION

#### General Introduction

In the vast array of proteins, hemoglobin (Hb) stands out as one of the most studied. Hemoglobin's ability to bind oxygen reversibly and its role in oxygen delivery in mammals have been known since the 1800's. Hemoglobin transports oxygen from the lungs to the tissues in the body and completes the respiratory cycle by transporting CO<sub>2</sub> from the tissues to the lungs. The delivery of oxygen is dependent on blood flow to tissues. Dilation or constriction of microvascular beds controls blood flow in the microcirculation, matching oxygen delivery to oxygen demand in a process known as hypoxic vasodilation [1]. However, a crucial question regarding hemoglobin in the blood remains unanswered: what is the molecular basis that allows hemoglobin to transduce the oxygen signal and induce vasodilation?

#### Background and Significance

##### Hemoglobin and Allostery

Hemoglobin is a tetrameric metalloprotein consisting of two  $\alpha$  and two  $\beta$  subunits, the crystal structure being solved by Max Perutz and coworkers in 1960 [2]. Each subunit contains a heme prosthetic group consisting of a porphyrin ring with an iron atom bound at the center. The two sides of the heme plane are known as the proximal and distal sides. On the proximal side, the iron atom in each heme typically binds to an

imidazole nitrogen of a histidine residue. It is on the distal side of the heme plane that iron ligates  $O_2$ , as well as a variety of other ligands. Early studies of oxygen binding to hemoglobin revealed a sigmoidal binding curve (Figure 1-1), distinct from that of other oxygen carrying proteins, such as myoglobin. The binding curve demonstrates that the affinity of Hb for  $O_2$  increases as  $pO_2$  increases. This change in oxygen binding affinity, which occurs as successive subunits of Hb become occupied, led to the development of the concept of allostery [3].

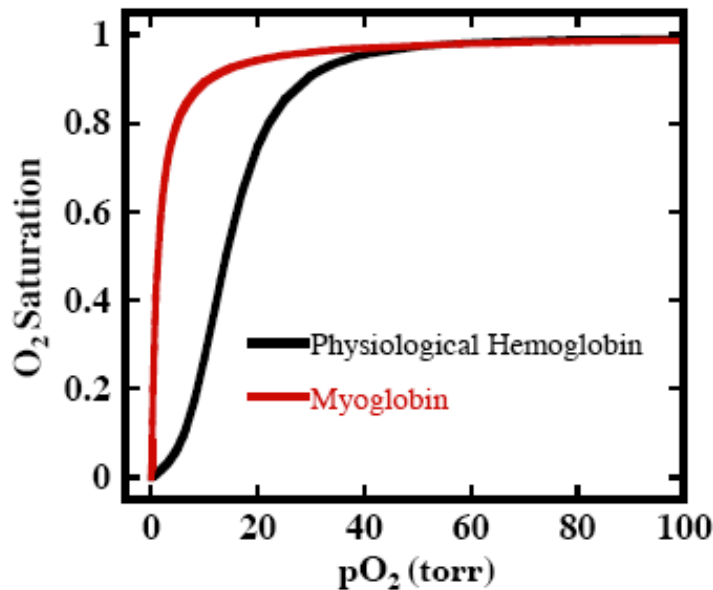


Figure 1-1: Oxygen saturation curves for hemoglobin and myoglobin as a function of  $pO_2$ . [4]

An allosteric protein is one in which substrate affinity is altered by the presence (or absence) of a ligand at a different binding site of the same protein as the result of a conformational change. Hemoglobin's ability to change between two conformational states allows for cooperative binding of oxygen, in which the binding of an  $O_2$  molecule to one subunit increases the  $O_2$  affinity of the other hemes of the tetramer. This

cooperativity allows Hb to deliver  $O_2$  efficiently by binding multiple  $O_2$  molecules in the lungs at high  $pO_2$  and release most, or all, of the  $O_2$  in tissues where the  $pO_2$  is lower. In contrast, monomeric myoglobin binds oxygen efficiently, but the lack of cooperativity prevents the release of oxygen in significant amounts until very low  $pO_2$  is achieved, as illustrated in Figure 1-1.

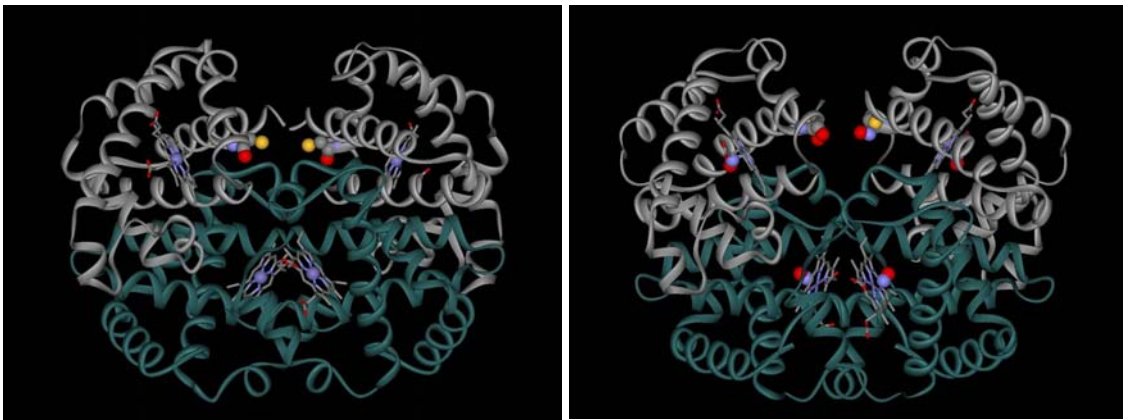


Figure 1-2: Crystal structures of T-state deoxy-Hb [5] (left) and R-state SNO-Hb(NO)<sub>4</sub> (right) [6].

In allosteric proteins, there are both homotropic and heterotropic allosteric modulators. Homotropic modulators bind to the substrate active site (or sites) of the protein, while heterotropic modulators bind to an alternative site (or sites) on the protein. Ligands which bind to the heme iron, such as  $O_2$ , CO, and NO, as well as the oxidation of iron from Fe(II) to Fe(III), are homotropic allosteric modulators. When heme occupancy exceeds 50% in a tetramer, the molecule undergoes a conformational change from the tensed state (T-state) to the relaxed state (R-state), shown in Figure 1-2. T-state is hemoglobin's low affinity state, while the R-state is the high affinity state.  $H^+$ ,  $CO_2$  and inositol hexaphosphate (IHP) are heterotropic allosteric modulators of hemoglobin and

induce the T-state conformation in hemoglobin. Because these effectors induce T-state and therefore decrease Hb's affinity for substrates, they are considered negative allosteric modulators. But not all heterotropic effectors are negative effectors; S-nitrosylation of the  $\beta$ Cys93 residue of the protein (SNO-Hb) favors R-state and has been shown to increase O<sub>2</sub> affinity of hemoglobin [7].

### Blood Flow and Nitric Oxide

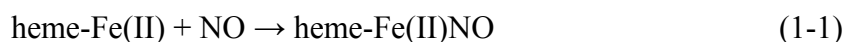
Hemoglobin's allosterically enhanced oxygen binding ability accomplishes nothing if the oxygen saturated Hb does not reach tissues in demand for oxygen. The delivery of oxygen is dependent on blood flow, which, in the microcirculation, is determined by the local physiological oxygen gradients [1,8]. Areas under high metabolic demand will have decreased oxygen content, which will result in increased blood flow and, therefore, the delivery of oxygen. The converse holds true as well, with high oxygen content yielding reduced blood flow. Hb acts as the sensor of the oxygen content of the blood and it is Hb's O<sub>2</sub> saturation, rather than pO<sub>2</sub>, that ultimately determines blood flow [9,10].

The increase and decrease of blood flow is the result of dilation and constriction, respectively, of the microcirculation. In 1987, the endothelium-derived relaxing factor, which induces vasodilation, was identified as nitric oxide [11,12]. Prior to this discovery, nitric oxide was considered a toxic free radical, useful only as a surrogate ligand for O<sub>2</sub> in electron paramagnetic resonance (EPR) studies of hemoglobin [13].

### Hemoglobin Interaction with NO

The connection between EDRF and NO was, in part, discovered because of the inactivation of both by hemoglobin. This, however, raises an important query: in light of the graded vasodilatory response to Hb O<sub>2</sub> saturation, how is balance maintained between the vasodilatory activity of NO and hemoglobin's propensity for NO scavenging?

The NO scavenging reactions of hemoglobin are:



and



In reaction 1-1, deoxy-Hb (heme-Fe(II)) rapidly binds to NO, forming nitrosyl-Hb (heme-Fe(II)NO), with a binding constant 10<sup>5</sup>-fold greater than that of O<sub>2</sub>. [14] In the second reaction, 1-2, oxy-Hb (heme-Fe(II)O<sub>2</sub>) reacts with NO, resulting in heme oxidation to methemoglobin (Met-Hb or heme-Fe(III)) and the formation of nitrate, which is considered biologically inactive [15,16].

While the cellular packaging of Hb in red blood cells and the spatial arrangements of red blood cells in blood vessels may retard hemoglobin's ability to quench NO bioactivity [17-21], the most significant means of NO bioactivity preservation is the formation of S-nitrosothiols (RSNOs), known to be potent vasodilators [22-25]. Formation of RSNOs, termed S-nitrosylation, allows NO to elude inactivation by the reactions shown above. Possible targets of S-nitrosylation range from low molecular weight thiols to proteins [26], including serum albumin [25] and hemoglobin [27].

### SNO-Hemoglobin

In proteins, S-nitrosylation is a redox-based, post-translational modification of the thiol group of a reactive cysteine residue. S-nitrosylation has been reported in almost every class of protein, with identified substrates for S-nitrosylation numbering over one hundred and serving a wide array of functions in biology [28]. Additionally, altered levels of nitrosylated functional groups (RSNOs) have been measured in conjunction with diseases such as asthma, arthritis, cystic fibrosis, and lung disease [22]. Modified S-nitroso-hemoglobin (SNO-Hb) levels have been linked to diabetes and pulmonary hypertension [22], being elevated in the former and depressed in the latter.

SNO-Hb was shown to be involved in vascular control in 1996 [27]. Soon thereafter, SNO-Hb's ability to regulate blood flow in a manner dependent on the physiological oxygen gradient was also reported [29]. When O<sub>2</sub> content is high, blood vessels are constricted; when O<sub>2</sub> content is low, SNO-Hb induces vasodilation. The graded response of SNO-Hb to O<sub>2</sub> levels is in marked contrast to S-nitrosoglutathione (GSNO), a low molecular weight S-nitrosothiol. In bioassays measuring tension of aortic rings (meant to mimic vasodilation in vivo), addition of GSNO resulted in relaxation, independent of O<sub>2</sub>-levels [8,29]. SNO-Hb, however, was able to transduce the O<sub>2</sub> signal, inducing relaxation at low O<sub>2</sub> levels and constriction when O<sub>2</sub> levels were elevated [8,29].

In hemoglobin, S-nitrosylation occurs on the thiol of the  $\beta$ Cys93 residue, which is highly conserved among species [14,27]. SNO-Hb has been generated in vitro from a variety of reactions. Transnitrosation, in which the NO moiety of a S-nitrosylated low-molecular weight thiol, such as cysteine or glutathione, is transferred to  $\beta$ Cys93, results

in SNO-Hb formation. Oxidation of Hb(NO)<sub>4</sub> by ferricyanide results in the preferential oxidation of  $\beta$ -heme-Fe(II)NO and the formation of SNO-Hb and Met-Hb [30]. Additionally, under appropriate conditions, the reaction of Met-Hb with NO, known as reductive nitrosylation, can also form SNO-Hb, as well as nitrosyl-Hb and nitrite [30]. The redox-coupled formation of SNO-Hb in the last two reactions suggests a possible role for Met-Hb in SNO-Hb formation in vivo.

### Methemoglobin

The oxidized form of hemoglobin, Met-Hb (heme-Fe(III)), accounts for less than 1% of total heme under normal, physiological conditions [31]. The majority of ferric hemes are reduced back to the ferrous state, but some form irreversible denatured species which are subsequently removed in the spleen [32].

Ferric iron in Met-Hb has five 3d-orbital electrons that, depending on the ligand field strength, can assume either high- or low-spin configurations,  $s=5/2$  or  $s=1/2$ , respectively. Both spin states facilitate characterization by EPR spectroscopy. Peisach and Blumberg [33] developed a method to categorize low-spin Fe(III) heme proteins, known as hemichromes, using tetragonal and rhombic ligand field parameters determined by the g-values measured with EPR spectroscopy. This method allows comparison of hemichromes, even with unknown ligands, as complexes with different types of axial ligands fall into distinct clusters when their ligand field parameters are plotted.

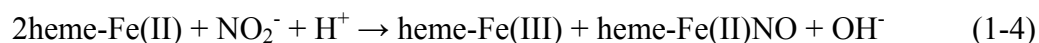
Considerable attention has been directed towards low-spin ferric heme complexes [33-38]. In hemoglobin, hemichromes are formed when a high-field ligand is bound to iron in the distal position of the heme. These ligands include endogenous ligands like the

imidazole nitrogen of histidine, as well as exogenous ligands such as  $\text{CN}^-$ ,  $\text{OH}^-$  and  $\text{N}_3^-$ . In one species, hemichrome formation involving a cysteine thiol has been shown to result in S-nitrosylation following addition of nitric oxide [39].

While the majority of hemichromes have been well characterized by EPR, the hemichrome formed by nitrite addition to Met-Hb has been almost completely ignored, save a single EPR spectrum [40] and binding constants determined by UV-VIS spectroscopy [41-43]. The recent focus by many on the purported role of  $\text{NO}_2^-$  in hypoxic vasodilation [44,45], including a report claiming Met-Hb: $\text{NO}_2^-$  to be EPR silent [46], highlights the need for further examination of this species by EPR spectroscopy.

#### Reactions of Nitrite and Hemoglobin

In addition to binding to Met-Hb, nitrite reacts with both the oxygenated and deoxygenated forms of ferrous hemoglobin, as seen in the following reactions:



The product distribution of the reaction of deoxy-Hb with nitrite has been the source of much debate. Some have measured equal populations of Met-Hb and heme-Fe(II)NO as indicated in reaction 1-4 [47]. Others have found the formation of Met-Hb to exceed that of heme-Fe(II)NO [48], with some attributing the “missing NO” to be involved in SNO-Hb formation [49].

Reutov et al. [45] suggested that, in light of the NO produced in the deoxy-Hb/nitrite reaction, nitrite could serve as a pool of NO-bioactivity under anaerobic conditions. Others have noted Hb’s ability to function as a nitrite reductase, as well

[44,47,50,51]. What these proposals lack is rational for how the generated NO avoids quenching by the reactions mentioned earlier (1-1 and 1-2).

While a direct role for nitrite in NO-induced hypoxic vasodilation appears unlikely, nitrite could possibly be indirectly involved through participation in SNO-Hb formation. Luchsinger et al. [49] observed SNO-Hb formation in the reaction of deoxy-Hb with nitrite, though the major products of the reaction were Met-Hb and heme-Fe(II)NO as predicted by reaction 1-4. A similar study by Angelo et al. [52] found that in the reaction of nitrite with deoxy-Hb, a Fe(III)NO-like species forms that, upon oxygenation (and T-state to R-state conversion), quantitatively generates SNO-Hb. In this reaction scheme,  $\text{NO}^+$  would be released to react with  $\text{RS}^-$  of Cys $\beta$ 93, leaving behind the reduced heme-Fe(II), which would subsequently bind  $\text{O}_2$ . Others have suggested that the reactive intermediate in this reaction is actually  $\text{Fe(III)NO}_2^-$ , which reacts with NO to form  $\text{N}_2\text{O}_3$  [46].  $\text{N}_2\text{O}_3$ , a highly reactive molecule, could then S-nitrosylate Cys $\beta$ 93, forming SNO-Hb, as well as homolyze to NO. These studies demonstrate that the reaction of nitrite with hemoglobin is capable of producing SNO-Hb, yet specifics of SNO-Hb formation by nitrite and the possibility for its indirect role in hypoxic vasodilation remain unresolved [53,54].

The reaction of nitrite with hemoglobin raises the important distinction between pharmacological vasodilation and physiological hypoxic vasodilation. By definition, hypoxic vasodilation is “the rapid dilation of microvascular beds in response to increased local metabolic demand, which is critically coupled to decreased Hb  $\text{O}_2$  saturation and occurs in the time that blood transits a capillary bed from the arteries to the veins.” [1] The timescale of hypoxic vasodilation is seconds. Some have attempted to link the

relaxation observed with the administration to supraphysiological doses of nitrite to a direct role for nitrite in hypoxic vasodilation [44,55,56]. However, the timescale of the response (several minutes, rather than seconds) and the nitrite levels required are indicative of a pharmacological response rather than a physiological response. Moreover, others have reported that physiological amounts of nitrite were unable to induce vasodilation in the presence of red blood cells [57].

### Summary

The reactions of hemoglobin are as numerous as they are diverse. The connection between these many reactions and the physiological formation of SNO-Hb in vivo remains elusive. This thesis employs EPR spectroscopy to investigate the nature of interactions between heme-iron, both Fe(II) and Fe(III), and physiologically relevant ligands. Given the pivotal role of SNO-Hb in hypoxic vasodilation [1], the characterization of species with potential roles in SNO-Hb formation is of considerable importance. As a whole, this work extends our knowledge base of hemoglobin behavior, particularly with regard to the interaction of heme-Fe(III) with  $\text{NO}_2^-$  and heme-Fe(II) with NO.

## CHAPTER 2

## EPR SPECTROSCOPY OF METHEMOGLOBIN:NITRITE

Introduction

The chemical interaction of nitrite with hemoglobin (Hb) has attracted considerable, recent attention because of its potential significance in the mechanism of NO-related vasoactivity regulated by Hb, namely, hypoxic vasodilation. While the specific nature of nitrite's possible roles in this physiological process has been debated, the critical assessment of all of the available data, recently published by Allen et al. [1], consolidates the view that the central signaling entity in hypoxic vasodilation is the S-nitroso-derivative of Hb, SNO-Hb. SNO-Hb has the unique capacity to effect a prompt NO-dependent modulation of blood flow in response to hemoglobin oxygen-saturation over physiological oxygen gradients, as red blood cells (RBCs) pass from arterial to venous circulation. This assessment allows only an indirect, albeit potentially important, role for nitrite, which, for example, could, through slower biochemical pathways, raise stores of SNO-Hb.

Luchsinger et al. [8,30], had already in 2003, used the well-known reaction of nitrite with deoxy-Hb to produce SNO-Hb, and thus to exemplify one of several routes of SNO-Hb synthesis that involve redox coupling of heme-iron and NO to support nitrosative chemistry. This work brought increased attention to the role of Fe(III)-containing met-hemes, and their complexes with nitrogen oxides in such transformations [46,49,52], and prompted renewed interest in the spectroscopic characterization of such

complexes to facilitate analysis of this chemistry.

This interest was further piqued recently by the report of Basu et al. [46] who measured the affinity of Met-Hb for nitrite by an indirect EPR technique. Specifically, they monitored the progressive loss of the high-spin Met-Hb EPR signal with successive additions of nitrite, and, assuming a simple equilibrium, determined a substantially higher affinity than previously determined by UV-Vis spectroscopy [41]. Intriguingly, they did not detect the EPR spectrum of the complex— an outcome that was surprising, inasmuch as EPR spectra have been previously reported both for low-spin nitrite complexes with metmyoglobin [58] and for RBCs treated with nitrite [59]. We therefore undertook a re-investigation of the EPR spectroscopy of the nitrite:Met-Hb complex. We were able to elicit the expected the nitrite:Met-Hb spectrum, to demonstrate, through mass balance, that it was essentially the sole reaction product, and, by quantitative analysis of both the protein reactant and product, to determine an affinity in agreement with the previous studies that had been questioned by Basu et al. These findings were reported in a brief account published elsewhere [54].

The observed EPR spectra exhibited a distinctive structure— a doubling of certain spectral features— that motivated further study. This motivation is enhanced by recent X-ray crystallographic studies that have demonstrated structural and linkage isomerization in nitrite coordination to Met-Hb [60], and thus raised the possibility that the spectral features might arise from structurally distinct coordination complexes. Here we report a comprehensive EPR study of the nitrite:Met-Hb complex, in which we test different possible origins of the spectral structure. We also elaborate our previous, brief remarks [54], on evidence for the weak affinity between Met-Hb and the nitrite ligand.

## Materials and Methods

### Hemoglobin

Hb was purified from human red blood cells obtained from Innovative Research (Novi, Michigan), following the procedure of Geraci et al. [61] Hb was stored in aqueous solution at -80 °C for later usage. Prior to use, Hb was passed through Sephadex G-25 (GE Healthcare) chromatography gel, equilibrated with the appropriate buffer, either 100 mM HEPES or PBS. All buffered solutions also contained 0.1 M KCl and 0.1 mM DTPA (diethylene triamine pentaacetic acid). In light of the well-known pH artifacts associated with the freezing of sodium phosphate buffer [62,63], we utilized HEPES buffer primarily, and, to illuminate buffer-effects, potassium PBS.

Met-Hb was prepared by treatment of Hb with potassium ferricyanide followed by G-25 filtration to remove excess oxidant. To prepare Met-Hb:NO<sub>2</sub><sup>-</sup>, aliquots of buffered (HEPES or PBS) aqueous solutions of NaNO<sub>2</sub> were added to Met-Hb solutions with nitrite at twenty-fold excess over heme.

### Fe(II)NO/Fe(III)NO<sub>2</sub><sup>-</sup>-Hb hybrids

To probe for subunit specificity of the nitrite:Met-Hb complexes, reactions were carried out with Met-Hb/nitrosyl-Hb hybrids, which were prepared in two distinct ways. First, to obtain Hb with preferentially oxidized β-subunits (and nitrosylated α-subunits), Hb was initially incubated with sodium nitrite and sodium dithionite under anaerobic conditions to generate Hb(NO)<sub>4</sub>; the solution was then subjected to gel filtration to remove any excess reagents. The resulting Hb(NO)<sub>4</sub> solution was then exposed to room

air for approximately 7 hours at 20 °C. This procedure results in preferential oxidation of  $\beta$ -Fe(II)NO to Fe(III) [30]. The concentration of Met-Hb present was assayed by UV-Vis spectroscopy, while subunit specificity was determined by EPR spectroscopy [30]. Concentrated  $\text{NaNO}_2$  solution was then added to form the  $\alpha$ -Fe(II)NO/ $\beta$ -Fe(III)NO $_2^-$  hybrid complexes.

Complementary Hb hybrids, with oxidized  $\alpha$ -subunits and nitrosylated  $\beta$ -subunits, were prepared by reductive nitrosylation of Met-Hb with a [NO]:[heme] ratio of 0.9 to 1 using DEANO (diethylamine NONOate (Cayman Chemical)) as the NO donor [30]. Reaction progress was monitored using UV-Vis spectroscopy. Following reductive nitrosylation, concentrated  $\text{NaNO}_2$  was added in molar excess over the remaining Fe(III), to furnish  $\alpha$ -Fe(III)NO $_2^-$ / $\beta$ -Fe(II)NO hybrid complexes.

### SNO-Hb

SNO-Hb was prepared by reacting oxygenated Hb in pH 9.2 borate buffer with acidified nitrite. Following incubation, the SNO-Hb solution was passed through a G-25 column equilibrated with pH 7.4 HEPES buffer. SNO-Hb yield was determined by Greiss and Saville assays, as described previously [64]. SNO-Hb was then oxidized with potassium ferricyanide with subsequent G-25 filtration. Concentrated  $\text{NaNO}_2$  was added in molar excess, as determined by UV-Vis spectroscopy to furnish SNO-Met-Hb:nitrite.

### D<sub>2</sub>O Solutions

To prepare solution of Met-Hb:NO $_2^-$  in D $_2$ O, hemoglobin was first treated with potassium ferricyanide followed by G-25 filtration, then concentrated using a Microcon 30 centrifugal filter (Millipore, Billerica, MA). The protein was reconstituted in 1:10

(vol:vol) HEPES buffered deuterium oxide (Cambridge Isotope Laboratories Inc, Cambridge, MA). pD of the solution set to 7.4, as determined with a glass electrode using pH+0.4 [65].

### EPR Spectroscopy

X-band EPR data were collected on a Varian E-109 spectrometer modified with a National Instruments computer interface for data collection and field control. For spectra obtained at liquid helium temperatures, a Heli-Tran LTD-3-110 (Air Products and Chemicals Inc, Allentown, PA) liquid helium transfer system and dewar was employed. For X-Band spectra obtained at 100K and above, sample cooling was provided by a flow through set-up utilizing a constant stream of liquid nitrogen cooled gas. S-band EPR data collection was conducted on a Bruker EMX spectrometer with an ER061ST microwave bridge, and a flexline cavity assembly. Liquid helium temperatures were achieved through the use of an Oxford Instruments CF-905 cryostat. Detailed simulation of experimental EPR data was conducted using the program EasySpin [66]. Observed alterations in the quality of the fit with changes in parameter values were used as a guide to the precision of the determination of the values. Simulated spectra were then used as basis spectra for least-squares decomposition of multi-component EPR spectra, using a fitting program similar to that described by us previously [30].

### UV-Vis Spectroscopy

UV-Vis spectra were collected using a Cary 300 spectrometer. Least-squares fitting of spectra [30] was used to determine the concentration of UV-Vis detectable of heme species.

## Results

### Doublet Structure

Low-temperature EPR spectra of our neutral pH, neat Met-Hb preparations consist, generally, of spectral contributions from three distinct chemical species: 1) high spin aquo-Met-Hb; 2) low spin hydroxy-Met-Hb; and 3) an additional low spin species that has been proposed to result from the coordination of a nitrogen atom of the distal histidine as the sixth heme-iron ligand [67]. Detailed simulations of our experimental Met-Hb spectra (not shown) agree well with the results of Svistunenko and co-workers, both in regard to the spectral properties and the relative amounts of each of the three species [67].

Addition of excess sodium nitrite to neutral pH Met-Hb solutions results in the substantial replacement of the Met-Hb EPR signals with new features in the region associated with low-spin Fe(III) hemichromes. In the X-band EPR spectra shown in Figure 2-1, these new features entail a broad, high-field feature at ~4500 G; a closely spaced doublet, low-field feature at ~2200 G; and a well-resolved doublet, intermediate field feature at ~3000 G. As evidenced in Figure 2-1, the resolution of the low-field doublet exhibits some sensitivity to the nature of the buffer. It is better resolved, with sharper component lines and minor changes in line position in PBS (Figure 2-1, bottom). Nevertheless the fundamental features are the same; intrinsic buffer effects represent a modest perturbation, in contrast to suggestions made by others [53].

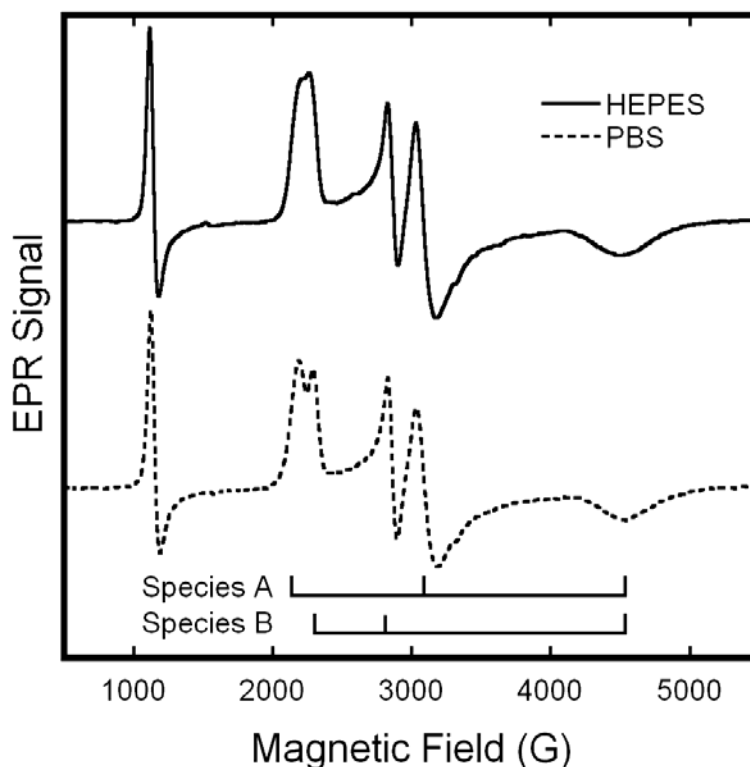


Figure 2-1: X-Band EPR spectra of solutions of Met-Hb:NO<sub>2</sub><sup>-</sup> in HEPES (—) or PBS (---) buffers at 20 K. The samples included Met-Hb at 0.5 M and twenty-fold molar excess (per heme) of NaNO<sub>2</sub>; the buffer concentration was 0.1 M and the pH 7.4. EPR spectra were obtained with the following spectrometer parameter values: 0.5 s time constant, 5 G modulation amplitude, 16.67 G/s sweep rate, 5 mW microwave power, and 9.24 GHz microwave frequency.

We considered two alternative hypotheses for the origin of this structure: 1) the splittings reflect hyperfine structure; or 2) they reflect the overlap of the unstructured spectra of two low-spin hemichromes with slight difference in their high and intermediate *g*-values. To distinguish between these possibilities we undertook two experiments. First, we obtained the EPR spectrum of isotopically labeled Met-Hb:NO<sub>2</sub><sup>-</sup> samples. Given the size of the splittings, the coupling would most likely involve an H-atom whose 1s orbital has substantial overlap with iron *t*<sub>2g</sub> orbitals— perhaps a proton associated with the nitrite ligand. To test this possibility we obtained the EPR spectrum of the Met-Hb:nitrite complex in HEPES buffer in D<sub>2</sub>O (Figure 2-2). The spectra are essentially identical to

ones obtained in H<sub>2</sub>O; in particular, the splitting of the two central features is unchanged. (Analogous results were obtained in complexes formed with <sup>15</sup>N-nitrite (data not shown)).

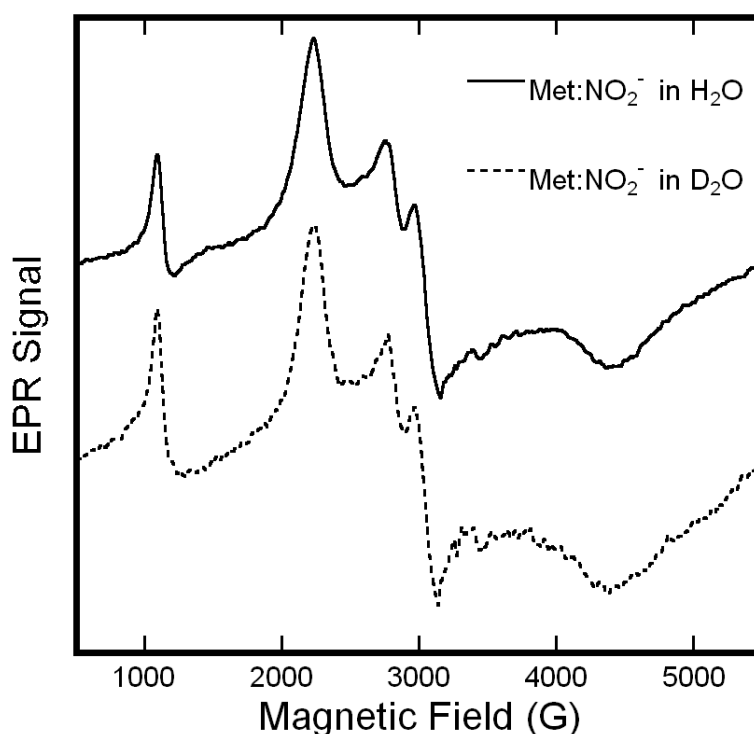


Figure 2-2: EPR spectra of solutions of Met-Hb:NO<sub>2</sub><sup>-</sup> in H<sub>2</sub>O and D<sub>2</sub>O in boiling nitrogen (76 K). The protein concentration was 0.5 M in the H<sub>2</sub>O sample and 0.4 M in the D<sub>2</sub>O sample. Both samples contained a twenty-fold molar excess (per heme) of NaNO<sub>2</sub>, and buffered at an effective pH of 7.4 in HEPES. Spectral amplitudes were corrected for difference in concentration. Both EPR spectra were recorded at 9.12 GHz with a 16.67 G/s sweep rate, a 0.5 s time constant, 5 G modulation amplitude, and 10 mW of microwave power.

To validate this result, we compared EPR spectra obtained at X-band, with spectra obtained at S-band (3.9 GHz). The S-band spectrum (Figure 2-3) exhibits splittings in both the low-field and intermediate-field features that scale in proportion to the reduction in microwave frequency from X-band to S-band. If the observed splitting had originated from a hyperfine interaction, then the splitting would be expected to remain constant over

this microwave frequency range. Collectively, the multi-frequency EPR and the isotopic labeling experiments indicate that the EPR spectrum of Met-Hb:NO<sub>2</sub> is caused by the presence of two distinct species. Accordingly, returning to the upper spectrum of Figure 2-1, we determine the Met-Hb:nitrite EPR spectra to have principal g-values of: (3.006, 2.887), (2.299, 2.129), and 1.45 (HEPES, 20K). The assignment of the pairs of values in parentheses to unique species is not obvious from the spectra, but can be made on the basis of observations of the differential effects of pH on the size of the components of each doublet (*vide infra*).

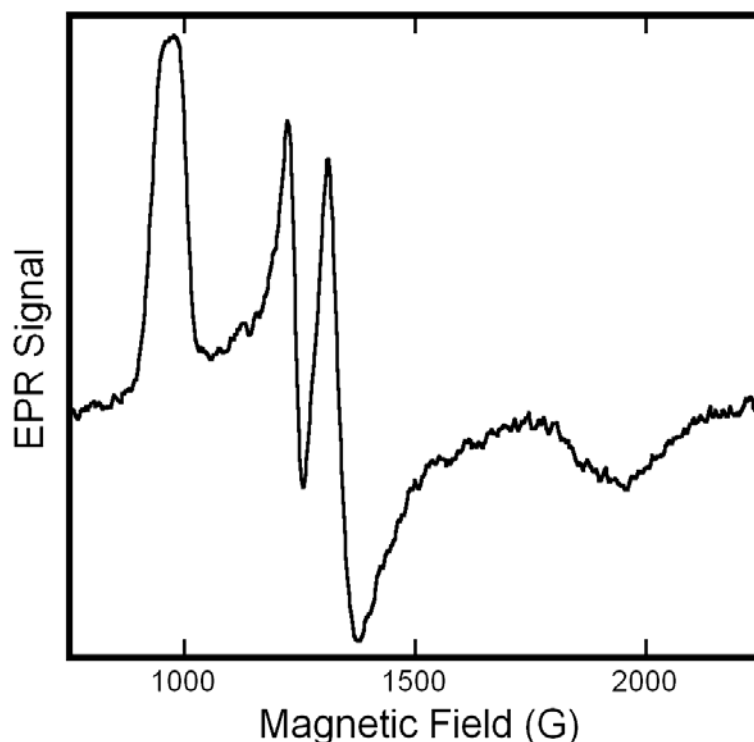


Figure 2-3: S-Band EPR spectrum of solutions of Met-Hb:NO<sub>2</sub><sup>-</sup>. The sample was prepared in pH 7.4 HEPES buffer with a protein concentration of 0.75 M and a twenty-fold molar excess (per heme) of NaNO<sub>2</sub>. The spectrum was obtained with the sample at ~40 K, and at a frequency of 3.98 GHz, with a sweep rate of 17.88 G/s, a time constant of 0.328 s, 5 G modulation amplitude, and 9.7 mW microwave power.

### pH Dependence

As illustrated in Figure 2-4, the relative intensities of the features of each doublet in the EPR spectra of Met-Hb:NO<sub>2</sub><sup>-</sup> exhibit notable variation with pH over the range pH 5 to pH 10. As the pH increases, the intensity of the feature at  $g \approx 2.9$  increases relative to the  $g \approx 3.0$  feature. This change in intensity is mirrored by the increase in intensity of the  $g \approx 2.3$  feature relative to the  $g \approx 2.1$  feature. This concerted variation allows for the assignment of features to two species, Met-Hb:NO<sub>2</sub><sup>-</sup> A and B, with  $g$ -values of ( $g_z, g_y, g_x$ ) of (3.018, 2.122, 1.45) and (2.870, 2.304, 1.45) (PBS, 20K); and thus of (3.006, 2.129, 1.45) and (2.887, 2.299, 1.45) (HEPES, 20K). This assignment balances the sizes of the  $g$ -values, consistent with the general rule for hemichrome principal  $g$ -values that the sum of their squares be  $\sim 16$  [38].

In addition to changes in complexation, this series of EPR spectra also reveals changes in the positions of certain features in the Met-Hb:NO<sub>2</sub><sup>-</sup> spectra with pH. The greatest change is sustained by the low field feature of Met-Hb:NO<sub>2</sub><sup>-</sup> species A: it appears at  $g \approx 3.00$  at pH 5.0;  $g \approx 3.02$  at pH 7.4, and  $g \approx 3.04$  at pH 10.0. The central feature of species A ( $g = 2.12$ ) also shifts as a function of pH, although its exact position is difficult to follow because it is masked at higher pH by the Met-Hb:OH<sup>-</sup> spectrum. Changes to Met-Hb:NO<sub>2</sub><sup>-</sup> B features are more subtle; the low field feature of species B varies from  $g = 2.86$  at pH 5.0 to  $g = 2.87$  at pH 10.0. The broad high field features of both species A and B do not show discernible, pH-dependent changes in position.

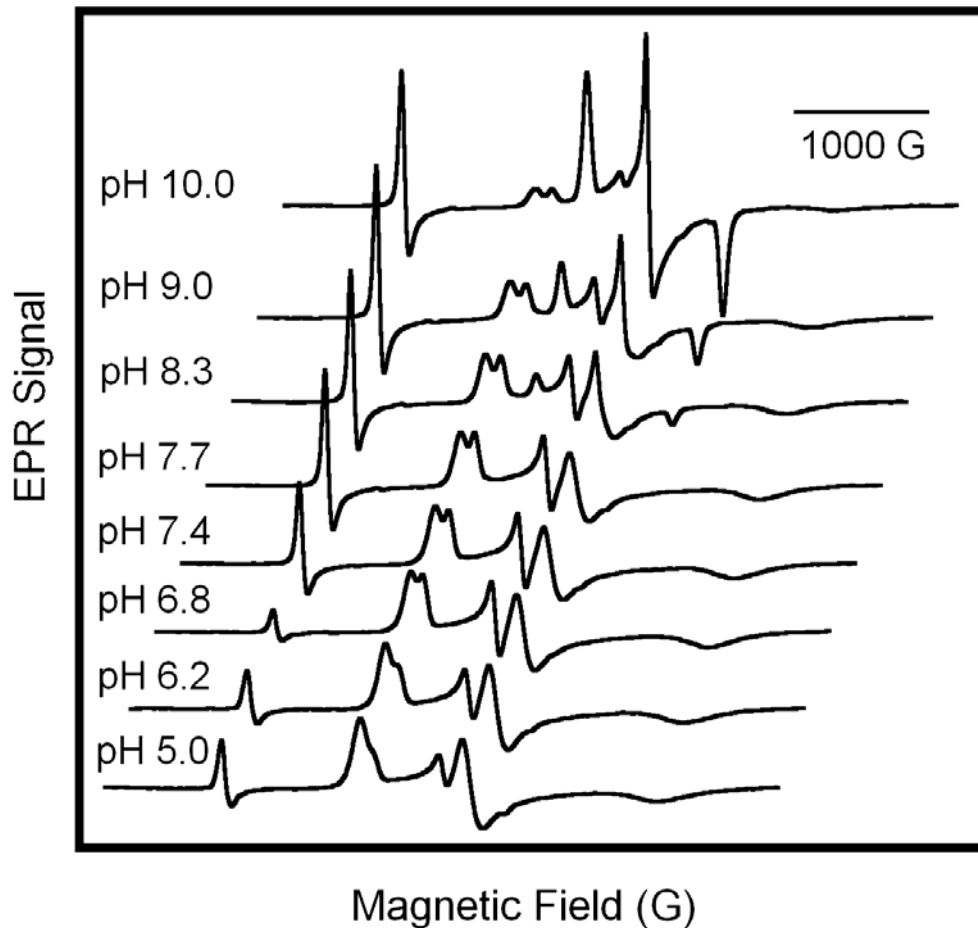


Figure 2-4: pH dependence of EPR spectra of Met-Hb:NO<sub>2</sub><sup>-</sup>. Solutions of Met-Hb in PBS poised at pH values as indicated in figure, 0.5 mM in protein and 40 mM in NaNO<sub>2</sub> for all samples. The EPR spectra were recorded at 9.24 GHz with a 16.67 G/s sweep rate, 0.5 s time constant, 5 G modulation amplitude, and 5 mW of microwave power.

Figure 2-5 plots the relative percentages of the components of the Met-Hb:NO<sub>2</sub><sup>-</sup> EPR spectrum as a function of pH. The contribution of Met-Hb:NO<sub>2</sub><sup>-</sup> species A steadily decreases from pH 5 to pH 10, while the percentage of species B increases from pH 5 to pH ~8 and then decreases as the pH increases above pH 8. The ratio of species A:B varies from about 7:1 at pH 5 to about 2:1 at pH 10. The aquo-Met-Hb component of the EPR spectrum declines as the pH is varied from pH 5 to pH 6.8. As the pH is raised above 6.8, the aquo-Met-Hb contribution steadily increases. Additionally, at pH 8.3,

Met-Hb:OH<sup>-</sup> is first detected in the Met-Hb:NO<sub>2</sub><sup>-</sup> EPR spectrum. At pH 10.0, Met-Hb:OH<sup>-</sup> accounts for approximately 60% of the detected species.

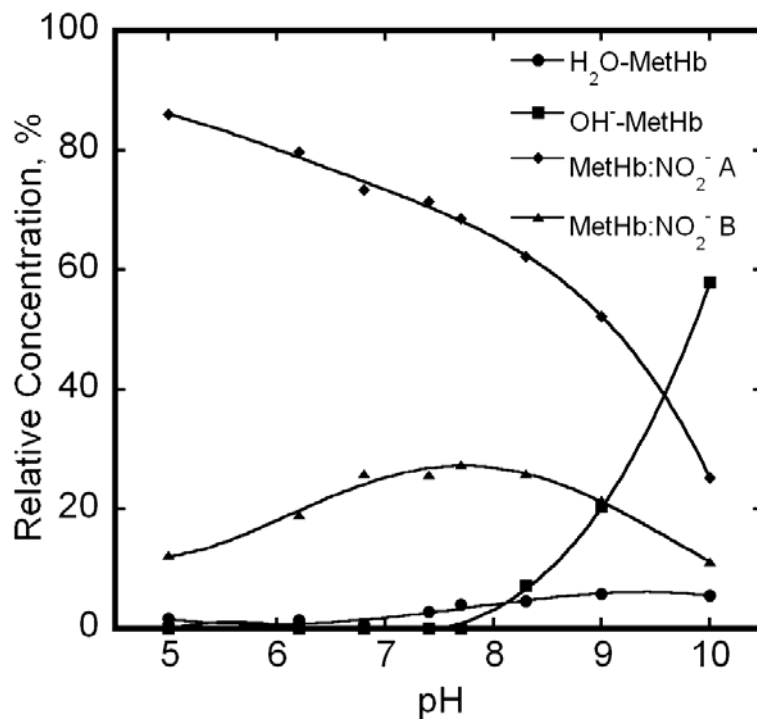


Figure 2-5: Relative concentrations of MetHb species as a function of pH as determined by fitting X-Band EPR spectra shown in Figure 2-4.

#### Variable Temperature EPR

The presence of multiple species that are distinguished by EPR in samples of Met-Hb:NO<sub>2</sub><sup>-</sup> is reminiscent of the behavior of Fe(II)NO in Hb(NO)<sub>4</sub>. EPR spectra in Hb(NO)<sub>4</sub> show two different species (axial and rhombic) with, moreover, subunit distinctions that are most clearly illuminated in variable temperature EPR studies [68,69]. In light of this precedent, we undertook variable temperature EPR studies of Met-Hb:NO<sub>2</sub><sup>-</sup>. Exemplary spectra are shown in Figures 2-6 and 2-7.

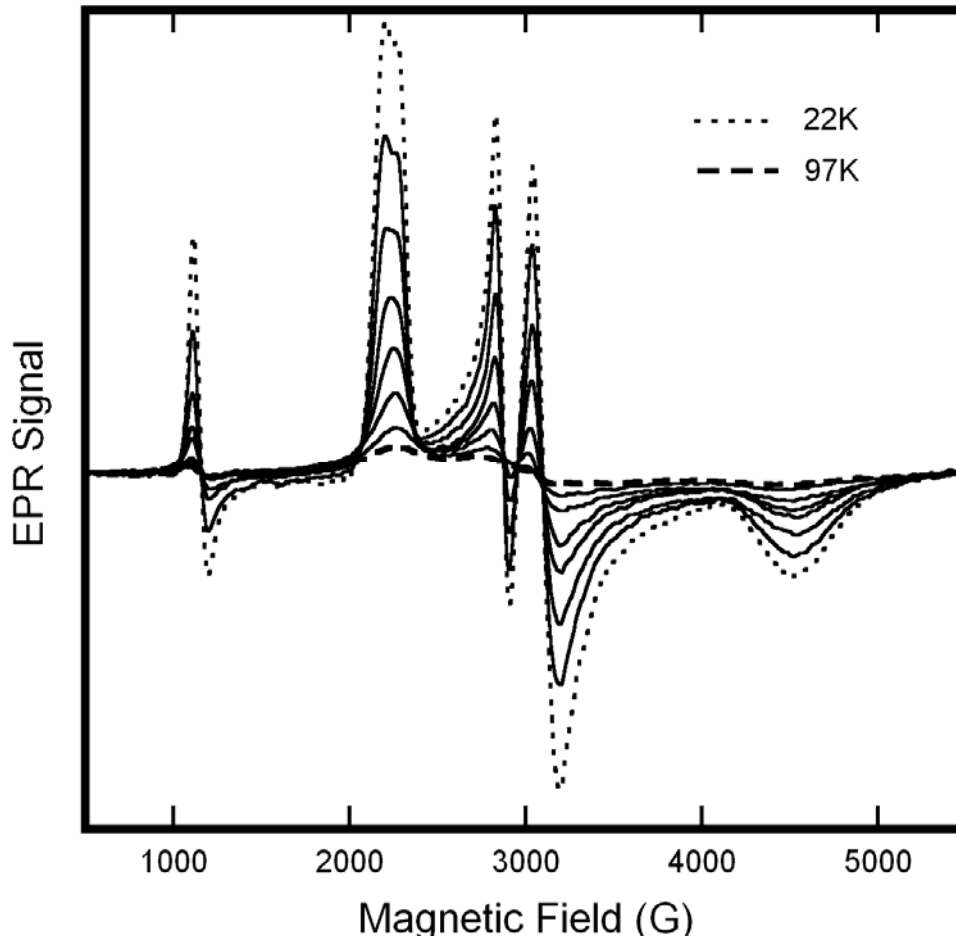


Figure 2-6: Variable temperature EPR spectra of solutions of Met-Hb:NO<sub>2</sub><sup>-</sup> in HEPES buffer at pH 7.4. The sample included Met-Hb at 0.65 M and a twenty-fold molar excess (per heme) of NaNO<sub>2</sub><sup>-</sup>. Spectra were obtained at 22, 32, 43, 54, 65, 76, 86, and 97 K. The EPR spectra were recorded at 9.24 GHz with a 16.67 G/s sweep rate, a 0.5 s time constant, 5 G modulation amplitude, and 5 mW of microwave power.

At temperatures below 20 K, the Met-Hb:NO<sub>2</sub><sup>-</sup> spectrum is readily saturated and, absent sufficient care, subject to lineshape and intensity distortion, as has been recently realized by others [53]. Spectra are obtained with facility in the temperature range of 20 to 100 K, and display only very subtle changes in the position and shape of spectral features. The separate components of the low-field feature remain resolved until the temperature is raised to ~54 K, while the central doublet remains resolved until the temperature exceeds ~100 K. There appears to be little, if any, net interconversion

between the two species, in contrast to the spectrum of  $\text{Hb}(\text{NO})_4$ , which over a similar temperature range, shows striking changes reflective of a temperature-dependent equilibrium between the axial and rhombic species (see Chapter 5 and [69]). This effect was first noted in the EPR spectrum of  $\text{Fe}(\text{II})\text{NO}$  myoglobin by Morse and Chan [70]. As illustrated in Figure 2-7, once the sample temperature exceeds 115 K, there appears to be sufficiently rapid and unrestricted motion of the nitrite ligand that the spectra of both of the  $\text{Met-Hb:NO}_2^-$  species no longer exhibit  $g$ -anisotropy.

In light of the motional averaging that ensues at cryogenic temperatures, the apparent lack of a temperature-dependent interconversion between the  $\text{Met-Hb:NO}_2^-$  A and B species at the lower temperatures is intriguing. It is possible that the temperature dependence of an equilibrium constant between the A and B species is small enough (e.g., if A and B were isoenthalpic) that no temperature dependence of the partitioning into A and B spectra is observed. Alternatively, it may be the case that the motion that the ligand undergoes cannot support species interconversion. This possibility is very difficult to reconcile with a conjecture that species A and B entail structural or linkage isomers; rather, it strongly suggests that the A and B reflect differences in nitrite binding between  $\alpha$ - and  $\beta$ -subunits of hemoglobin, in which case motion leading to spectral averaging could occur entirely within a given subunit's heme pocket, without inter-subunit ligand exchange. However, if species A and B are each associated with a particular subunit, equal populations of each are expected in the presence of putatively saturating nitrite. Detailed simulation of the spectra revealed that the A:B ratio is not 1:1, and thus suggest binding modes that entail greater complexity than simple subunit inequalities.

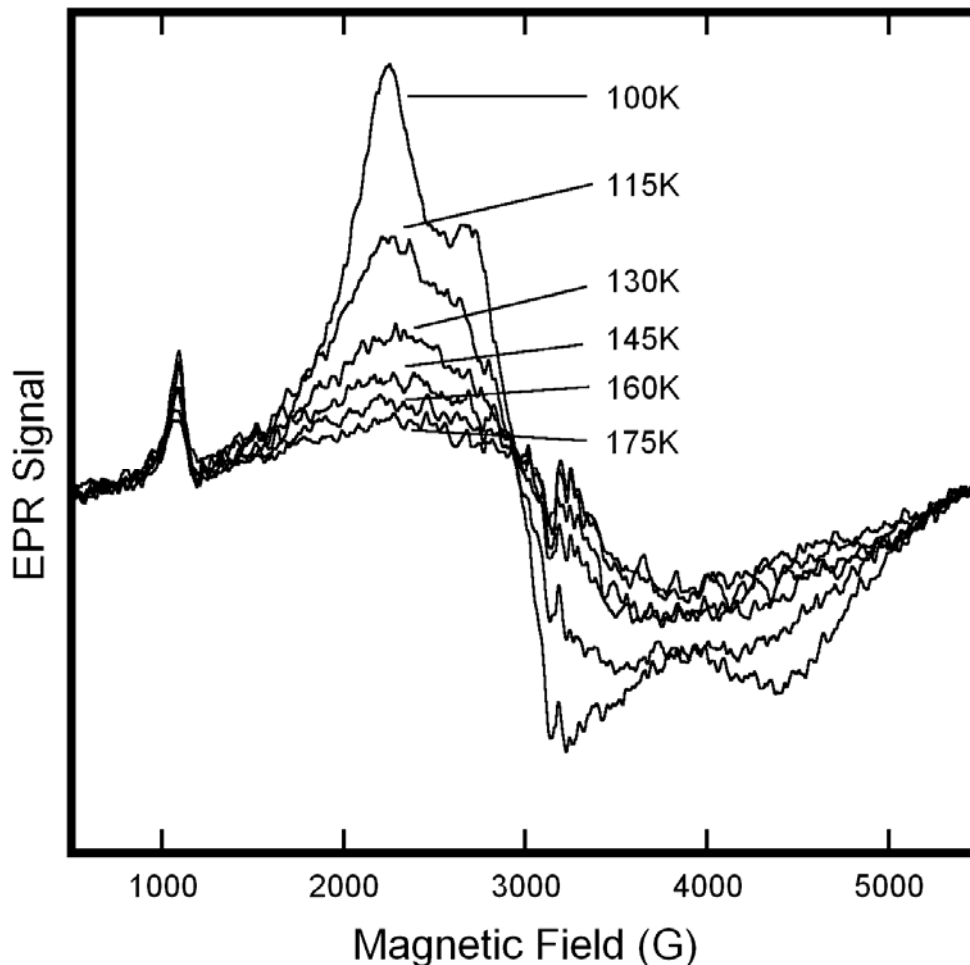


Figure 2-7: Variable temperature EPR spectra of solutions of Met-Hb:NO<sub>2</sub><sup>-</sup> in HEPES buffer at pH 7.4. The sample included Met-Hb at 0.65 M and a twenty-fold molar excess (per heme) of NaNO<sub>2</sub><sup>-</sup>. Spectra were obtained at the indicated temperatures in the range 100 K to 175 K. EPR spectra were recorded at 9.1 GHz with a 16.67 G/s sweep rate, a 0.5 s time constant, 5 G modulation amplitude, and 10 mW of microwave power.

### Hb Hybrids

In an effort to further illuminate possible subunit differences in nitrite binding to hemoglobin, we prepared hybrids of the form:  $\alpha$ -Fe(II)NO/  $\beta$ -Fe(III) Hb, and  $\beta$ -Fe(II)NO/  $\alpha$ -Fe(III) Hb and examined the EPR spectra of their nitrite complexes. In these experiments, the balance between ferrous-nitrosyl and Met-Hb species was assayed by

UV-Vis spectroscopy, while the subunit populations were monitored by examination of their Fe(II)NO EPR spectra [30].

A first class of samples was prepared by reductive nitrosylation with limiting NO [30]. An exemplary preparation, the spectrum of which is shown in Figure 2-8B, was analyzed as 30% Fe(II)NO and 70% Fe(III), with the Fe(III) distributed as >66%  $\alpha$  and <33%  $\beta$ . A second class of samples (Figure 2-8D) was created through partial autoxidation of Hb(NO)<sub>4</sub>, which resulted in 56% Fe(II)NO and 44% Fe(III), 2% of which was  $\alpha$ -Fe(III) and the remaining 98%  $\beta$ -Fe(III). To each hybrid, NaNO<sub>2</sub> was then added to twenty-fold molar excess over the ferric heme present.

As compared to the spectrum of the nitrite complex of the standard Met-Hb (Figure 2-8A), the spectrum of the hybrid with excess  $\alpha$ -Fe(III) (Figure 2-8B), exhibited a reduction in intensity of the B component of the low-field feature ( $g \approx 2.89$ ), as well as a shift of that component to a slightly higher field ( $g \approx 2.85$ ). The ratio of species A to B was 3.2:1. In the hybrid with excess  $\beta$ -Fe(III) (Figure 2-8D), the position of the two low field features remains constant, but the  $g=3.006$  feature displays a reduction in intensity compared to normal Met-Hb:NO<sub>2</sub><sup>-</sup>. The A/B ratio was determined to be 0.8:1. Comparison of the central features is impeded by the much more intense Fe(II)NO signal (which begins to exhibit appreciable intensity  $\sim 3150$ G).

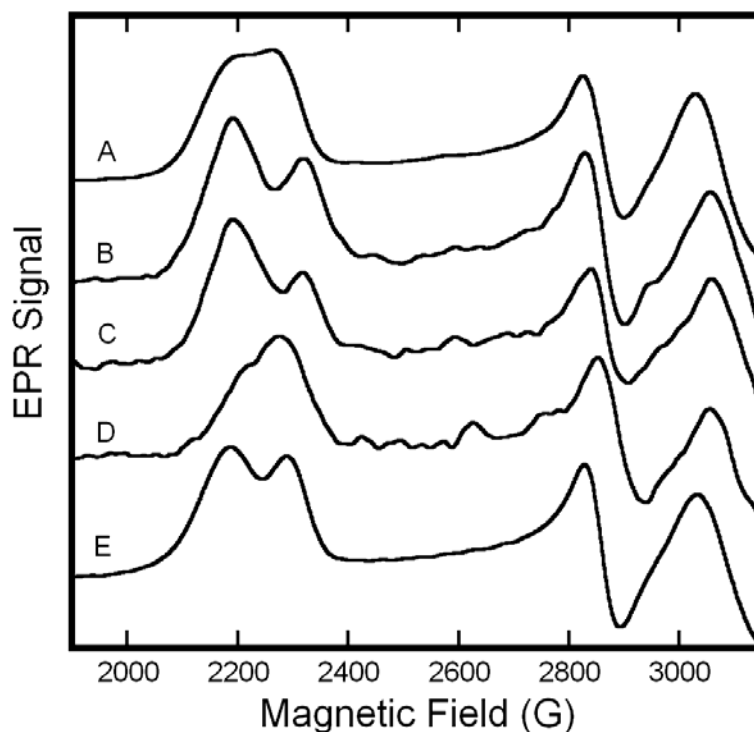


Figure 2-8: EPR spectra of Fe(II)NO/Fe(III)NO<sub>2</sub><sup>-</sup> hybrids and related hemoglobins. For detail, only the variable, low-field portion of the spectrum is shown. (A) Met-Hb:NO<sub>2</sub><sup>-</sup> in HEPES, pH 7.4; (B)  $\alpha$ -Fe(III)NO<sub>2</sub><sup>-</sup>/ $\beta$ -Fe(II)NO in HEPES, pH 7.4; (C) SNO-Met-Hb:NO<sub>2</sub><sup>-</sup> in HEPES pH 7.4; (D)  $\alpha$ -Fe(II)NO/ $\beta$ -Fe(III)NO<sub>2</sub><sup>-</sup> hybrid in HEPES pH 7.4; (E) Met-Hb:NO<sub>2</sub><sup>-</sup> in PBS pH 7.4. All spectra were recorded at 20 K with a frequency of 9.24 GHz, 0.5 s time constant and sweep rate of 16.67 G/s. For spectra A and E the modulation amplitude was 5 G and the microwave power was 5 mW. Spectra B-D were recorded with 1 G modulation amplitude and 10 mW microwave power.

The spectroscopic results of these hybrids experiments are intriguing on multiple levels. First, since the shift of the  $g \approx 2.89$  feature to  $g \approx 2.85$  was only observed in hybrids prepared through reductive nitrosylation, we hypothesized that the shift might be caused by S-nitrosylation of the  $\beta$ Cys93 thiol, a known product of this reaction [30]. To test this notion, we prepared an authentic SNO-Met-Hb:NO<sub>2</sub><sup>-</sup> complex. The EPR spectrum of this species, shown in Figure 2-8C, manifests a similar perturbation of the  $g \approx 2.89$  feature as does the hybrid prepared by reductive nitrosylation. Since S-nitrosylation occurs solely on the  $\beta$ -subunit, species B must be associated with the  $\beta$ -Fe(III):NO<sub>2</sub><sup>-</sup>. However, the

A:B ratios of the two hybrids reveals the simple  $\alpha=A$  and  $\beta=B$  assignment to be inadequate. In the oxidized Hb(NO)<sub>4</sub> hybrid, the  $\alpha:\beta$  Fe(III) ratio was 1:49, yet the A:B ratio was 0.8:1; the hybrid prepared through reductive nitrosylation had an  $\alpha:\beta$  Fe(III) ratio 2:1 and an A:B ratio of 3.2:1.

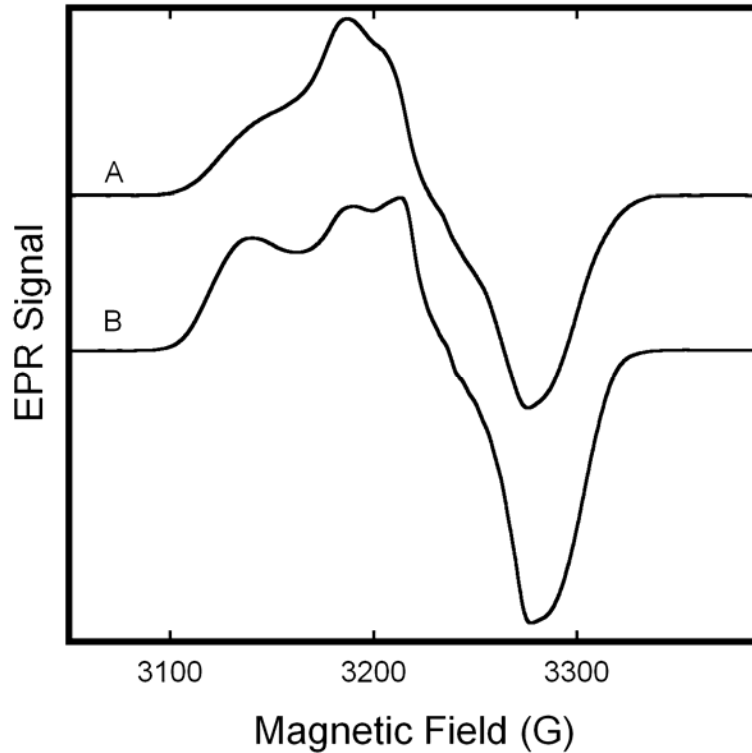


Figure 2-9: Fe(II)NO EPR spectra of Fe(II)NO/Fe(III)NO<sub>2</sub><sup>-</sup> hybrid hemoglobins. Only the central region of the spectrum, featuring the ferrous nitrosyl EPR signal is shown. (A)  $\alpha$ -Fe(III)NO<sub>2</sub><sup>-</sup>/  $\beta$ -Fe(II)NO, as in Figure 2.6B. (B)  $\alpha$ -Fe(II)NO/ $\beta$ -Fe(III)NO<sub>2</sub><sup>-</sup> hybrid as in Figure 2.6D. Spectra were obtained with the sample in boiling nitrogen, at a microwave frequency of 9.12 GHz, 10 mW microwave power, 5 G modulation amplitude, a sweep rate of 3.33 G/s, and a time constant of 0.128 s.

### Affinity

Dissociation constants ( $K_d$ ) of Met-Hb:NO<sub>2</sub><sup>-</sup> were determined by means of the Hill analysis [71] detailed in Figure 2-10. In these experiments, we examined samples in both PBS and HEPES, and added nitrite at molar equivalence and in five-, ten- and

twenty-fold excess over met-heme. The analysis utilized concentrations determined by UV-Vis spectroscopy, with differentiation of the Fe(III) products and reactants being determined by EPR spectroscopy. The assayed concentrations confirmed mass balance of protein before and after the addition of nitrite; no evidence for formation of EPR silent products was observed. The slope of the Hill plot ( $\sim 1$ ) indicates the absence of cooperativity in ligand binding and affords values for  $K_d$  of Met-Hb: $\text{NO}_2^-$  of  $1.24 \pm 0.5$  mM in HEPES pH 7.4, and  $1.68 \pm 0.4$  mM in KPBS pH 7.4.

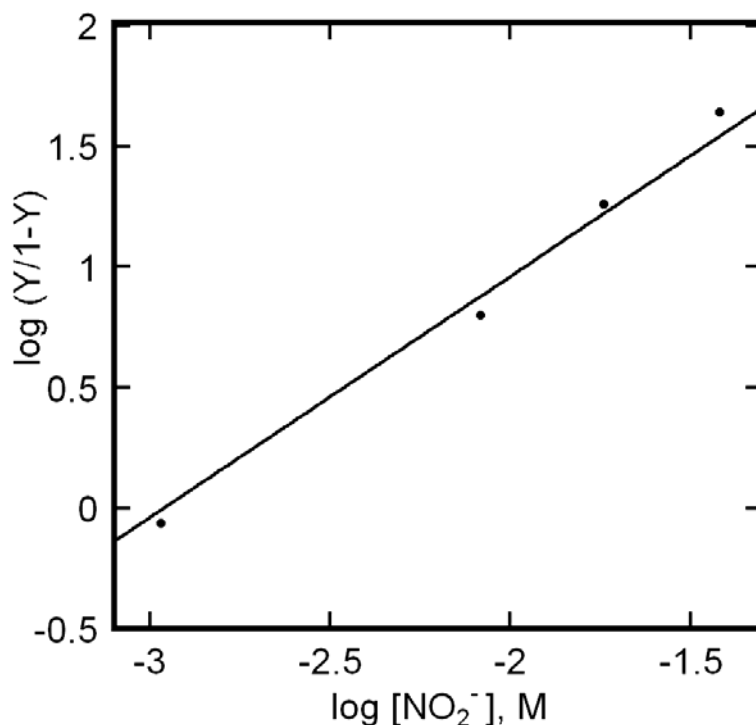


Figure 2-10: Exemplary Hill plot summarizing the titration of Met-Hb with  $\text{NaNO}_2$ . The species concentrations used in the plot were obtained from detailed simulation of experimental EPR spectra. For the particular trial depicted in this plot, the protein concentration was 0.5 mM (pH 7.4 HEPES), with  $\text{NaNO}_2$  at, alternatively, one-, five-, ten- and twenty-fold excess over heme.

The affinity of nitrite and MetHb was also determined from the EPR data collected at multiple pHs, Figure 2-4. A cursory examination of the peak heights of aquo-Met-Hb versus Met-Hb: $\text{NO}_2^-$  reveals a pH dependence of the affinity of Met-Hb for

nitrite. The affinity of Met-Hb for nitrite is greatest at pH 6.8, though the change in affinity with pH is less dramatic than the sharp nature of the  $\lambda=6$  aquo-Met-Hb would lead one to believe. Additionally, having obtained the relative concentrations of the various components in experimental spectra (Figure 2-5), we determined the pKa ( $K_a = K_{AB}$  in Figure 2-11) of the water ligand to be 8.15 at pH 8.3, which is in good agreement with the values determined previously [72,73]. Using  $K_{AB}$  and  $K_{BC}$  and equation (2-5), the  $K_d$  of  $\text{MetHb:NO}_2^-$  ( $1/K_{AC}$ ) was calculated to be 2.0 mM, 3.1 mM and 6.0 mM at pH 8.3, 9.0 and 10.0, respectively. As seen in the equations (2-2) and (2-3), the absence of  $\text{MetHb:OH}^-$  when  $\text{pH} < 8.3$  prohibited the determination of the  $K_d$  of  $\text{MetHb:NO}_2^-$  by this method at pHs below 8.3.

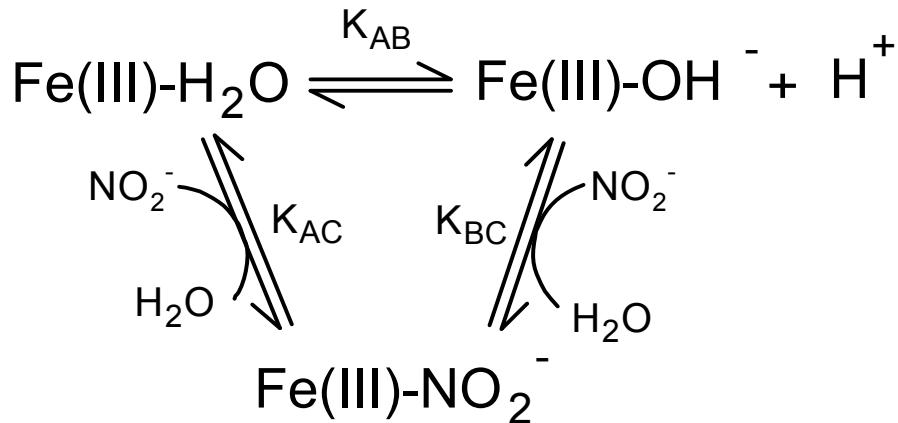


Figure 2-11: Scheme depicting the reactions of  $\text{MetHb:NO}_2^-$ ,  $\text{MetHb:H}_2\text{O}$  and  $\text{MetHb:OH}^-$ ; and the corresponding equilibrium constants.

$$K_{AB} = [\text{Met-Hb:OH}^-][\text{H}^+] / [\text{Met-Hb:H}_2\text{O}] \quad (2-2)$$

$$K_{BC} = [\text{Met-Hb:NO}_2^-] / [\text{Met-Hb:OH}^-][\text{NO}_2^-][\text{H}^+] \quad (2-3)$$

$$K_{AC} = [\text{Met-Hb:NO}_2^-] / [\text{Met-Hb:H}_2\text{O}][\text{NO}_2^-] \quad (2-4)$$

$$K_{AB}K_{BC} = K_{AC} \quad (2-5)$$

Discussion

In their pioneering EPR studies of hemichromes, Peisach and Blumberg [33] used g-values to categorize low-spin Fe(III) heme proteins and model complexes according to the relative sizes of the tetragonal and rhombic ligand field components that they imply. Complexes with different types of axial ligands lie in distinct neighborhoods when mapped with their ligand field parameters as coordinates. Both sets of g-values reported here for Met-Hb:NO<sub>2</sub><sup>-</sup> fall into the region associated with B-type hemichromes (since termed Type II hemichromes [38]). This type of hemichrome typically has an Fe(III)-N bond, such as the imidazole nitrogen of the eponymous cytochrome B. Characterization as a B-type hemichrome naturally suggests that nitrite coordination to Met-Hb assumes N-nitro, rather than O-nitrito, binding mode, or binds through an atom with electronegativity similar to an imidazole nitrogen. The recent crystallographic studies of Richter-Addo and co-workers [60], however, reveal O- rather than N-nitro coordination, and, moreover, revealed the presence of distinct nitrito conformers in the  $\alpha$ - vs.  $\beta$ -subunits of Met-Hb:NO<sub>2</sub><sup>-</sup>. The crystallographic and EPR results seem difficult to reconcile. Such discrepancies between solution and crystallographic studies, however, are not without precedent in Hb. In particular, EPR studies of Hb(NO)<sub>4</sub> show marked differences in g-values obtained in single crystal versus frozen solution EPR samples [74,75]. DFT calculations presented by Basu and co-worker found N-nitro coordination to be about 7 kcal/mol more stable than O-nitrito coordination; calculations of g-values for the different species may be very illuminating [46].

Combining the information gained from the variable pH and the hybrid data, assignment of the two Met-Hb:NO<sub>2</sub><sup>-</sup> species can be proposed. At pH 5, the ratio of species A:B is 7:1 and the two Met-Hb:NO<sub>2</sub><sup>-</sup> species account for >98% of the Met-Hb species detected, ruling out assigning the assignment of one species to the  $\alpha$ -subunit and the other species to the  $\beta$ -subunit. The spectrum of the SNO-Met-Hb:NO<sub>2</sub><sup>-</sup> hybrid does link the species B spectrum to the  $\beta$ -subunit. Yet, the spectrum of the  $\alpha$ -Fe(II)NO/ $\beta$ -Fe(III)-hybrid Hb demonstrates that the  $\beta$ -subunit can assume the conformation of both species A and B, while the  $\alpha$ -Fe(III)/ $\beta$ -Fe(II)NO-hybrid Hb seems to indicate that the  $\alpha$ -subunit is only found in the species A form.

The pH dependence of the ratio of the two species suggests a possible origin of the two species. The distal pocket, the site of ligand binding, is larger in the  $\alpha$ -subunit than in the  $\beta$ -subunit [69]. Moreover, the distal histidine of the  $\beta$ -subunit ( $\beta$ His63) has been shown to swing out of the distal pocket [76], creating more space in the distal pocket and alleviating steric interference with ligands, as originally suggested by Perutz [77,78]. This distal histidine rotation is pH dependent [76] and has been reported in a variety of heme proteins [79-83]. These conformational changes of the distal histidine and pocket occur only in the  $\beta$ -subunit not the  $\alpha$ -subunit [76,84], consistent with our results that indicate the  $\alpha$ -subunit exists only as Met-Hb:NO<sub>2</sub><sup>-</sup> species A and the  $\beta$ -subunit can interconvert between species A and B.

In Figure 2-4 and 2-5, the relative percentage of species A increases as pH decreases. Concomitant with this increase is the decrease in the relative percentage of species B, while all other species remain constant, demonstrating the conversion of species B to species A as pH decreases. The pH dependent conversion between Met-

Hb:NO<sub>2</sub><sup>-</sup> species is consistent with the pH dependent rotation of the distal histidine of the β-subunit. The movement of the distal histidine opens the distal pocket, allowing nitrite to assume the same conformation as in the larger α-heme distal pocket, species A.

Movement of the distal histidine would also affect the affinity of Met-Hb for nitrite. At higher pH, the position of the distal histidine of the β-heme sterically hinders ligand binding [76,78]. Additionally, at high pH, nitrite must compete with hydroxide for Met-Hb, the more compact hydroxide having easier access to the heme pocket. As the pH is lowered and the distal histidine swings out of the heme pocket, ligand binding is enhanced by the additional space created, allowing the β-subunits to assume the most energetically favorable conformation. The modest decrease in affinity below pH 6.8 could possibly result from continued rotation of distal histidine, especially if species A is stabilized by a hydrogen bond from the imidazole nitrogen. Additionally, the pKa of nitrite (3.16 at 298K [85]), in conjunction with the reduction of pH that occurs upon freezing PBS buffer [62,63], could result in a substantial portion of nitrite being protonated in the pH 5.0 and 6.2 Met-Hb:NO<sub>2</sub><sup>-</sup> samples, causing an apparent reduction in Met-Hb affinity for nitrite.

Hemoglobin is known to be a robust protein, resisting denaturation over a wide pH range. Hollecher and Buckley demonstrated the efficacy of EPR spectroscopy in measurements of Met-Hb over the range from pH 3 to pH 12 [86]. Others have shown acid induced denaturation to occur below pH 4 [87] and alkaline denaturation to occur above pH 11 [88]. Using a pH range similar to ours, Svistunenko et al. conducted an EPR investigation of the pH dependence of Met-Hb hemichrome species, noting that all species detected were also present in whole blood [67]. Moreover, the modest changes

we observe in the Met-Hb:NO<sub>2</sub><sup>-</sup> EPR spectrum (Figure 2-4) over the pH range employed demonstrate the absence of any protein unfolding that would abrogate the conclusions drawn.

Moreover, we reiterate the weak binding of nitrite to Met-Hb, with the K<sub>d</sub> of Met-Hb:NO<sub>2</sub><sup>-</sup> in the mM range in both HEPES and PBS buffers. The dissociation constants of Met-Hb:NO<sub>2</sub><sup>-</sup> presented here are calculated from direct EPR measurements of the various Hb species: aquo-Met-Hb, hydroxy-Met-Hb, and Met-Hb:NO<sub>2</sub><sup>-</sup>, in contrast to the work of Basu et al., in which only aquo-Met-Hb was measured. Our approach allows a check for mass balance and clear demonstration that the Met-Hb:NO<sub>2</sub><sup>-</sup> species detected by EPR account for all heme products formed during the reaction. With this check on the sufficiency of the analysis, we obtain dissociation constants that are more reliable than those obtained indirectly [46], and which are in good agreement to previously reported optical data [41,42].

We also note, that the UV-Vis data of Basu et al. [46], that were obtained to monitor the progress of the reaction of deoxyHb with nitrite, provide an alternative means to estimate the nitrite dissociation constant. In experiments with excess nitrite (for example, Figure 1e of Basu et al. [46]) the reaction reaches an endpoint in which the Met-Hb formed is in equilibrium with the excess nitrite. From the observed concentrations of Met-Hb, Met-Hb:NO<sub>2</sub><sup>-</sup>, and the reported nitrite exposure, dissociation constants can be inferred that are two orders of magnitude larger than those determined by their EPR measurements.

The discrepancy provokes one additional comment. In their experimental design, the Met-Hb:NO<sub>2</sub><sup>-</sup> complex was often formed, as noted above, as a *reaction product*. As

such, a Met-Hb:NO<sub>2</sub><sup>-</sup> basis spectrum must certainly be included in the least squares decomposition of composite UV-Vis spectra, and will obviously improve the least squares fit. This situation, however, does not justify a claim that Met-Hb:NO<sub>2</sub><sup>-</sup> is a reaction intermediate. Indeed, their reported data make a better case for the intermediacy of Fe(III)NO, as it is observed to improve the least-squares fit only during the reaction, not at its endpoint (Basu et al. [46] Figure 1f).

It is also worth noting some pitfalls that can occur in quantitative analyses of EPR spectra in multi-component systems. First, care must obviously be taken to ensure that the microwave power applied is appropriate to avoid saturation of all spin components to avoid errors in the interpretation of relative intensities. Second, it is of clear importance, when measuring species with broad spectra, that data be collected over the full magnetic field range; broad high-field features are regularly encountered in low-spin Fe(III)-heme species. If the full spectrum is not measured, substantial errors in quantitation are possible [58]. Finally, since transition moments differ for spin systems with different spin multiplicities – even for transitions between nominal  $m_s \pm 1/2$  spins states, detailed simulation are required to quantify interconversion among such species – relative integrated intensities can be misleading. Thus, although we observed that the addition of NO<sub>2</sub><sup>-</sup> to Met-Hb resulted in an overall loss of (integrated) EPR signal, detailed simulation of experimental spectra for both high-spin and low-spin species demonstrated that the number of spins was conserved after nitrite addition [54]. Apart from spectral simulation this conservation would not be readily apparent, and might be mistaken for the formation of an EPR “silent” species.

### Conclusion

The EPR measurements of Met-Hb:NO<sub>2</sub><sup>-</sup> presented here indicate that addition of NaNO<sub>2</sub> to Met-Hb results in the formation of two distinct heme-Fe(III):NO<sub>2</sub><sup>-</sup> species. EPR measurements at multiple frequencies and measurements in D<sub>2</sub>O rule out assignment of this splitting as hyperfine structure. Systematic changes in the EPR spectra with pH enable the assignment of each component of the doublet features to the spectra of two species. Thus, we conclude that the EPR spectrum of Met-Hb:NO<sub>2</sub><sup>-</sup> is a composite of two species with g-values of 3.018, 2.122, 1.45 and 2.870, 2.304, 1.45 at pH 7.4 in PBS and 3.006, 2.129, 1.45 and 2.887, 2.299, 1.45 at pH 7.4 in HEPES buffer. On the basis of EPR studies of Fe(III)NO<sub>2</sub><sup>-</sup>/Fe(II)NO hybrids, we propose that one of the species is present in both the  $\alpha$ - and  $\beta$ -subunit, while the other is exclusive to  $\beta$ -subunit. The two species most likely originate from differences in the distal heme pockets and histidine residues of the  $\alpha$ - and  $\beta$ -subunits, with the pH dependent rotation of the  $\beta$ -subunit distal histidine allowing the  $\beta$ -subunit to interconvert between the two species. EPR experiments on hybrids also led to the discovery of an effect of S-nitrosylation on the  $\beta$ -subunit Fe(III)NO<sub>2</sub><sup>-</sup> EPR spectrum.

## CHAPTER 3

## ELECTRONIC STRUCTURE OF METHEMOGLOBIN:NITRITE

Introduction

Low-spin Fe(III) is found in a plethora of both purely inorganic complexes and protein prosthetic groups. In biology, low-spin Fe(III) is typically found in the center of the porphyrin ring of heme proteins, such as cytochromes, myoglobins, and hemoglobins [38].

The non-integer spin of low-spin heme Fe(III) complexes allows for their characterization by electron paramagnetic resonance (EPR) spectroscopy. The theory relating  $g$ -values of  $d^5$  complexes to the relative energies of the  $t_{2g}$  orbitals and their contributions to the ground state wavefunction was first presented by Bleaney and O'Brien [89]. It was soon thereafter applied to hemoglobin by Griffith [35,90] and later simplified by Taylor [91]. Peisach and Blumberg [33,37] developed a method to compare low-spin ferric compounds using the theory as presented by Griffith [35].

In the previous chapter, the EPR spectrum of methemoglobin:nitrite (Met-Hb:NO<sub>2</sub><sup>-</sup>) was reported. The spectrum was found to be the composite of the spectra of two distinct species, A and B. Presented here is an evaluation of the electronic structure of the two Met-Hb:NO<sub>2</sub><sup>-</sup> species as probed by EPR spectroscopy.

## Materials and Methods

The data used in this study was obtained from the previous chapter (using the methods described there) or from other sources as noted [36,38,91].

### Low-Spin $d^5$ Hole Theory

Methemoglobin is the oxidized form of hemoglobin, with iron being in the Fe(III) oxidation state. These iron centers coordinate six ligands: four nitrogens of the porphyrin ring and two axial ligands— one above and one below the porphyrin plane. This ligand field results in the lifting of the degeneracy of the five 3d orbitals of iron, which elevates the  $e_g$  orbitals ( $d_{z^2}$ ,  $d_{x^2-y^2}$ ) and reduces the  $t_{2g}$  orbitals ( $d_{xz}$ ,  $d_{yz}$ ,  $d_{xy}$ ) in energy. The distal ligand of iron is variable and affects the magnitude of the splitting between the  $e_g$  and  $t_{2g}$  manifolds. When the ligand field is large, all five 3d electrons of Fe(III) occupy the  $t_{2g}$  orbitals— the energy of pairing electrons being less than that of occupying the  $e_g$  orbitals. The pairing of electrons in the  $t_{2g}$  orbitals yields a low-spin complex ( $s=1/2$ ), in contrast to  $s=5/2$  in high spin Fe(III) complexes when the ligand field splitting is small.

In Met-Hb, the  $t_{2g}$  orbitals of iron are not degenerate, as would be the case in an octahedral ligand field. The orientation of the imidazole ring of the proximal histidine creates an inequality between the x- and y-axes [92], assuming z-axis to be normal to the heme plane. This orientation precludes axial symmetry, resulting in rhombic symmetry and lifting the degeneracy of the three  $t_{2g}$  orbitals, as shown in Figure 3-1. In low-spin Met-Hb species, these three  $t_{2g}$  orbitals are probed by EPR spectroscopy.

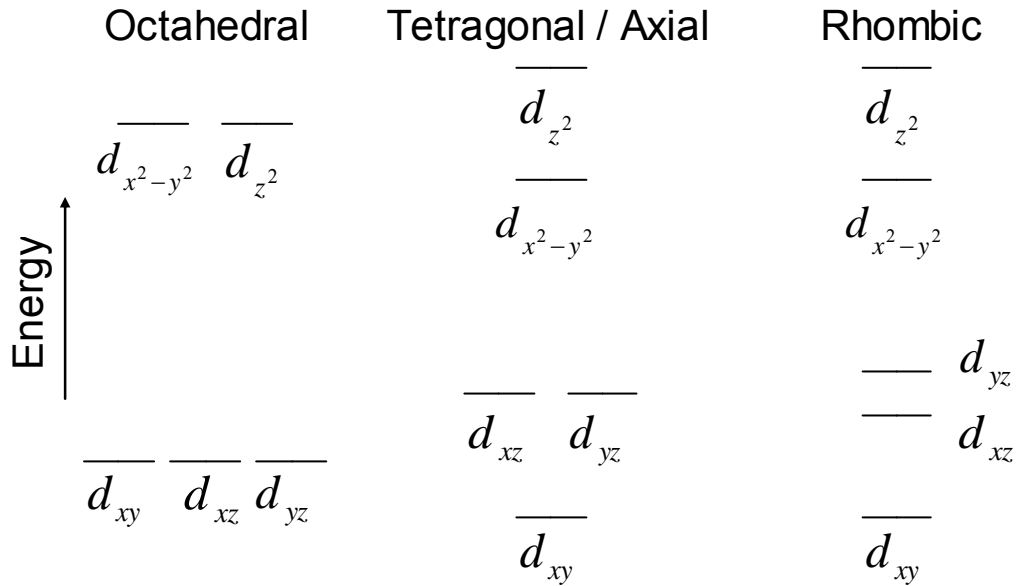


Figure 3-1: Splitting of the 3d orbitals as a function of ligand environment. The relative energy of the orbitals is consistent with contraction along the y- and z-axes. Energy is in arbitrary units.

The Hamiltonian has many contributions, from spin-orbit interactions to hyperfine structure, but we will only concern ourselves with the Zeeman energy, all other terms being insignificant in this application. Therefore, the Hamiltonian being employed is

$$\hat{H} = \beta \mathbf{B} \cdot (\mathbf{L} + g_e \mathbf{S}), \quad (3-1)$$

which equals

$$\hat{H} = \beta (g_x B_x S_x + g_y B_y S_y + g_z B_z S_z), \quad (3-2)$$

where  $\beta$  is the Bohr magneton;  $B$ , the magnetic field;  $L$ , the orbital angular momentum;  $S$ , the spin angular momentum;  $g_e$ , the free electron g-factor; and  $g_x$ ,  $g_y$ , and  $g_z$ , the x, y, and z components of the diagonalized g-tensor, respectively.

The large ligand field splitting between the  $e_g$  and  $t_{2g}$  orbitals of iron, results in the five 3d electrons occupy solely the  $t_{2g}$  orbitals,  $d(t_{2g})^5$ , leaving one hole. Calculating the

parameters of the single hole, using the  $t_{2g}$  hole model of Bleaney and O'Brien [89], allows for a simplified analysis. The hole model is equivalent to that of the single electron case, but with the reverse sign of the spin-orbit coupling constant. This inverts the energy splitting between the orbitals, as shown in Figure 3-2.

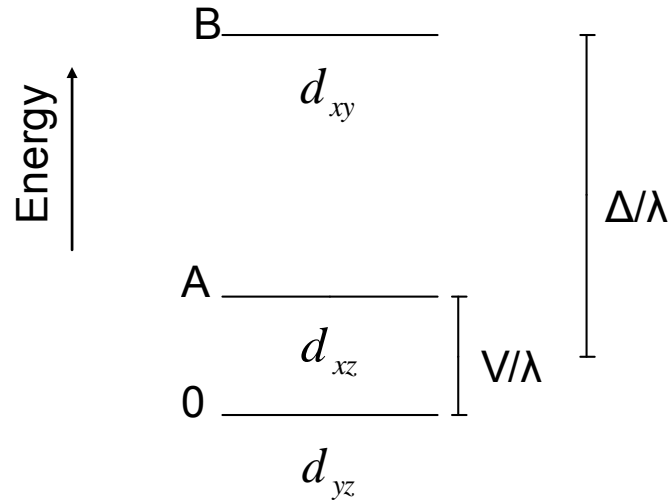


Figure 3-2: Splitting of the  $t_{2g}$  orbitals as viewed according to the hole model.  $V/\lambda$  is the rhombic distortion,  $\Delta/\lambda$  is the tetragonal distortion, where  $\lambda$  is the spin-orbit coupling constant. Energy is in arbitrary units.

The states of the system are also influenced by spin-orbit coupling, in addition to the ligand field effects. As a result of spin-orbit coupling, the states of the system are no longer pure  $t_{2g}$  orbitals, but are mixtures of orbitals and spin types. Because of the possible combinations of orbital and spin angular momentum, each of the three states also has an energetically degenerate counterpart. These degenerate states are known as Kramer's doublets. The wavefunctions of the ground state Kramer's doublet as given by Taylor [91] are:

$$|+\rangle = a|d_{yz}\alpha\rangle - ib|d_{xz}\alpha\rangle - c|d_{xy}\beta\rangle \quad (3-3a)$$

and

$$|-\rangle = -a|d_{yz}\beta\rangle - ib|d_{xz}\beta\rangle - c|d_{xy}\alpha\rangle. \quad (3-3b)$$

The wavefunction coefficients are  $a$ ,  $b$ , and  $c$  and must be real numbers.  $\alpha$  and  $\beta$  represent the electron spin  $s=1/2$  and  $-1/2$ , respectively.

The coefficients  $a$ ,  $b$  and  $c$  can be determined from the three  $g$ -values using the following equations:

$$g_z = 2[(a + b)^2 - c^2], \quad (3-4a)$$

$$g_y = 2[(a + c)^2 - b^2], \quad (3-4b)$$

$$g_x = 2[a^2 - (b + c)^2]. \quad (3-4c)$$

The coefficients reveal the contribution of each  $t_{2g}$  orbital to the ground state wavefunction. Additionally, the coefficients can also be used to calculate the relative energies of the three states.

$$-\lambda \cdot \begin{bmatrix} 0 & i/2 & -1/2 \\ -i/2 & -A & i/2 \\ -1/2 & -i/2 & -B \end{bmatrix} \cdot \begin{bmatrix} a \\ -ib \\ -c \end{bmatrix} = E \cdot \begin{bmatrix} a \\ -ib \\ -c \end{bmatrix} \quad (3-5)$$

From equation 3-5 the following solutions are derived:

$$\frac{E}{\lambda} = -\frac{b+c}{2a} = \frac{g_x}{g_z + g_y} - \frac{1}{2}, \quad (3-6)$$

$$A = \frac{E}{\lambda} + \frac{a+c}{2b} = \frac{g_x}{g_z + g_y} + \frac{g_y}{g_z - g_x}, \quad (3-7)$$

$$B = \frac{E}{\lambda} + \frac{a+b}{2c} = \frac{g_x}{g_z + g_y} + \frac{g_z}{g_y - g_x}. \quad (3-8)$$

Also, as denoted in Figure 3-2,

$$A = \frac{V}{\lambda} \quad (3-9)$$

and

$$B - \frac{A}{2} = \frac{\Delta}{\lambda}, \quad (3-10)$$

with  $V/\lambda$  being the rhombic splitting and  $\Delta/\lambda$  being the tetragonal splitting.

At this point, all one needs to do is insert the measured g-values and solve the appropriate equations. However, this is not as straightforward as it first appears. While EPR spectroscopy determines the magnitude of the g-values, it does not determine their signs [38,93]. Additionally, when EPR data is collected from molecules randomly oriented in frozen solution, rather than from a single crystal, the magnetic axes of the system are initially unknown. However, Taylor proved that  $g_z+g_y-g_x$  must be positive [91]. Also, the determinate of the g-tensor matrix ( $g_z g_y g_x$ ) is positive for tetragonal complexes [38,91]. These two criteria eliminate the majority of the possible g-value assignments.

For the few g-value assignments that do yield positive solutions to  $g_z+g_y-g_x$  and  $g_z g_y g_x$ , consistency can be maintained by requiring the tetragonal distortion to be greater than the rhombic distortion and assigning the tetragonal distortion to the z-axis. This is achieved by using only results that have the quantity  $|V/\Delta| < 2/3$ . For Met-Hb:NO<sub>2</sub><sup>-</sup>, a proper axis system is achieved by assigning all g-values to be positive and  $g_z > g_y > g_x$ .

This assignment is in agreement with the g-values measured in single crystals in low-spin ferrimyoglobin complexes [94].

It should be noted that in their method, Peisach and Blumberg [33,37] use a different axis system, in which  $|V/\Delta|$  is allowed to exceed 2/3. In their axis system, the largest g-value is assigned as  $g_y$  and is considered positive. The remaining two g-values are negative, assigning  $|g_x| > |g_z|$ . Accordingly, one must employ their axis system in order to compare hemichromes using the “truth table” of Peisach and Blumberg.

### Results and Discussion

Assigning the g-values of Met-Hb:NO<sub>2</sub><sup>-</sup> in HEPES buffer (Table 3-1) as outlined by Taylor [91], all positive with  $g_z > g_y > g_x$ , the coefficients of the ground state wavefunction and the rhombic and tetragonal splittings were calculated for the two species detected in the Met-Hb:NO<sub>2</sub><sup>-</sup> EPR spectrum (Figure 3-3). For both species, the primary contributor to the wavefunction was the  $d_{yz}$  orbital, followed by the  $d_{xz}$  and then  $d_{xy}$  orbital. For species A, the tetragonal splitting ( $\Delta/\lambda$ ) was 3.884 and the rhombic splitting ( $V/\lambda$ ) was 1.651, resulting  $V/\Delta$  being 0.425. The energy differences for species B were 3.072, 1.834 and 0.597, for  $\Delta/\lambda$ ,  $V/\lambda$ , and  $V/\Delta$ , respectively.

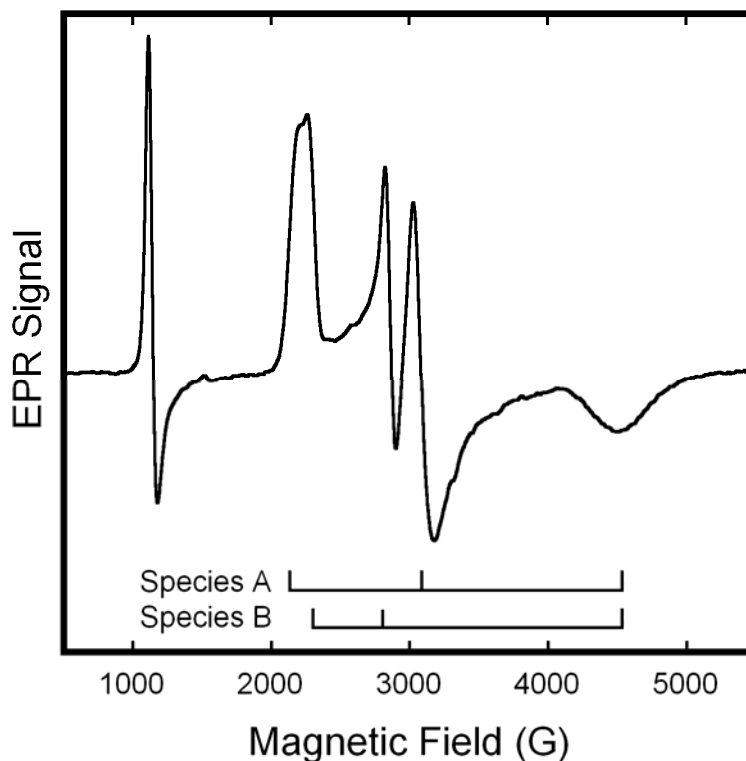


Figure 3-3: X-band EPR spectrum of Met-Hb:NO<sub>2</sub><sup>-</sup> in aqueous HEPES buffer at 20 K. Met-Hb was 0.5 M with twenty-fold molar excess (per heme) of NaNO<sub>2</sub>; the buffer concentration was 0.1 M and the pH was 7.4. The spectrum was obtained with the following spectrometer parameter values: 0.5 s time constant, 5 G modulation amplitude, 16.67 G/s sweep rate, 5 mW microwave power, and 9.24 GHz microwave frequency.

The tetragonal and rhombic splittings calculated are given in relation to the spin-orbit coupling constant. Since the hole model employs the negative value of the spin-orbit coupling constant, while the single electron model uses the positive value, the energy level diagram for the single electron is obtained by simply inverting the energy level scheme determined by the hole model. For Met-Hb:NO<sub>2</sub><sup>-</sup>, these results indicate that the majority of unpaired electron density is located in the d<sub>yz</sub> orbital. Moreover, the lowest lying iron 3d orbital is the d<sub>xy</sub> orbital, consistent with calculations by others on low-spin heme systems [38,90,91], with the d<sub>xz</sub> orbital lying between the d<sub>yz</sub> and d<sub>xy</sub> orbitals. The spin-orbit coupling constant is 460 cm<sup>-1</sup> for the free ferric ion [38] and is

reduced by covalent bonding in many ferric complexes ( $\sim 280 \text{ cm}^{-1}$  in  $\text{K}_3\text{Fe}(\text{CN})_6$  [89]). Using a spin orbital coupling constant of  $400 \text{ cm}^{-1}$  (as done by others [38]), we find the tetragonal splitting to be  $1554 \text{ cm}^{-1}$  and the rhombic splitting to be  $660 \text{ cm}^{-1}$  in Met-Hb: $\text{NO}_2^-$  Species A. In Species B,  $\Delta$  is  $1229 \text{ cm}^{-1}$  and  $V$  is  $734 \text{ cm}^{-1}$ .

Analyzing the orbital mixing coefficients of the ground state wavefunctions of the two Met-Hb: $\text{NO}_2^-$  species, we see almost identical contributions from the  $d_{yz}$  orbitals,  $a$ , and that  $b > c$  in both species. In the wavefunction of species B, the contribution of the  $d_{xz}$  orbital is less than, and the  $d_{xy}$  orbital is greater than, those in the wavefunction of species A. This is a reflection of the differences in tetragonality and rhombicity of the two species. The reduction in tetragonality of species B compared to species A results in an increased contribution of the  $d_{xy}$  orbital, whereas the increased rhombicity of species B over species A results in the reduction of the  $d_{xz}$  orbital contribution to the wavefunction of species B compared to species A. These differences are most likely the result of dissimilarities in ligand orientation and/or bond length of species A and B.

In the previous chapter, we proposed that the  $\alpha$ -subunit of hemoglobin assumes only the species A conformation and the  $\beta$ -subunit converts between species A and B in a pH dependent fashion. Though the crystal structure of Met-Hb: $\text{NO}_2^-$  of Yi et al. [60] indicates O-nitrito binding of nitrite to Fe(III), in conflict with our EPR data, the structure does provide some insight into the electronic structure determined here. As shown in Figure 3-4, in the structure of the  $\alpha$ -subunit, the Fe-O-N plane of nitrite-iron bond projects between two iron-porphyrin bonds. In the  $\beta$ -subunit, the Fe-O-N plane is directly aligned with one iron-porphyrin bond and the imidazole plane of the proximal histidine below the heme. Comparing the two structures, one would expect the  $\beta$ -subunit

to have a larger splitting between the  $d_{yz}$  and  $d_{xz}$  orbitals ( $V/\lambda$ ) than that of the  $\alpha$ -subunit. Indeed, our calculations show that  $V/\lambda$  for species A is smaller than  $V/\lambda$  for species B. This is consistent with our finding that the  $\alpha$ -subunit is associated with species A while the  $\beta$ -subunit can assume the species B conformation. However, in contrast to our findings, Yi et al. [60] did not report a second conformation for  $\beta$ -subunit similar to the  $\alpha$ -subunit conformation.

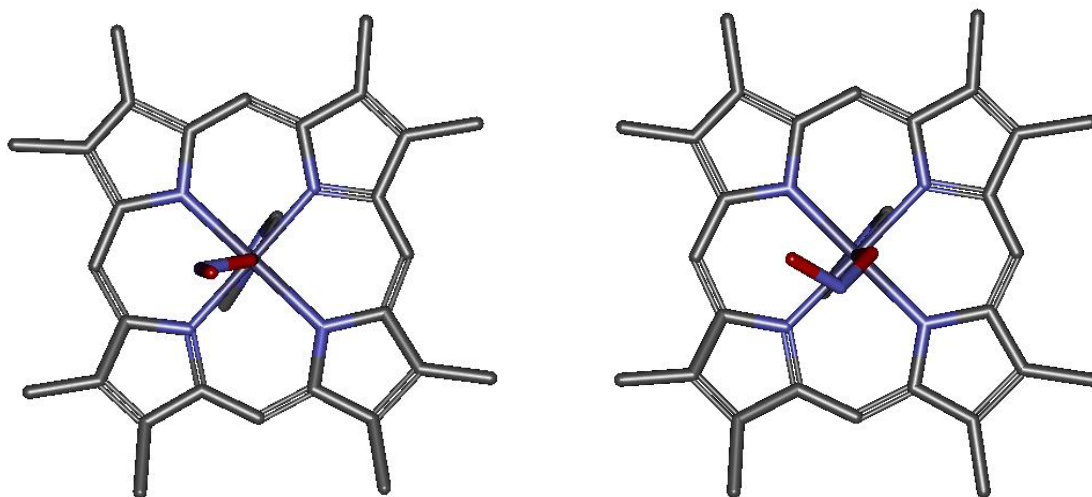


Figure 3-4: The abbreviated structures of  $\alpha$ -Met-Hb:NO<sub>2</sub><sup>-</sup> (left) and  $\beta$ -Met-Hb:NO<sub>2</sub><sup>-</sup> (right) as viewed along the z-axis. Crystal structure coordinates were obtained from PDB entry 3D7O [60]. Nitrite in these structures coordinates to iron via an O-nitrito binding mode, in contrast to our EPR data as presented in Chapter 2.

For comparison, the tetragonal and rhombic parameters for several other Met-Hb hemichromes were calculated, as seen in Table 3-1. The primary contribution to the ground state wavefunctions of the hemichromes investigated was from the  $d_{yz}$  orbital. Additionally, in each of these hemichromes, the relative energies of the  $t_{2g}$  orbitals follow the same sequence as those of the two Met-Hb:NO<sub>2</sub><sup>-</sup> species, with the energy of  $d_{yz} > d_{xz} > d_{xy}$ .

Table 3-1: The ground state wave function coefficients and the tetragonal and rhombic distortions for various Met-Hb adducts. The ligands (nitrite (Species A and B) [Chapter 2], azide [36], imidazole nitrogen of the distal histidine [33,37], and hydroxide [Chapter 2]) are bound to the distal face of the heme iron and their respective g-values were obtained from the references noted.

<b>Ligand</b>	<b><math>g_z</math></b>	<b><math>g_y</math></b>	<b><math>g_x</math></b>	<b><math>\Delta/\lambda</math></b>	<b><math>V/\lambda</math></b>	<b><math>V/\Delta</math></b>	<b><math>a</math></b>	<b><math>b</math></b>	<b><math>c</math></b>	<b><math>a^2+b^2+c^2</math></b>
NO <sub>2</sub> <sup>-</sup> A	3.006	2.129	1.45	3.884	1.651	0.425	0.946	0.287	0.125	0.992
NO <sub>2</sub> <sup>-</sup> B	2.887	2.229	1.45	3.072	1.834	0.597	0.945	0.265	0.144	0.984
N <sub>3</sub> <sup>-</sup>	2.82	2.20	1.71	4.934	2.323	0.471	0.976	0.216	0.095	1.007
N <sub>His</sub>	2.70	2.21	1.69	4.270	2.532	0.593	0.967	0.199	0.102	0.986
OH <sup>-</sup>	2.56	2.18	1.88	7.129	3.602	0.505	0.991	0.142	0.063	1.006

In Figure 3-5, the three mixing coefficients of the ground state wavefunction are plotted as a function of g-anisotropy, as given by  $g_z - g_x$ . The plot links the anisotropy in EPR spectrum of the hemichromes to the amount of  $t_{2g}$  orbital mixing in the ground state wavefunctions. As mixing of the  $t_{2g}$  orbitals increases, the g-anisotropy increases. Conversely, reduction in mixing of orbitals in the ground state wavefunction results in a more isotropic EPR spectrum. In the limit where the unpaired electron resides in a pure orbital, the EPR signal will be isotropic, like a free electron. The amount of mixing of  $t_{2g}$  orbitals in the ground state wavefunction is dependent on the energy difference of the orbitals. When there is a large difference in energy between the  $t_{2g}$  orbitals, as is the case in Met-Hb:OH<sup>-</sup>, the wavefunction has very little mixing, giving a more isotropic EPR spectrum. For example, the energy differences between the  $t_{2g}$  orbitals of Me-Hb:NO<sub>2</sub><sup>-</sup> species A are less than those of the  $t_{2g}$  orbitals of Met-Hb:OH<sup>-</sup>, resulting in more orbital mixing in the Met-Hb:NO<sub>2</sub><sup>-</sup> wavefunction and increased g-anisotropy.

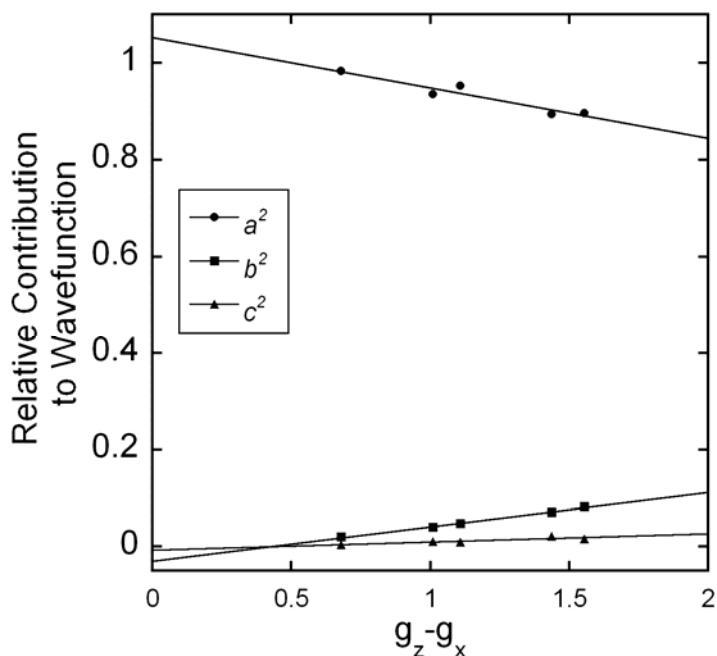


Figure 3-5: Plot of the squares of the orbital mixing coefficients of the ground state wavefunction as a function of  $g$ -anisotropy ( $g_z - g_x$ ).

Figure 3-5 also shows that there are other contributions to the ground state wavefunction not accounted for by this model. This results from the assumption of Taylor's model that there is no covalency in the ligand-iron bonding. Deviation of the sum of the squares of the orbital mixing coefficients,  $a^2 + b^2 + c^2$  in Table 3-1, from unity demonstrates there to be slight covalency in the bonding. In the extrapolation of the data in Figure 3-5 to  $g_z - g_x = 0$ , the isotropic limit, the deviation from the expected value (unity for  $a$ , and zero for  $b$  and  $c$ ) is greater for  $a$  and  $b$  than that of  $c$ . This indicates that the covalency is greater in the  $d_{yz}$  and  $d_{xz}$  orbitals than in the  $d_{xy}$  orbital. The increased covalency is consistent with the  $d_{yz}$  and  $d_{xz}$  orbitals' ability to  $\pi$ -bond with the porphyrin ring, and possibly the axial ligands. In  $\text{Met-Hb:N}_3^-$  and  $\text{Met-Hb:OH}^-$ ,  $a^2 + b^2 + c^2$  exceeds unity, which Griffith suggest could be the result of mixing of the ground state wavefunction with low-lying excited states [90].

### Conclusion

We have determined that the majority of unpaired electron density in Met-Hb:NO<sub>2</sub><sup>-</sup> species A and B to be localized in the iron d<sub>yz</sub> orbital. In species A and B, the relative positions of the t<sub>2g</sub> orbitals are the same, though the energy differences between them, tetragonality and rhombicity, are different. The disparity between the tetragonality and rhombicity of the two species results in slight differences in the composition of the ground state wavefunction. Of the Met-Hb hemichromes surveyed here, the Met-Hb:NO<sub>2</sub><sup>-</sup> species exhibited the greatest g-anisotropy, as well as the greatest mixing of the t<sub>2g</sub> orbitals in their ground state wavefunction. Finally, each of the ground state wavefunctions determined here were within 2% of normalization when considering only the t<sub>2g</sub> orbitals. It thus appears that the effects of covalency and excited state mixing on the ground state wavefunction are minor.

## CHAPTER 4

## X-BAND EPR INVESTIGATION OF METHEMOGLOBIN: TEMPERATURE AND BUFFER DEPENDENCE

Introduction

Iron in the heme centers of hemoglobin is typically found in one of two oxidation states, Fe(II) and Fe(III). Methemoglobin (Met-Hb), the oxidized form of hemoglobin, makes up less than 1% of the total hemoglobin in the bloodstream of healthy individuals [31]. In methemoglobin, the  $d^5$  electrons of iron exist in either a high- or low-spin state,  $s=5/2$  or  $s=1/2$ , respectively, depending on the ligation environment of iron. High-field ligands, such as  $\text{OH}^-$ ,  $\text{NO}_2^-$  or  $\text{CN}^-$ , bound to the distal face of the heme result in low-spin Fe(III), whereas the high-spin form has ligands such as  $\text{H}_2\text{O}$  or  $\text{F}^-$  bound. Both Met-Hb spin states are EPR active. The high-spin state has characteristic signals at  $g \approx 6$  and  $g \approx 2$ ; the low-spin states are typically characterized by a rhombic EPR spectrum having three distinct g-factors, two greater than, and one less than, 2.

Met-Hb can form from a multiplicity of reactions, including: the autoxidation of oxyhemoglobin ( $\text{Fe(II)O}_2$ ) [95]; the reaction of nitrosyl-hemoglobin ( $\text{Fe(II)NO}$ ) with  $\text{O}_2$  [30]; the reaction of oxyHb with NO [30]; and the reaction of deoxyhemoglobin with nitrite [44,47-49]. Recently, significant attention has been focused on possible roles of Met-Hb in hypoxic vasodilation. A study by Angelo et al. [52] found that incubation of deoxyHb with nitrite resulted in the formation of a Fe(III)NO-like species that, upon oxygenation, quantitatively formed S-nitrosyl-hemoglobin (SNO-Hb), a potent vasodilator [96]. The reaction of met-Hb-nitrite with NO has been shown to generate

$\text{N}_2\text{O}_3$ , a highly reactive molecule that could function in vasodilation through S-nitrosylation of thiols or homolysis to NO (and  $\text{NO}_2$ ) [46]. Additionally, nitrite addition to Met-Hb is known to result in the formation of both nitrosyl-Hb and SNO-Hb [30].

In addition to the reactions mentioned above, many studies have been conducted on the interaction of Met-Hb (and other heme proteins) with exogenous ligands [37,38,59,97,98]. The variable temperature characterization of neat Met-Hb by EPR, however, has not yet been carried out. Met-Hb in aqueous solution is in equilibrium between the high-spin state and two or more low spin states. Svistunenko et al. measured the pH dependence of the various Met-Hb species by EPR [67]. Because many hemoglobin derivatives [99-102], as well as those of other heme-proteins [70,103], have been shown to have temperature dependent EPR spectra, here we report the temperature dependence of the EPR spectra of Met-Hb in potassium phosphate and HEPES buffers.

## Materials and Methods

### Hemoglobin

Hb was purified from human red blood cells obtained from Innovative Research (Novi, Michigan), following the procedure of Geraci et al. [61] Hb was stored in aqueous solution at  $-80\text{ }^\circ\text{C}$  for later use. Prior to use, Hb was passed through Sephadex G-25 (GE Healthcare) chromatography gel, equilibrated with the appropriate buffer, either 100 mM HEPES or PBS. All buffered solutions also contained 0.1M KCl and 0.1 mM DTPA (diethylene triamine pentaacetic acid). Met-Hb was prepared by treatment of Hb with potassium ferricyanide followed by G-25 filtration to remove excess oxidant. All solutions were prepared to be 2 mM in heme.

### EPR Spectroscopy

X-band EPR data were collected on a Varian E-109 spectrometer modified with a National Instruments computer interface for data collection and field control. Sample cooling to cryogenic temperatures was provided by a Heli-Tran LTD-3-110 (Air Products and Chemicals Inc, Allentown, PA) liquid helium transfer system and dewar. Spectra were collected with the following spectrometer settings: microwave frequency of 9.24 GHz, 5 mW of microwave power, 0.5 s time constant, modulation amplitude of 5 G and a sweep rate of 16.67 G/s.

### EPR Spectra Simulations

Simulations of EPR spectra were conducted with the program EasySpin [66]. EasySpin enables the user to simulate experimental EPR spectra through the specification of a variety of parameters, accounting for such things as microwave frequency, field position, hyperfine interactions and line broadening. At each temperature, individual components of the multi-component Met-Hb spectrum were determined by adjusting parameters to satisfactorily reproduce the features in the spectrum. Simulated spectra were then used as basis spectra for least-squares decomposition of multi-component EPR spectra, using a fitting program similar to that described by us previously [30].

## Results

### Buffer Dependence at 10 K

The EPR spectrum of Met-Hb shows a high-spin signal ( $s=5/2$ ) and multiple low-spin signals ( $s=1/2$ ), as seen in Figure 4-1. The high-spin signal, with features at  $g \approx 6$  and

$g \approx 2$ , originates from aquo-Met-Hb, which coordinates  $\text{H}_2\text{O}$  as the sixth iron ligand [104]. There are three rhombic, low-spin signals which appear between 2000 and 4500G when measured at X-band. The first is hydroxy-Met-Hb, having  $\text{OH}^-$  coordinated as the distal ligand [86], with  $g$ -values of 2.58, 2.17 and 1.84, in HEPES at 10 K. The second low-spin species, a bis-histidine adduct of Met-Hb (bishis-Met-Hb) with iron coordinating an imidazole nitrogen of distal histidine [67], has  $g$ -values of 2.77, 2.25 and 1.67, in HEPES at 10 K. There is a third low-spin Met-Hb species, speculated to also be a bis-histidine complex with altered protein structure. Only the low field feature ( $g=3.08$ ) of this minority species is visible in the conditions employed here, the remaining two features being obscured by other low-spin signals or undetected because of substantial line broadening.

The same high- and low-spin Met-Hb signals are present when measured in PBS or HEPES buffers, however, the relative percentages of each species is buffer dependent. At 10 K in HEPES, the Met-Hb spectrum is composed of 56.6% aquo-Met-Hb, 18.8% hydroxy-Met-Hb, and 24.6% bishis-Met-Hb. At 10 K in PBS buffer, the relative percentages are 81.8%, 3.5% and 14.7% for aquo-, hydroxy- and bishis-Met-Hb, respectively. In this analysis, the minor bis-histidine species was neglected, only being detected at 10 K and 20 K and accounting for  $\sim 1\%$  of the total Met-Hb.

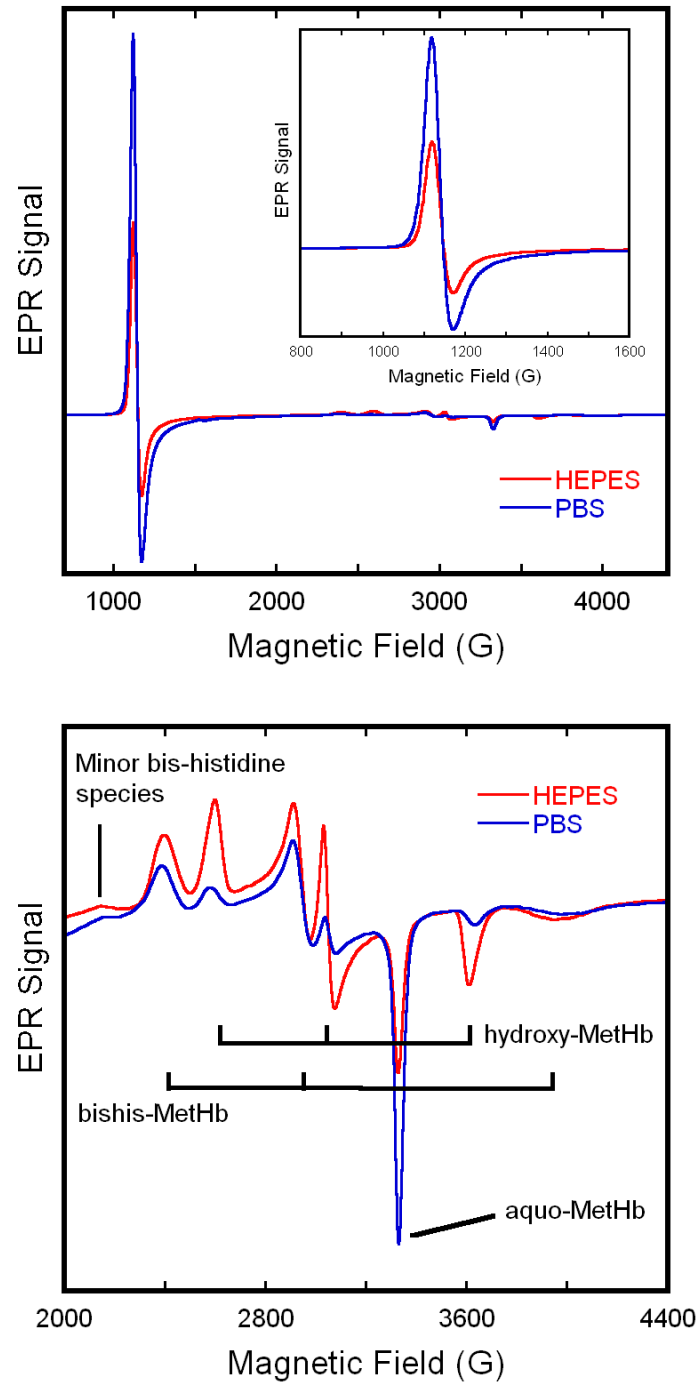


Figure 4-1: X-band EPR spectra of Met-Hb in aqueous HEPES and PBS buffer, shown in red and blue, respectively, at 10 K.

### Temperature Dependence

The EPR spectra of Met-Hb in PBS and HEPES buffer at various temperatures are shown in Figures 4-2 and 4-3, respectively. The total signal decreases with increasing temperature as the population difference between the ground and excited states decreases, as predicted by the Boltzmann distribution, resulting in a reduction in microwave absorption as temperature increases. As mentioned above, the spectra in both buffers consist of three major components: aquo-, hydroxy-, and bishis-Met-Hb. The spectral features of the two low-spin components, hydroxy- and bishis-Met-Hb, show very little change in field position and slight broadening in linewidth as the temperature increases. The high spin signal from aquo-Met-Hb maintains a constant field position but undergoes much more substantial broadening than the low-spin signals.

The relative percentages of each component as a function of temperature, are shown in Figure 4-4. In PBS and in HEPES, the percentage of aquo-Met-Hb decreases with the increase in temperature between 10 K to ~50 K. Above 50 K, the percentage of aquo-Met-Hb increases with increasing temperature. In PBS, the initial decrease in aquo-Met-Hb results in the increase in percentages of both hydroxy- and bishis-Met-Hb. Above 35 K, the percentage of bishis-Met-Hb decreases sharply with temperature, while hydroxy-Met-Hb remains almost constant, decreasing slightly. In PBS, at all temperatures measured, bishis-Met-Hb always maintains a greater relative percentage than hydroxy-Met-Hb.

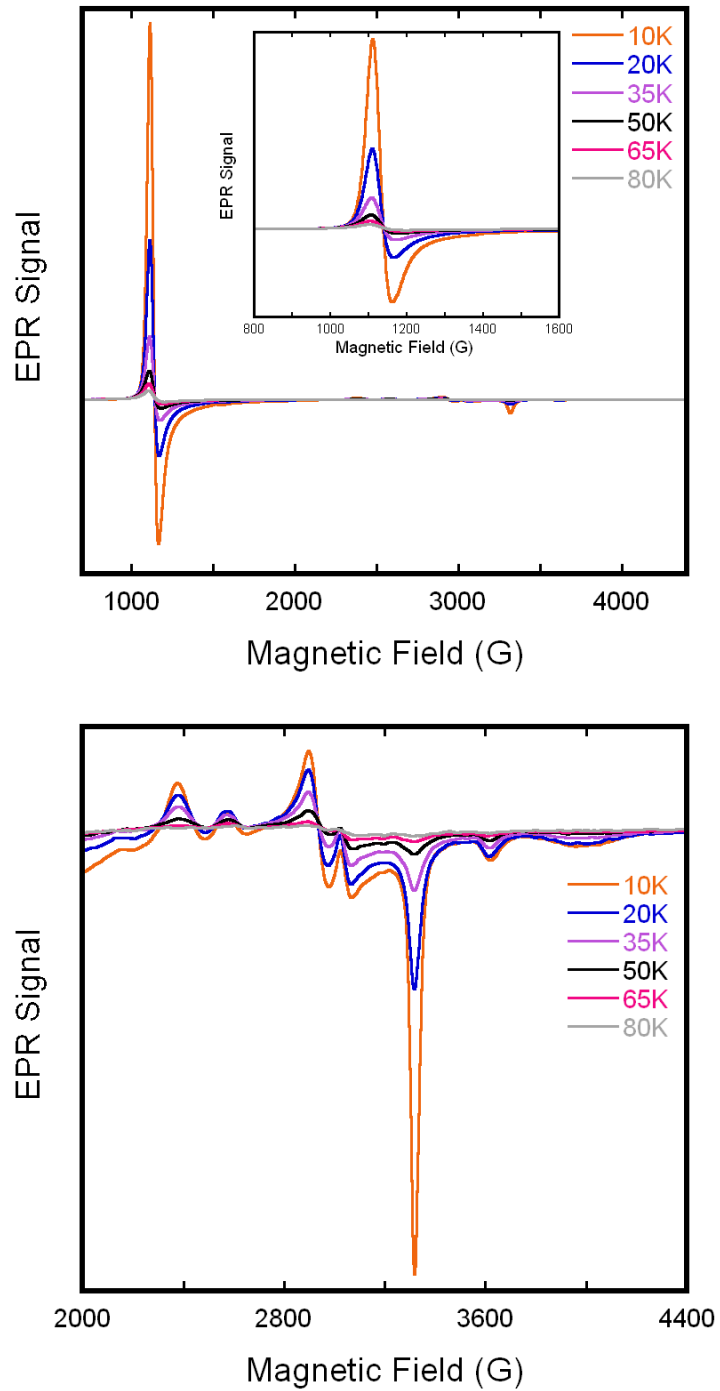


Figure 4-2: X-band EPR spectra of Met-Hb in aqueous PBS buffer at various temperatures, as labeled.

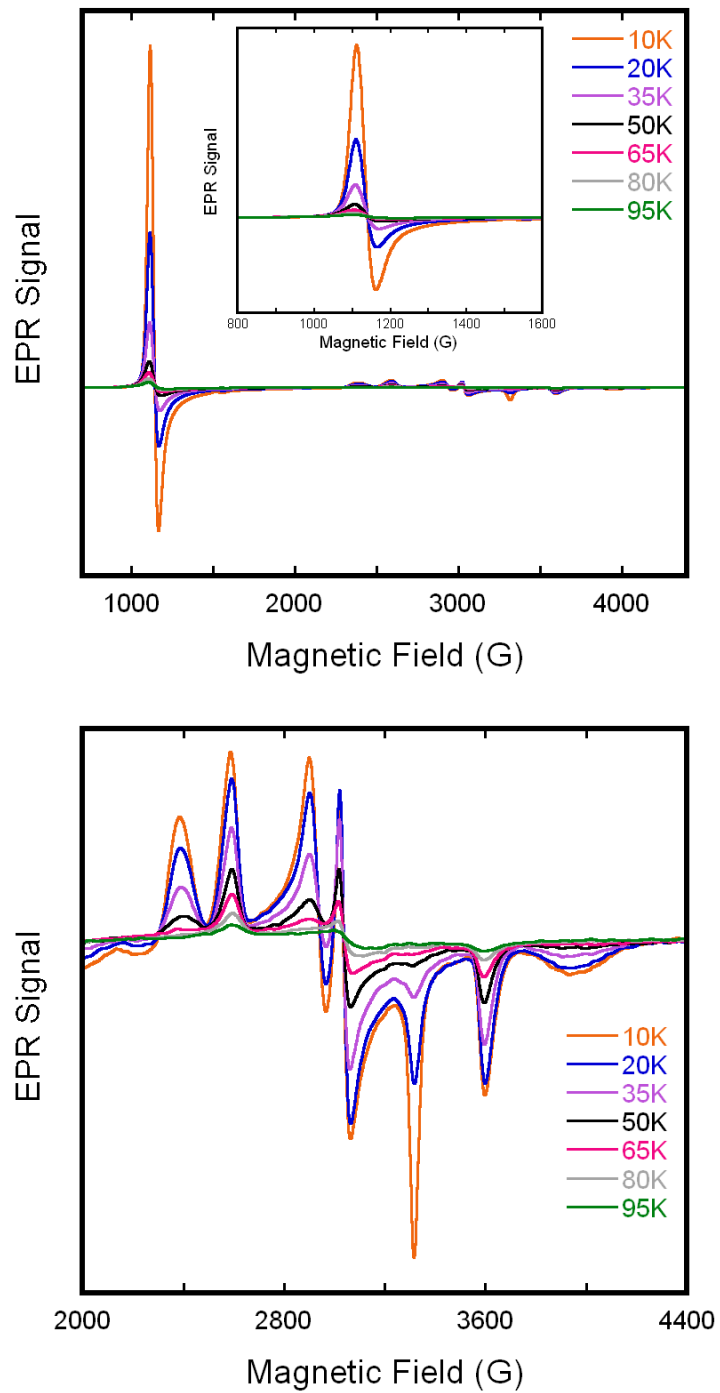


Figure 4-3: X-band EPR spectra of Met-Hb in aqueous HEPES buffer at various temperatures, as labeled.

In HEPES buffer, the percentage of bishis-Met-Hb increases between 10 K and 20 K and gradually declines as the temperature is increased above ~20 K. The percentage of hydroxy-Met-Hb increases steadily as the temperature increases from 10 K to 50 K. Above 50 K, the percentage of hydroxy-Met-Hb remains reasonably constant, similar to the result in PBS buffer, though at a higher relative percentage when measured in HEPES buffer. Unlike measurements in PBS buffer, in HEPES buffer, the amount of hydroxy-Met-Hb detected exceeds that of bishis-Met-Hb at 35 K and above.

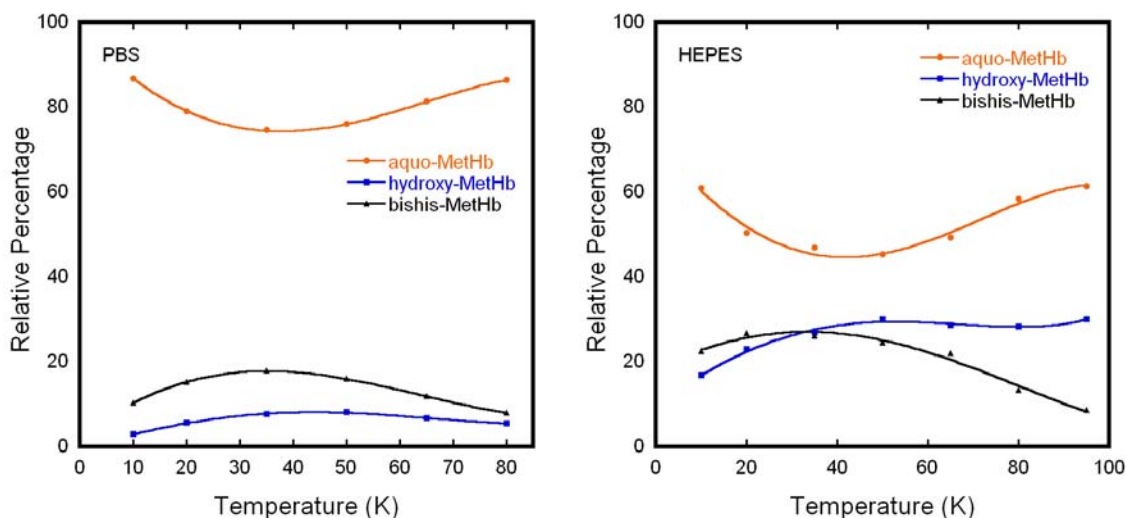


Figure 4-4: Relative percentages of Met-heme species as a function of temperature. Percentages were obtained by spectral simulation and least-squares analysis of experimental EPR spectra shown in Figures 4-2 and 4-3. Lines drawn are to aid the eye.

## Discussion

### Bis-histidine Hemichromes

Bis-histidine, low-spin Fe(III) complexes have been observed by EPR in proteins such as myoglobin [34], cytochrome  $b_5$  [97], and horse and fish hemoglobins [105], in addition to those formed in human hemoglobin, as seen in the EPR spectra shown in

Figures 4-2 and 4-3, and elsewhere [67,97]. We detected two low-spin Fe(III) complexes, a major and a minor species, both believed to be bis-histidine hemichromes [67,97,106], though no crystal structures have yet been reported. The detection of only one feature of the minor bis-histidine species is consistent with the observations of Levy et al. [107,108], who additionally noted that the formation of this species is dependent on the method of sample freezing. The two bis-histidine adducts bind the same histidine residue, therefore the electronic environment of the heme must be altered such that they are distinguishable by EPR. In their study of the pH dependence of low-spin Met-Hb species, Svistuneko and coworkers [67] postulated that the difference between the two bis-histidine hemichromes is the presence or absence of a proton on an undetermined ionizable functional group, the major species having the group deprotonated. Levy et al. [107] suggested that the difference between the two species is whether or not a water molecule remains in the distal heme pocket. In each hypothesis, the deprotonation, or presence of water, lengthens the iron-imidazole bond, resulting in reduced  $g$ -anisotropy when compared to the minor bis-histidine species.

As the temperature was increased to above 35 K (Figure 4-4), the relative percentage of bishis-Met-Hb decreased with a concomitant increase in the percentage of aquo-Met-Hb, indicative of the two species being in equilibrium with each other. The limited motion at cryogenic temperatures would make conversion from the bishis-Met-Hb adduct to the aquo-Met-Hb adduct unlikely if a water molecule was not already present in the distal heme pocket. Therefore, our results appear to be in agreement with the proposal of Levy et al. [97,107], that the presence or absence of a water molecule distinguishes the two bis-histidine hemichromes.

What the Levy et al. scheme does not rectify is the difference in relative percentages of the bishis-Met-Hb hemichrome in PBS and HEPES buffers; in PBS, the percentage of bishis-Met-Hb is about half the percentage measured in HEPES buffer at all temperatures employed. The reduction of bishis-Met-Hb by fifty percent in PBS buffer is suggestive of a subunit inequality (the Hb tetramer being half  $\alpha$  and half  $\beta$  subunits) and possibly pH dependent, given the pH drop associated with freezing PBS buffered solutions [62,63]. So described, the situation is reminiscent of the distal histidine rotation described in Chapter 2, which occurs only in the  $\beta$ -subunit and is pH dependent [76,84]. In PBS, the reduction in pH upon freezing could result in the rotation of the distal histidine residue of the  $\beta$ -subunit in a manner that prevents its coordination to iron in the  $\beta$ -subunit, effectively reducing the bishis-Met-Hb population by fifty percent. This suggests that the reaction scheme for bis-histidine hemichrome formation should incorporate both (1) the presence or absence of H<sub>2</sub>O in the distal heme pocket to distinguish between the two bis-histidine hemichromes [107] and (2) a pH dependent equilibrium between aquo-Met-Hb and bishis-Met-Hb [67].

The alteration of pH in the PBS buffered solutions was also evident in the partitioning between aquo-Met-Hb and hydroxy-Met-Hb. The pK<sub>a</sub> for aquo-Met-Hb, where the proton being lost is from the iron bound water ligand, was calculated at each temperature in both buffers. Given the variation of relative concentrations of Met-Hb species with temperature (Figure 4-4), the pK<sub>a</sub> was found to vary, as well. In HEPES, the pK<sub>a</sub> varied from a low of 7.58 (50 K) to a high of 7.96 (10 K), with an average of 7.71. In PBS, the pK<sub>a</sub> varied from 8.37 at 50K to 8.89 at 10 K, with mean value of 8.54. Previous studies have determined the pK<sub>a</sub> to be around 8 [72,73,109]. Using the pK<sub>a</sub> of

aquo-Met-Hb in HEPES, the pH of the frozen PBS solution can be estimated. Correcting the  $pK_a$  in PBS to be consistent with the  $pK_a$  in HEPES indicated the pH of the frozen PBS buffered solution to be  $\sim 6.5$ , rather than the room temperature pH of 7.4, consistent with the reduction in pH determined by others [63].

### Hb(NO)<sub>4</sub>

The variable temperature EPR study of Hb(NO)<sub>4</sub> in Chapter 5 of this work shows that as the temperature increases, the Hb(NO)<sub>4</sub> spectrum gradually changes from being predominately characterized by a rhombic signal to axial signal. In this progression, there is a continuum of states between the purely rhombic and purely axial states. In the EPR spectra of Met-Hb, intermediate states are not detected in the temperature dependent equilibrium between spectral components. This difference is most likely the result of the major spectral components of the Met-Hb spectrum each possessing distinct distal ligands, in contrast to Hb(NO)<sub>4</sub>, which maintains the identical distal ligand, but undergoes temperature induced conformation changes.

### Conclusion

The results presented here indicate that the buffer dependence observed in the EPR spectrum of Met-Hb is actually a pH effect which results from the freezing induced pH change when using PBS buffer rather than an interaction between the buffer and hemoglobin. This “buffer effect” observed in the EPR spectra of solutions of Met-Hb in PBS and HEPES buffers indicates some pH dependence on bishis-Met-Hb formation [67], however, the temperature dependent conversion of bishis-Met-Hb to aquo-Met-Hb

reinforces the hypothesis of the presence of water in the distal heme pocket of the major bishis-Met-Hb complex [107]. Additionally, the freezing artifact associated with PBS buffer may explain the differences observed in the dissociation constant of Met-Hb:nitrite when measured in PBS versus HEPES buffered solutions. These findings underscore the importance of exercising care in all aspect of experimental planning and analysis, as easily overlooked factors such as choice of buffer may covertly influence the results obtained.

## CHAPTER 5

TEMPERATURE DEPENDENCE OF THE W-BAND EPR SPECTRUM OF  $\text{Hb}(\text{NO})_4$ Introduction

The nitrosyl-adduct of ferrous hemoglobin (Hb) was originally employed as an EPR-active surrogate for the EPR-silent  $\text{Fe}(\text{II})\text{O}_2\text{-Hb}$  [13]. Over the last two decades, the ubiquitous role of nitric oxide (NO) in biology has been increasingly exposed [110], giving greater importance to the investigation of  $\text{Fe}(\text{II})\text{NO-Hb}$ . Moreover, oxidation of  $\text{Hb}(\text{NO})_4$  has been shown to generate S-nitrosohemoglobin (SNO-Hb) [30], a crucial component in hypoxic vasodilation [27,111].

At 77 K, the isolated, hexacoordinate,  $\alpha$ - and  $\beta$ - subunits of nitrosyl-Hb were found to have distinct EPR spectra [112]. Additionally, upon cleavage of the proximal histidine, the  $\alpha$  heme- $\text{Fe}(\text{II})\text{NO}$  displays striking triplet hyperfine structure in its EPR spectrum [113,114]. This pentacoordinate form ( $\alpha_5$  heme-NO) is associated with the T- or tensed state, one of Hb's two allosteric conformations. The hexacoordinate nitrosylated  $\alpha$ -chain ( $\alpha_6$  heme-NO) is formed when the Hb tetramer assumes the R- or relaxed state, the normal state of  $\text{Hb}(\text{NO})_4$  under standard conditions [115]. The allosteric state of the tetramer has not been shown to influence the  $\text{Fe}(\text{II})\text{NO}$  EPR spectrum of the  $\beta$ -subunit.

Variable temperature EPR [99,100] revealed the presence of both axial and rhombic signals in the spectrum of  $\text{Hb}(\text{NO})_4$ . However, the two signals do not arise solely from subunit differences in Hb. Similar temperature dependent spectral changes

were also measured in nitrosyl-myoglobin (MbNO), a monomeric protein, by Morse and Chan [70], who proposed a simple two state model, comprised of an axial and a rhombic state, for the temperature dependent behavior. A later study showed axial and rhombic components to be present in the Fe(II)NO spectra of the isolated subunits of Hb [69], as well.

The spectral features in the EPR spectra of Hb(NO)<sub>4</sub> collected at lower microwave frequencies, such as X-band (9 GHz) and even Q-band (34 GHz), are subject to substantial overlap. EPR spectra collected at higher microwave frequencies typically display enhanced resolution of spectral features. Reported here are the W-band (95 GHz) EPR spectra of Hb(NO)<sub>4</sub> at temperatures from 10 K-200 K from our lab, complete with detailed spectral simulation and component analysis that has not yet been reported.

## Materials and Methods

### Hemoglobin

Human hemoglobin A<sub>0</sub> (Apex Bioscience) solutions were prepared in an aqueous stock solution containing 150 mM NaCl, 0.1 mM DTPA, and 100 mM HEPES pH 7.4. Hb was initially incubated with sodium nitrite and sodium dithionite under anaerobic conditions to generate Hb(NO)<sub>4</sub>. Excess reagent was removed by gel filtration using Sephadex G-25 (GE Healthcare) chromatography gel equilibrated with the HEPES buffer described above.

### EPR Spectroscopy

Electron paramagnetic resonance spectra were recorded on a W-band spectrometer consisting of an Oxford Instruments Teslatron split-pair superconducting magnet system; with a 94.9 GHz microwave bridge operating in continuous-wave (CW) mode and a TE<sub>011</sub> cavity, both obtained from the Physico-Technical Institute of Donetsk, Ukraine; and a locally constructed probe. Cooling of the probe was provided by an Oxford Instruments CF935G dynamic, continuous flow cryostat.

### EPR Spectra Simulation

Simulations of EPR spectra were conducted with the program EasySpin [66]. EasySpin enables the user to simulate experimental EPR spectra through the specification of a variety of parameters, accounting for such things as microwave frequency, field position, hyperfine interactions and line broadening. At each temperature, individual components of the multi-component Hb(NO)<sub>4</sub> spectrum were determined by adjusting parameters, bounded by previous studies of Hb(NO)<sub>4</sub> and other heme proteins' EPR spectra at lower frequencies, to obtain a satisfactory quality of fit. As will be detailed below, the experimental spectrum will frequently demand the inclusion or exclusion of one or more spectral components. Fitting of the experimental data was done by visual inspection using a linear combination of the simulated component spectra for each temperature, altering the contribution of the necessary components to obtain a reasonable reproduction of the salient features of the experimental data. The broad nature of the features in the Hb(NO)<sub>4</sub> EPR spectra reduce the effectiveness of least-squared decomposition (employed in Chapters 2, 4 and 6), which seeks to minimize chi-squared,

favoring the sharp, intense features over features whose broadening results in reduced intensity. It should be noted, however, that fits obtained by least-squares decomposition were generally within 10 percent agreement with fits obtained by visual inspection.

## Results

### General Observations

Cursory examination of the series of EPR spectra of Hb(NO)<sub>4</sub> shown in Figure 5-1 reveals that at low temperatures, the primary contribution to the spectrum is rhombic in nature, while at higher temperatures, the spectrum is comprised principally of an axial signal. This rhombic to axial trend is consistent with measurements at lower microwave frequencies on both nitrosylated hemoglobin and myoglobin reported by others [69,70,103,116]. Also readily apparent is the narrowing of the rhombic signal as a whole (reduction in the g-anisotropy) as sample temperature is increased, notwithstanding the reduction in its intensity relative to the axial signal.

The presence of both axial and rhombic components is visible at all of the temperatures reported here. At 10 K, the  $g_1$ ,  $g_2$ , and  $g_3$  (appearing approximately at 3.26, 3.38 and 3.43 T, respectively) features of the rhombic spectrum are well defined, denoted by the blue vertical lines in Figure 5-1. As the sample temperature increases, the  $g_1$  feature moves progressively to higher field while also becoming increasingly broadened. The  $g_1$  feature remains well defined, with a clear turning point, until ~130 K. The  $g_3$  feature also exhibits positional dependence on temperature, moving to lower magnetic field as the temperature increases. While somewhat masked by the  $g_{||}$  of the axial spectrum, the  $g_3$  feature does not appear to undergo substantial broadening with

increasing temperature, in contrast to the broadening of the  $g_1$  feature, and retains a well-defined turning point up to  $\sim 160$  K. The  $g_2$  feature persists as a well-defined feature at all temperatures employed in this study, though its intensity decreases with increasing temperature. Additionally, the  $g_2$  feature is significantly broadened as the temperature increases. Though hyperfine splitting has been detected in the  $g_2$  feature of the nitrosyl adducts of Hb and other heme proteins at lower microwave frequencies [70,102,103], at W-band, no hyperfine interaction is observed in the  $g_2$  feature, consistent with the measurements of others [103]. Spectral simulations, discussed below, further elucidate the nature of the rhombic component of the  $\text{Hb}(\text{NO})_4$  EPR spectrum.

The axial component of the  $\text{Hb}(\text{NO})_4$  EPR spectrum has two features,  $g_{\parallel}$  and  $g_{\perp}$ , appearing at high and low magnetic field, respectively. At 200 K, these two features of the axial component dominate the spectrum, with  $g_{\perp}$  positioned at  $\sim 3.34$  T and  $g_{\parallel}$  at  $\sim 3.42$  T (red vertical lines in Figure 5-1). At 10 K, the  $g_{\parallel}$  feature appears as a faint shoulder on the  $g_3$  feature of the rhombic component, becoming equal in intensity with the  $g_3$  feature between 50 K and 76 K. The  $g_{\perp}$  feature also persists at 10 K, though the intensity is substantially reduced. Change in temperature appears to have little effect on the position of the features of the axial component, in contrast to the dramatic temperature induced changes on the position of rhombic species. Furthermore, broadening of the axial spectrum appears modest over the temperature range employed in this study.

At low temperature, 10 K-50 K, an additional component appears with features at  $\sim 3.35$  T and  $\sim 3.46$  T. It appears well defined at 10 K, gradually losing intensity as the

sample temperature is increased. The exact nature of this component is not readily apparent. Possible assignments are discussed below.

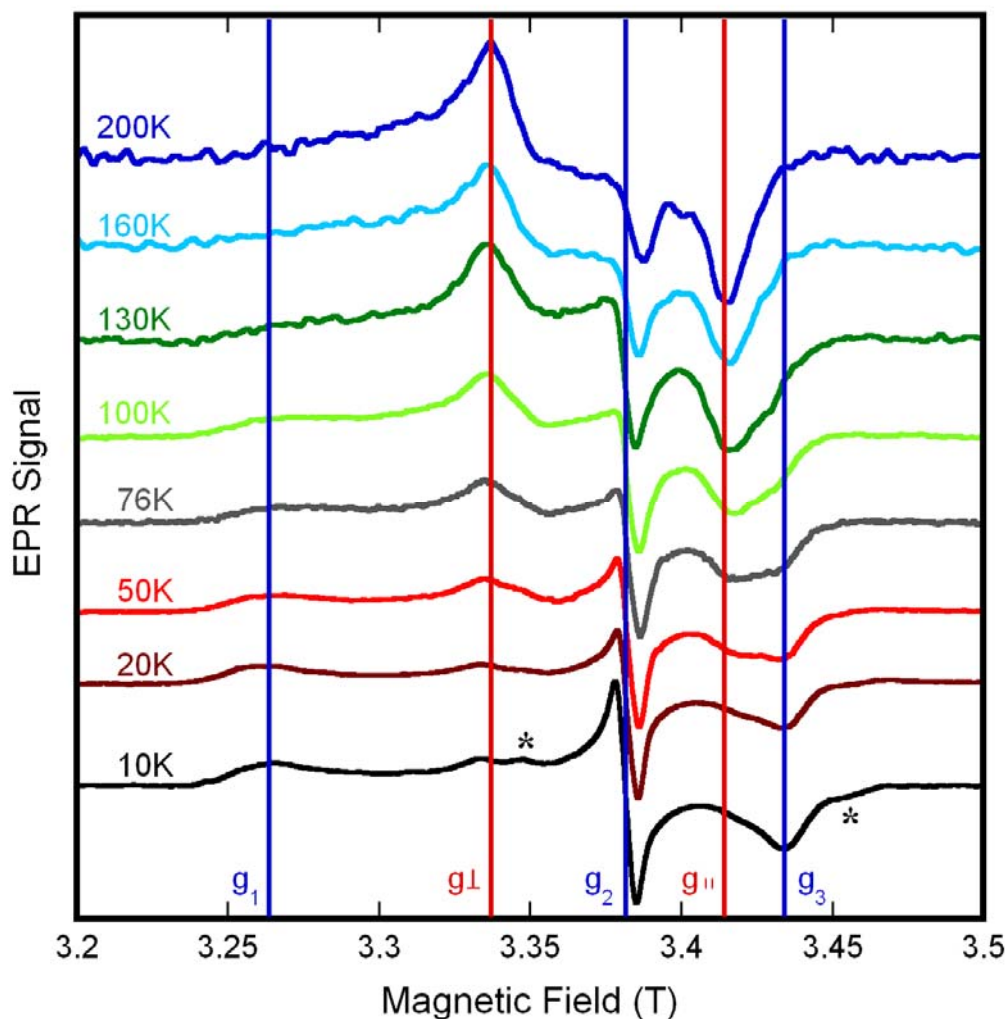


Figure 5-1: W-band EPR spectra of  $\text{Hb}(\text{NO})_4$  in aqueous solution at temperatures from 10 K-200 K. Spectra were collected with 94.9 GHz microwave frequency, microwave power ranging from 2.2-16.8  $\mu\text{W}$ , 0.1 s time constant, modulation amplitude of 10 G, and a 0.2 T/min sweep rate. Vertical lines highlight the major rhombic (blue, 10 K) and axial (red, 200 K) features. Asterisks mark minor features discussed in the text.

### Spectral Simulation

For a more detailed analysis of the temperature dependence of the  $\text{Hb}(\text{NO})_4$  EPR spectrum, simulations of the experimental spectra were conducted. Simulations at each temperature revealed characteristics of the spectra that would otherwise be imperceptible. The goal of the spectral simulations was to accurately reproduce the experimental spectrum with the minimum number of components, only adding additional basis spectra when demanded by the data. The simulated spectra are shown in Figure 5-2.

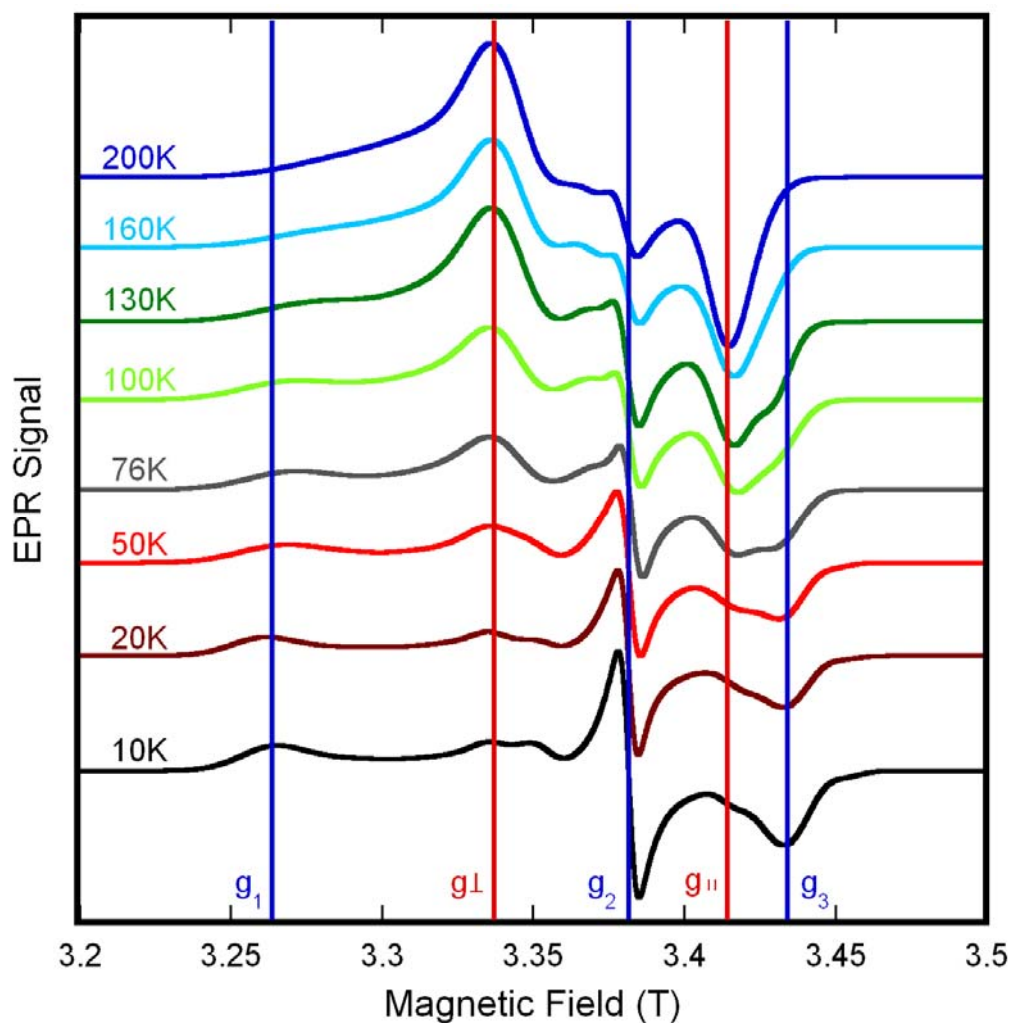


Figure 5-2: Simulated W-band EPR spectra corresponding to the spectra shown in Figure 5-1. Simulated spectra were prepared as described in the text. Vertical lines highlight the major rhombic (blue, 10 K) and axial (red, 200 K) features.

Accordingly, initial attempts to simulate the 10 K spectrum employed only a rhombic and an axial species (initially neglecting the unidentified features at  $\sim 3.35$  T and  $\sim 3.46$  T). However, after exhausting all reasonable adjustment of line broadening and shape, an acceptable fit of the 10 K spectrum could not be obtained with only two components. The residual intensity was too great, especially in the region between  $g_{\parallel}$  of the rhombic component and  $g_{\perp}$  of the axial. An additional rhombic component was necessary; one with broader, less well-defined features than the initial rhombic component. The inclusion of the second rhombic spectrum produced a simulated spectrum with good agreement to the experimental data.

The need for two rhombic components persists through 200 K, the broad area of the low field region not being sufficiently represented by a single rhombic component. Furthermore, at temperatures of 100 K and higher, the central feature of the rhombic spectrum, with its sharp, negative intensity and limited positive intensity, no longer resembles a typical rhombic  $g_2$  feature, such as  $g_2$  of the 10 K spectrum in Figure 5-1. Attempts to replicate the central features of the experimental spectra included: an axial spectrum with a  $g_{\perp}$  of  $\sim 2.0$ ; an axial spectrum with broad, but unresolved, hyperfine structure in the  $g_{\perp}$  feature; and two rhombic components, one with a sharper higher field  $g_2$  feature and one with a broader, lower field  $g_2$  feature. While the two proposed axial spectra could reasonably reproduce the unique structure of the experimental spectra, support for such axial spectra is lacking in earlier EPR studies of nitrosylated heme proteins. Moreover, the necessity for both a broad and a narrow rhombic component at lower temperatures strengthens the third hypothesis: two distinct  $g_2$  features, each with a different line width. The natural conclusion was to match the broader  $g_2$  feature with the

broader rhombic component, while the narrower  $g_2$  feature was paired with the rhombic component with sharper features.

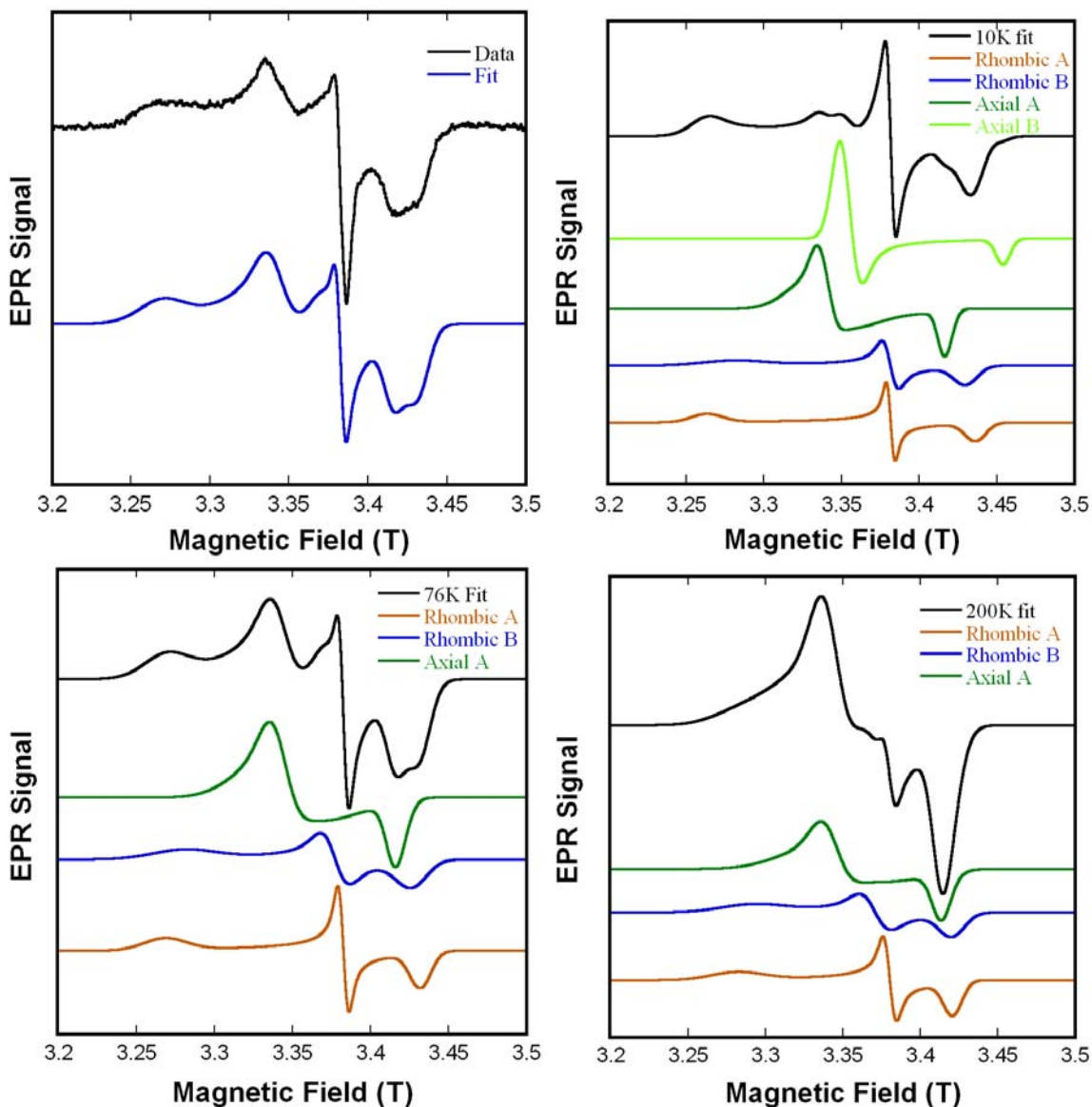


Figure 5-3: Exemplary experimental and simulated  $\text{Hb}(\text{NO})_4$  spectra, with component spectra, at 10 K, 76 K and 200 K. Top left: the experimental and simulated spectra of  $\text{Hb}(\text{NO})_4$  at 76 K. The remaining panels display the simulated  $\text{Hb}(\text{NO})_4$  spectra at 10 K (top right), 76 K (bottom left) and 200 K (bottom right), with their corresponding basis spectra used to generate the simulated spectra.

The axial features of the  $\text{Hb}(\text{NO})_4$  W-band EPR spectrum were originally fit with two axial spectra, one narrow and one broad. However, fitting the experimental spectra revealed that, at each temperature, the two axial spectra were being combined at nearly constant ratios to reproduce the experimental spectrum. The similarity of ratios indicates that the composite of the two axial spectra should be considered a single component, rather than two separate species. The need to simulate the axial component in such a way is a limitation of the simulation software employed, which does not allow Lorentzian line broadening to be applied to a single  $g$ -factor, but applies the line broadening to the spectrum as a whole. In fact,  $g_{\perp}$  of the composite axial spectrum could be simulated adequately; nevertheless, when good agreement with  $g_{\perp}$  was obtained, the  $g_{\parallel}$  feature was overly broadened. Therefore, the axial component was simulated by the linear combination of two spectra, which was then treated as a single spectrum.

At low temperatures (10-50 K), additional features at  $g=2.025$  and  $g=1.962$  (marked with asterisks in Figure 5-1, 10 K) were observed in the EPR spectra of  $\text{Hb}(\text{NO})_4$ . These features, which increase in intensity concurrently, could be fit as either  $g_2$  and  $g_3$  of a rhombic spectrum or as  $g_{\perp}$  and  $g_{\parallel}$  of an axial spectrum. If it is truly a rhombic spectrum, no  $g_1$  feature is evident, though it may possibly be obscured by the large contributions from the two prevailing rhombic components. Additionally, a rhombic spectrum has similar total area as an axial spectrum; however, the area of the rhombic spectrum is distributed over a broader range of magnetic field strengths. Consequently, fitting the two observed features with a rhombic spectrum results in a substantially higher population of this low temperature state than if the features were fit with an axial spectrum,  $>25\%$  or  $<5\%$  at 10 K, respectively. The line shape of the

$g=2.025$  feature is best simulated by an axial spectrum, rather than a rhombic spectrum, and the axial spectrum produces a better representation of the features of the  $\text{Hb}(\text{NO})_4$  spectrum overall. Accordingly, an axial spectrum, Axial B, was used to simulate the features arising only at low temperatures.

Representative basis spectra and fits are shown in Figure 5-3.

### Trends with Temperature

Several trends are observed as sample temperature increases. First, as the temperature increases, the percentage of rhombic contribution to the  $\text{Hb}(\text{NO})_4$  spectrum decreases while the axial contribution increases. At 10 K, the relative percentages are about 90% rhombic and 10% axial. At 200 K, the rhombic contribution is ~35% with axial assuming ~65%. The results for all temperatures recorded here are plotted in Figure 5-4, and are in good agreement with a prior study at Q-band [68].

Secondly, as the temperature increases, all component spectra display increased line broadening. This broadening was quantitated in the spectral simulations. At 200 K, each component was broadened by at least 50% compared to their respective 10 K spectrum. The notable exception is the  $g_2$  feature of the Rhombic B spectrum, which was broadened by 100%.

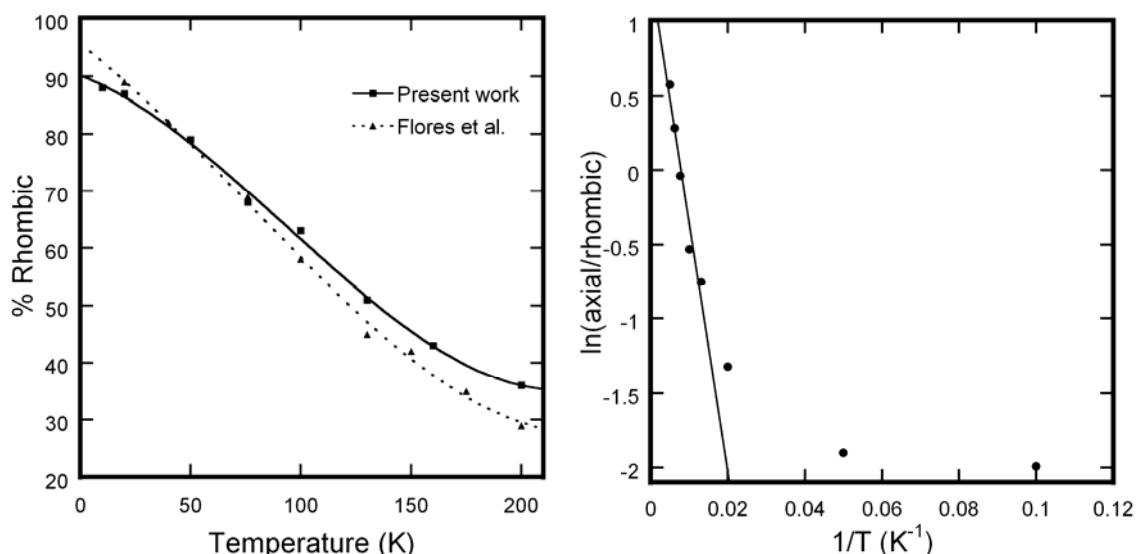


Figure 5-4: Left: plot of rhombic percentage vs. temperature. The rhombic percentage was determined from the simulated spectra (Figure 5-2) of the experimental data (Figure 5-1) at each temperature. For comparison, the data of Flores et al. [68] are also displayed. Right: plot of the relative fraction of axial/rhombic species as a function of inverse temperature. Plot also displays the linear fit of the data points corresponding to temperatures of 76 K and higher.

Third, in addition to the broadening of spectral features, the increase in temperature results in the changes in the position of spectral features. Change in magnetic field position was primarily seen in the rhombic components. For Rhombic A species,  $g_1$  decreases with increasing temperature, going from 2.078 to 2.067 at 10 K and 200 K respectively, and  $g_3$  increases with increasing temperature, from 1.973 at 10 K to 1.982 at 200 K. The  $g_2$  feature of Rhombic A remains relatively constant. The simulated spectra of Rhombic A at all temperatures are plotted in Figure 5-5, showing the variation in position and line width with temperature. Both  $g_1$  and  $g_3$  of Rhombic B display similar variations in position as those of Rhombic A,  $g_1$  decreasing from 2.068 to 2.061 and  $g_3$  increasing from 1.977 to 1.983, at 10 K and 200 K, respectively. Also,  $g_2$  of Rhombic B increased with increasing temperature, from 2.0055 at 10 K to 2.012 at 200 K. The axial component undergoes the similar changes in position as the rhombic spectra, but to a

much lesser degree; the  $g_{\perp}$  feature moves to higher field with increasing temperature, while the  $g_{\parallel}$  feature moved to lower field as the temperature increases.

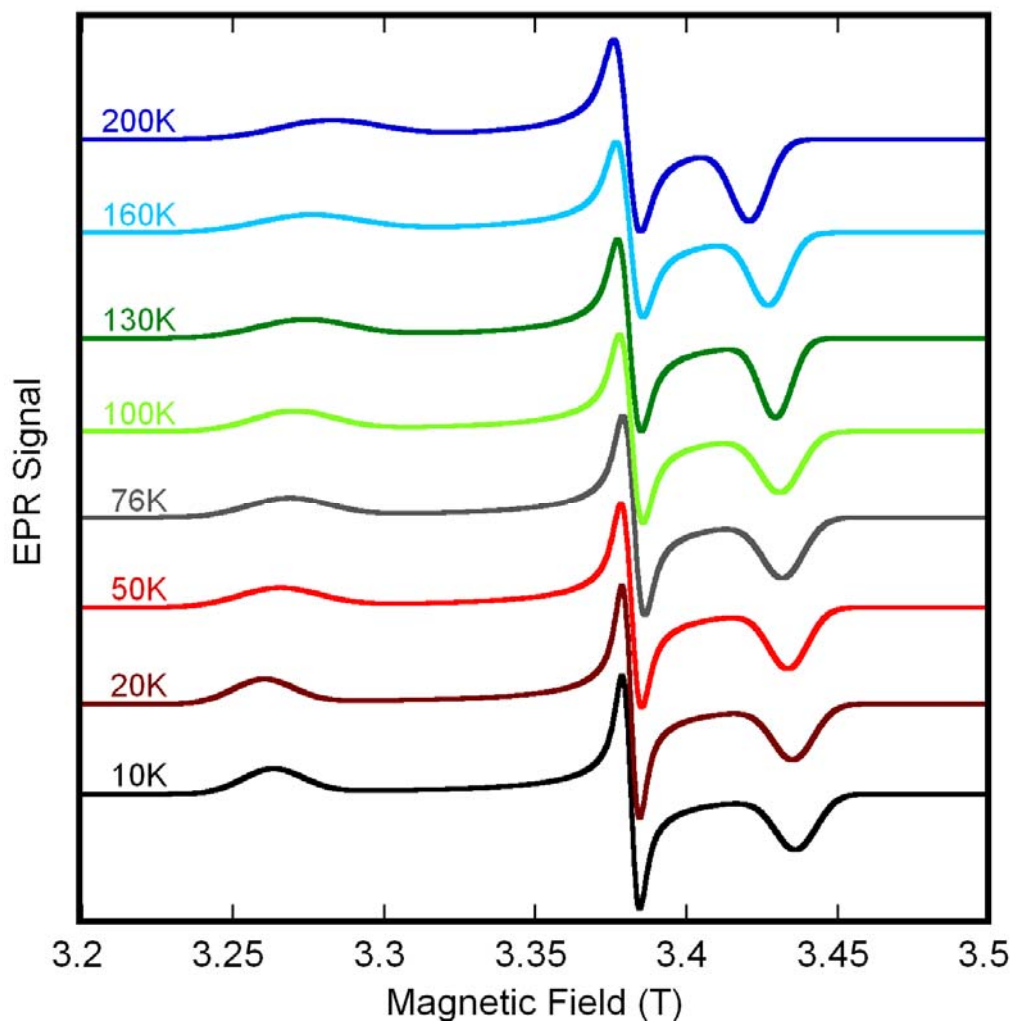


Figure 5-5: Simulated EPR spectra of Rhombic A at various temperatures. The reduction in  $g$ -anisotropy, as well as increasing linewidth, is evident as the temperature increases from 10 K to 200 K.

Also, the minority low temperature species, Axial B, visible only from 10 K to 50 K, appears to lose intensity as the temperature increases, while simultaneously shifting to lower fields. At 10 K, the  $g=2.025$  feature remains well resolved from the Axial A component, but at 50 K appears as a shoulder on the  $g_{\perp}$  feature of the Axial A spectrum.

The  $g=1.962$  feature undergoes similar temperature induced changes, disappearing into the  $g_3$  feature of the Rhombic A spectrum above 50 K.

### Discussion

At low microwave frequencies, such as X-band, there is significant overlap between the axial and rhombic components of the  $\text{Hb(NO)}_4$  EPR spectrum, as seen in Figure 5-6. In the same figure, the EPR spectra of the nitrosyl-derivatives of the isolated subunits of Hb measured at X-band can also be seen. At 76 K, the spectrum of the  $\alpha$  subunit is clearly discernible from the spectrum of the  $\beta$  subunit. While the  $\alpha$  subunit shows primarily rhombic character and the  $\beta$  subunit displays primarily axial character, neither subunit assumes solely one conformation (all axial or all rhombic) at 76 K. The  $\text{Hb(NO)}_4$  spectrum is simply the linear combination of the spectra of the two isolated subunits, as pointed out by Shiga et al. [100], with the  $\alpha$  and  $\beta$  spectra superimposed upon one another.

The rhombic and axial components of the EPR spectrum of  $\text{Hb(NO)}_4$  are better resolved in the W-band EPR measurements reported here than in previous studies employing lower microwave frequencies. However, these new data do not resolve distinct axial and rhombic components that can be assigned to specific subunits; there is no evidence here that the  $\alpha$ -subunit has a rhombic and an axial spectrum that is distinct from those of the  $\beta$ -subunit.

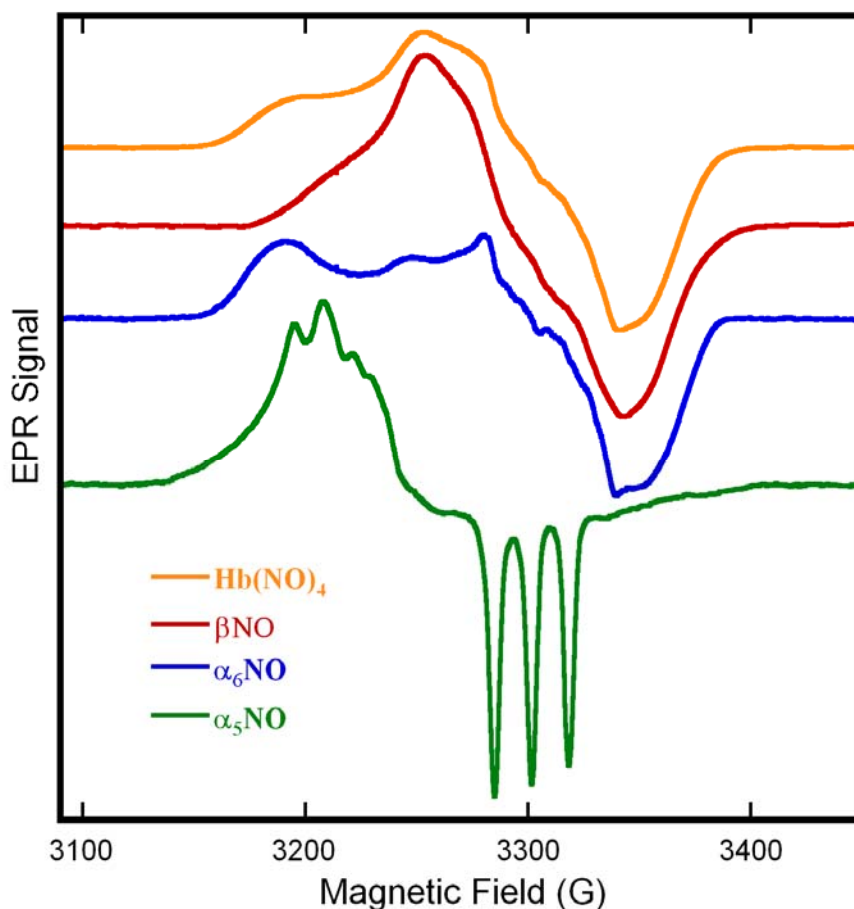


Figure 5-6: X-band EPR spectrum of Hb(NO)<sub>4</sub> and its derivatives. Data was collected at 9.29 GHz at 76 K with a modulation amplitude of 2 G, microwave power of 10 mW, 0.128 s time constant, and a sweep rate of 3.33 G/s.

Therefore, the component spectra Rhombic A cannot be rigorously identified as the  $\alpha$ -subunit rhombic conformation. The same is true of the  $\beta$ -subunit and Rhombic B. However, given the predilection of the  $\alpha$ -subunit for the rhombic conformation, the Rhombic A spectrum would have more  $\alpha$  character than  $\beta$  character and the Rhombic B spectrum would have more  $\beta$  character than  $\alpha$  character. The necessity for two rhombic components does not arise from the presence of distinct subunits, but from the manner of the conversion from the rhombic conformation to the axial conformation.

At 10 K, there is a well-defined rhombic spectrum (Rhombic A), which appears to be the rhombic limit of heme-Fe(II)NO, evidenced by the clear turning point of the  $g_1$  feature at  $g \approx 2.8$ . At the same time, however, there is an almost equal population of molecules with a less well-defined rhombic orientation (Rhombic B). As the temperature increases, molecules move away from the conformation with greater rhombic distortion to a state with reduced rhombic distortion, accounted for in simulations by changes in field position and increased line width. Therefore, though accurate simulation requires the use of two rhombic components, these components should not be thought of as two rigid, rhombic states. Rather, the two rhombic components are more a collection of molecules with various degrees of rhombicity.

The need for two rhombic components, coupled with the changes in field position and line width, indicates that the transition from rhombic to axial is a gradual progression. If Hb(NO)<sub>4</sub> had only two conformations, one rhombic species and one axial species, simulation of spectra would require changing only the relative contribution of each component to match the equilibrium at each temperature, as was originally proposed for MbNO [70]. This is not the case in the spectra of Hb(NO)<sub>4</sub>; changes in temperature require adjustment of field positions and line widths, in addition to varying component weights in the composite spectra. Clearly, as temperature increases, molecules shift from a rhombic conformation to an axial conformation in a graded progression. Studies at X-band, which facilitates measurement at room temperature, show more fully the rhombic component eventually converging to the axial conformation [103]. In this progression, molecules can assume a continuum of configurations between the two states, rather than a

simple two state model allowing molecules to assume only one strict conformation or the other.

The convergence from rhombic conformations and an axial conformation corresponds well with the structure of the heme centers in Hb. In its hexacoordinate state, the iron atom binds four equatorial atoms, the nitrogens of the porphyrin ring, and two axial atoms, an imidazole nitrogen of proximal histidine and the nitrogen of NO. When the porphyrin ring remains in the x-y plane and the  $N_{\text{His}}\text{-Fe-NO}$  bonds are oriented perpendicular to the heme plane, the resulting spectrum is that of an axial species, with  $x=y\neq z$ . Distortion in conformation that result in the inequivalence of x and y, such as tilting of the  $N_{\text{His}}\text{-Fe-NO}$  bonds from the heme-normal or puckering of the porphyrin ring, will yield a rhombic spectrum, with  $x\neq y\neq z$ . Therefore, as the temperature increases, the disparity between the x- and y-axes lessen, until ultimately an axial geometry is achieved.

### Subunit Differences

In  $\text{Hb}(\text{NO})_4$ , equal populations of axial and rhombic species are obtained at  $\sim 130$  K, as seen in Figure 5-4. While the axial:rhombic distribution is 50:50 when evaluating the tetramer as a whole, that is not the case if one were to examine the individual subunits. Previous work has demonstrated preference of the  $\alpha$ -subunit for rhombic geometry and that of the  $\beta$ -subunit for an axial conformation at 130 K [69,100,117]. The same preferences are observed at 76 K, as seen in Figure 5-6. Because the spectrum of  $\text{Hb}(\text{NO})_4$  is the sum of the isolated subunit spectra [100], the midpoint of the rhombic to

axial conversion of the  $\alpha$ -subunit must occur at a temperature greater than 130 K and the midpoint of the  $\beta$ -subunit conversion at a temperature less than 130 K.

For a system at equilibrium,

$$\Delta G^\circ = -RT \ln K \quad (5-1)$$

Additionally, when there are equal populations of products and reactants (ie.  $K=1$ ), then  $\Delta G^\circ = 0$ . Because

$$\Delta G^\circ = \Delta H^\circ - T \Delta S^\circ, \quad (5-2)$$

it follows that in a reaction with an equilibrium constant of unity,

$$\Delta H^\circ = T \Delta S^\circ. \quad (5-3)$$

The data plotted in Figure 5-4 represent the equilibrium populations of axial and rhombic species in the  $\text{Hb}(\text{NO})_4$  spectrum at each temperature, and therefore, equation 5-1 applies. Because of the different temperatures at which the subunits of Hb assume equal populations of axial and rhombic  $\text{Fe}(\text{II})\text{NO}$  contributions, it can be stated that  $\Delta H^\circ_\alpha / \Delta S_\alpha > \Delta H^\circ_\beta / \Delta S_\beta$ , using equation 5-3. If one assumes equal  $\Delta S^\circ$  for the two subunits, which is not unreasonable given similarities of their axial and rhombic spectra, it holds that  $\Delta H^\circ_\alpha > \Delta H^\circ_\beta$ . While equality of  $\Delta S^\circ_\alpha$  and  $\Delta S^\circ_\beta$  is speculative, it can be safely stated that the critical temperature of the  $\beta$ -subunit, the temperature at which the subunit possesses equal populations of axial and rhombic species, is substantially less than that of the  $\alpha$ -subunit. The dissimilar critical temperatures for the  $\alpha$  and  $\beta$  subunits, not subunit specific axial and rhombic spectra, allows for differentiation of the X-band EPR spectra of the isolated subunits at 77 K (Figure 5-6).

The temperature dependent behavior of  $\text{Hb}(\text{NO})_4$  is manifested in other  $\text{Fe}(\text{II})\text{NO}$  complexes. In fact, the temperature dependent conversion of  $\text{Fe}(\text{II})\text{NO}$  EPR spectra from

a rhombic state to an axial state has been observed in nitrosyl-heme proteins such as myoglobin [68,70,101,103], cytochrome c [118], neuroglobin [119], and catalase [118]; and even in nitrosylated iron-porphyrin coordination complexes [69,70]. The EPR spectra of these nitrosylated iron centers are surprisingly similar. Whether they are a monomeric or polymeric heme protein or an inorganic, model heme complex, they all display highly similar, temperature dependent, rhombic and axial EPR spectra. The significant difference between the various proteins or compounds is the conformation they preferentially assume at a given temperature (i.e. Hb(NO)<sub>4</sub> at 77 K,  $\alpha$  is more rhombic, while  $\beta$  is more axial). So, while the heme proteins and coordination complexes display similarities in their axial and rhombic EPR spectra, each protein/complex has a distinct  $\Delta H$  for rhombic to axial conversion. The  $\Delta H$  for each will depend on such factors as hydrogen bonding, space in the heme pocket, flexibility of the porphyrin ring, and the nature of the proximal ligand.

#### Axial to Rhombic Ratio

The percentage of rhombic contribution to the spectra of Hb(NO)<sub>4</sub> versus temperature are plotted in Figure 5-4. As shown, our results are consistent with those reported by others [68] at Q-band over a similar temperature range. At 10 K, we determined the rhombic contribution to the W-band spectrum to be 88%, with the remaining 12% being axial. Our results and those of Flores et al. [68] appear to be in conflict with the work of Tyryshkin et al. [120], who collected electron spin-echo envelope modulation (ESEEM) spectra on the nitrosyl adducts of the isolated subunits of hemoglobin. At 4 K, they report the  $\alpha$ -chain to be 80% rhombic and 20% axial

components and the  $\beta$ -chain to be 10% rhombic and 90% axial. They also report the  $\text{Hb(NO)}_4$  spectrum to be the linear combination of the individual  $\alpha$ - and  $\beta$ -chain spectra, making the total rhombic and axial contributions to the  $\text{Hb(NO)}_4$  spectrum equal, 50% each. Clearly, this result is inconsistent with the data presented above.

In Tyryshkin and coworkers' measurement of the isolated Hb subunits [120], they estimated the rhombic and axial contributions to the spectra of the  $\alpha$ - and  $\beta$ -chains. Support for their estimate, that percentage of rhombic is equal to  $0.7*\alpha+0.1$ , is not given. Furthermore, they employed the isolated  $\alpha$ - and  $\beta$ -chain spectra as basis spectra for the rhombic and axial components, respectively, based on their stated assumption that each represented nearly pure states.

The  $\text{Hb(NO)}_4$  spectrum has been shown to be the linear combination of the isolated subunit spectra at 4 K [120], 77 K [117], and 292 K [100], eliminating the possibility that the  $\beta$ -chain configuration is substantially altered when incorporated into the Hb tetramer. The discrepancy between the two data sets most likely arises from the underestimation of the rhombic character in the  $\beta$ -subunit  $\text{Fe(II)NO}$  spectrum by Tyryshkin and coworkers. The more limited motion of the  $\beta$ -chain inhibits adoption of the more extreme rhombic conformation of the  $\alpha$ -chain. Therefore, the rhombic component of the  $\beta$ -subunit exhibits narrower  $g$ -anisotropy in its EPR spectrum than that of the  $\alpha$ -chain, as evidenced by the need for multiple rhombic components when fitting the W-band spectra reported here. The more compact, rhombic spectral component of the  $\beta$ -chain, coupled with the increased component overlap at X-band, perhaps led to the overestimation of the axial contribution to the  $\beta$ - $\text{Fe(II)NO}$  spectrum by Tyryshkin et al. [120]

### Low Temperature Species

Schmidt et al. [103] mention a low temperature species detected at microwave frequencies above X-band. They tentatively define the feature ( $g \approx 2.015$ ) as  $g_2$  of minor rhombic conformation assumed by the  $\beta$  chain. The low temperature features we measure at 50 K and below, appear at  $g=2.025$  and  $g=1.962$ , but no feature is observed at  $g \approx 2.015$ . Additionally, in the handful of Y-band spectra Schmidt et al. display, the highlighted “low temperature” feature appears at all temperatures shown (including 180 K); and, though visible in their 5 K spectra, they make no mention of the  $g \approx 1.96$  feature.

The two low temperature features we measure are best simulated as an axial spectrum. At 10 K, employing a rhombic spectrum to fit these features results in this “minor” species accounting for greater than 25% of the total  $\text{Hb(NO)}_4$  spectrum. Fitting with a rhombic spectrum also compromises the quality of fit of other features in the  $\text{Hb(NO)}_4$  spectrum, particularly in the high field region. Additionally, EPR measurements of the isolated Hb subunits [69] have shown the axial spectrum of  $\alpha\text{-Fe(II)NO}$  to have a  $g_{\perp}$  of 2.024, similar to the “ $g_{\perp}$ ” value measured here, however, the  $g_{\parallel}$  feature of the Axial B spectrum is at higher field than typically found for an Fe(II) axial species. The coalescence of the  $g=2.025$  feature into  $g_{\perp}$  of the Axial A spectrum could indicate this to be a low temperature conformation of the  $\alpha$ -chain.

Additionally, the plot of axial/rhombic versus inverse temperature (Figure 5-4, right) deviates from linearity at temperature of 50 K and below. This deviation coincides with the appearance of the low temperature species, and indicates that, at low temperatures, the model either under represents the rhombic contributions or that a simple two state model does not adequately represent the data. Consequently, though the

line shape of two low temperature features are best modeled as an axial spectrum, the results here are not conclusive; association of the low-temperature features with an  $\alpha$ -chain axial conformation should be considered provisional until additional information is obtained.

#### Comparison to Met-Hb:NO<sub>2</sub><sup>-</sup> and Met-Hb

The temperature dependence of Hb(NO)<sub>4</sub> is in marked contrast to the temperature dependence of Met-Hb:NO<sub>2</sub><sup>-</sup>, which is contained in this work (Chapter 2) and published elsewhere [121]. In the EPR spectrum of Met-Hb:NO<sub>2</sub><sup>-</sup>, there is no observed temperature dependent interconversion between the two species between 20 K and 175 K, though alteration of pH does result in interconversion. Furthermore, each Met-Hb:NO<sub>2</sub><sup>-</sup> species retains its characteristic rhombic spectrum until motional averaging results in the loss of  $g$ -anisotropy, at temperatures above 115 K. In Met-Hb:NO<sub>2</sub><sup>-</sup>, it appears that the  $\alpha$  subunit can only assume one conformation, while the  $\beta$  subunit has the ability to assume both of the observed conformations, the partitioning of which is determined by pH. In the case of Fe(II)NO in Hb,  $\alpha$  and  $\beta$  can both assume an axial and a rhombic conformation, with the axial/rhombic distribution being temperature dependent and unique for each subunit.

Interestingly, the  $\alpha$ -heme's propensity toward rhombicity has been attributed to the greater range of motion afforded to the nitric oxide and proximal histidine in the heme pocket compared to the  $\beta$ -heme [69]. Yet, in Met-Hb:NO<sub>2</sub><sup>-</sup>, it is the  $\alpha$ -heme that appears to only assume one conformation, while the  $\beta$ -heme undergoes pH induced conversion between the two Met-Hb:NO<sub>2</sub><sup>-</sup> species detected.

Additionally, the variation in the EPR spectrum of Met-Hb over a range of cryogenic temperatures, as seen in Chapter 4, is distinct from that of Hb(NO)<sub>4</sub>. The components of the Met-Hb spectrum show little change in position and undergo lesser line broadening when compared to the components of the Hb(NO)<sub>4</sub> spectrum. Moreover, the various species of Met-Hb assume well defined conformations and spectra at all temperature measured, in contrast to the gradual coalescing of the rhombic species into the axial species observed in Hb(NO)<sub>4</sub> as the temperature increases. However, the major components of the Met-Hb spectrum all have distinct ligands which result in distinct EPR spectra, whereas the rhombic and axial components of the Hb(NO)<sub>4</sub> spectrum are simply conformational variants that, not surprisingly, can progressively interconvert.

### Conclusion

The W-band spectra of Hb(NO)<sub>4</sub> presented here show notably increased resolution over spectra collected at lower microwave frequencies. The spectra show features consistent with the presence of both rhombic and axial species. At low temperatures, the Hb(NO)<sub>4</sub> spectrum is dominated by rhombic contributions. At temperatures exceeding 130 K, the spectrum is primarily that of an axial conformation, consistent with studies at lower frequencies [68,69]. The rhombic components of the Hb(NO)<sub>4</sub> spectrum vary with temperature, showing increasing line broadening and decreasing g-anisotropy as the temperature increases. This indicates that the transition from the rhombic state to the axial state is a gradual conformational change, rather than equilibrium between two static states.

Despite the increased resolution achieved at W-band, there is no evidence for rhombic or axial spectra that can be assigned to specific chains ( $\alpha$  or  $\beta$ ) of the Hb tetramer. However, previous studies of the isolated subunits [69,100,117] demonstrate that the critical temperature of conversion between axial and rhombic conformations is unique for the  $\alpha$ - and  $\beta$ -chains. This result, coupled with a survey of EPR spectra of other proteins and complexes [68-70,101,103,118,119], indicates that spectra of heme-Fe(II)NO complexes generally possess the same salient axial and rhombic features, yet with distinct critical temperatures for axial to rhombic conversion.

Finally, the features appearing only in low temperature ( $\leq 50$  K) and high microwave frequency spectra are best simulated by an axial spectrum. Assignment of these features to an axial species is tentative and, as such, warrants additional investigation.

## CHAPTER 6

INVESTIGATION OF MIXED-VALENCE, PARTIALLY NITROSYLATED  
HEMOGLOBIN TETRAMERS AS SNO-PRECURSORSIntroduction

Human hemoglobin modulates the bioactivity of nitric oxide through chemical reactions of NO with the protein's hemes and thiols [96]. Details of these chemical dynamics, however, remain poorly understood. Angelo et al. [52] have identified the existence of a minority species that forms upon reaction of deoxy-Hb with nitrite, and quantitatively yields SNO-Hb upon oxygenation; the overall chemistry appears to involve the redox coupling of NO and oxidized hemes. Luchsinger and co-workers [30] previously established the coupling of heme-Fe(III) (Met-heme) and nitrosyl ligands in the formation of SNO-Hb.

Pentacoordinate  $\alpha$  heme-NO ( $\alpha_5$  heme-Fe(II)NO)— a species predominant in Hb's quaternary T-state (tensed state) and distinguished by a striking triplet hyperfine structure in its EPR signal— possesses considerable nitrosonium character [122], and could potentially serve as a nitrosation reagent if coupled to the reduction of a neighboring Met-heme. The reactive species would thus likely involve a Hb tetramer with an  $\alpha_5$  heme-NO, a Met-heme, and two vacant Fe(II) hemes, or  $\alpha$  heme-NO/Met-heme hybrids in the presence of allosteric effectors that induce the T-state. The physiological existence of such Hb species, while plausible, has no foundation in the literature.

Accordingly, we have initiated experiments to produce various mixed-valance, partially nitrosylated hemoglobin tetramers and to characterize their reactivity. Here we report the results of experiments that elucidate rate of formation and the final distribution of heme-nitrosyl species produced by incubation of deoxy-Hb with limiting amounts of NO from various NO donors, as a function of NO donor type, reactant concentrations, and presence of T-state inducing allosteric effectors.

### Methods and Materials

#### Hemoglobin

Human hemoglobin A<sub>0</sub> was obtained from Apex Bioscience (Research Triangle Park, NC). Reactions were carried out with Hb in 100 mM HEPES buffer, pH 6.8, or 100 mM sodium acetate buffer, pH 4.9. Both buffer solutions contained 0.1 mM DTPA and 0.1 M KCl. Deoxy-Hb was formed by gently vortexing in an ultra-high purity argon atmosphere with the addition of sodium dithionite to reduce any Met-Hb present. Hb(NO)<sub>4</sub> was formed by adding 5-fold molar excess sodium nitrite to deoxy-Hb. The solutions of sodium dithionite and sodium nitrite were prepared in the buffer corresponding to the buffer being used in the Hb solution and were thoroughly degassed before addition via gas-tight syringe. DEANO (Diethylamine NONOate, Cayman Chemical) was stabilized in 10 mM KOH, degassed, and added by gas-tight syringe. Concentrations of Hb solutions were determined using UV-Vis spectroscopy.

### EPR Spectroscopy

X-band EPR data were collected on a Varian E-109 spectrometer modified with a National Instruments computer interface for data collection and field control. Sample temperature during data collection was 76 K, obtained by placement in a dewar of boiling nitrogen. Data was collected at a microwave frequency of 9.14 GHz, with 10 mW microwave power, modulation amplitude of 2 G, a time constant of 0.128 s, and a sweep rate of 3.33 G/s. Spectra were normalized to aid in comparison.

### UV-Vis Spectroscopy

UV-Vis spectra were collected using a Cary 300 spectrometer. Least-squares fitting of spectra [30] was used to determine the concentration of UV-Vis detectable of heme species.

## Results

### Hb[ $\alpha$ (NO) $_2$ $\beta$ (Fe(II)) $_2$ ]

Hb(NO) $_4$  was generated by incubation of Hb with dithionite and nitrite under anaerobic conditions. The Hb(NO) $_4$  was then exposed to room air and the reaction progress was monitored by UV-Vis spectroscopy (Figure 6-1). Upon reaching 50% oxidation, where 50% of the hemes were Fe(II)NO and 50% Fe(III), the solution was deoxygenated and dithionite was added, reducing the oxidized subunits. This reaction sequence was carried out at both pH 4.9 and 6.8.

The UV-Vis spectra in Figure 6-1 clearly demonstrate the oxidation of heme-Fe(II)NO to heme-Fe(III), methemoglobin (Met-Hb). These spectra, however, tell only a

fraction of the story. Further characterization by EPR spectroscopy, shown in Figure 6-2, reveals subunit inequalities in the oxidation of heme-Fe(II)NO. The  $\beta$ -subunit displays substantially higher susceptibility to oxidation (from  $\beta$  heme-Fe(II)NO to  $\beta$  heme-Fe(III)) over  $\alpha$  heme-Fe(II)NO, evidenced by the relative loss of  $\beta$  heme-Fe(II)NO character in the EPR spectra. The  $\beta$ -subunit preference is observed at pH 4.9 and 6.8.

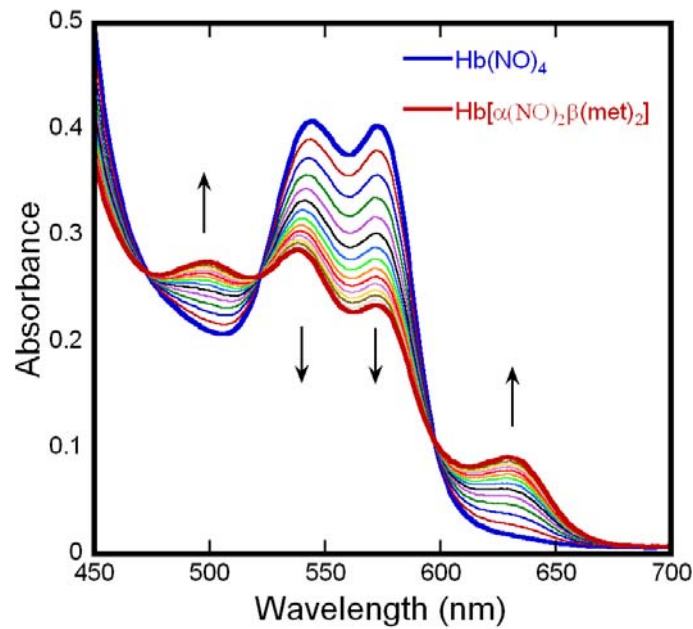


Figure 6-1: UV-Vis spectra tracking the oxidation of  $\text{Hb}(\text{NO})_4$ . The final trace (bold, red) results from 50% of the hemes forming heme-Fe(III) while the remaining hemes are Fe(II)NO.

Additionally, the pH difference between the two experiments affects the heme environment of the  $\alpha$ -subunit. In the  $\alpha$ -subunit of iron-nitrosyl hemoglobin, the bond between the heme-iron and the imidazole nitrogen of the proximal histidine is known to be intact when the Hb tetramer assumes R-state (relaxed) conformation and cleaved when the tetramer assumes the T-state (tensed) [115]. The cleavage of the proximal histidine bond gives a pentacoordinate ferrous configuration ( $\alpha_5$  heme-Fe(II)NO) with the aforementioned triplet hyperfine structure in its EPR spectrum [113,114]. No such

hyperfine structure is observed in R-state  $\alpha_6$  heme-Fe(II)NO or in  $\beta$  heme-Fe(II)NO, which is hexacoordinate in both allosteric conformations.

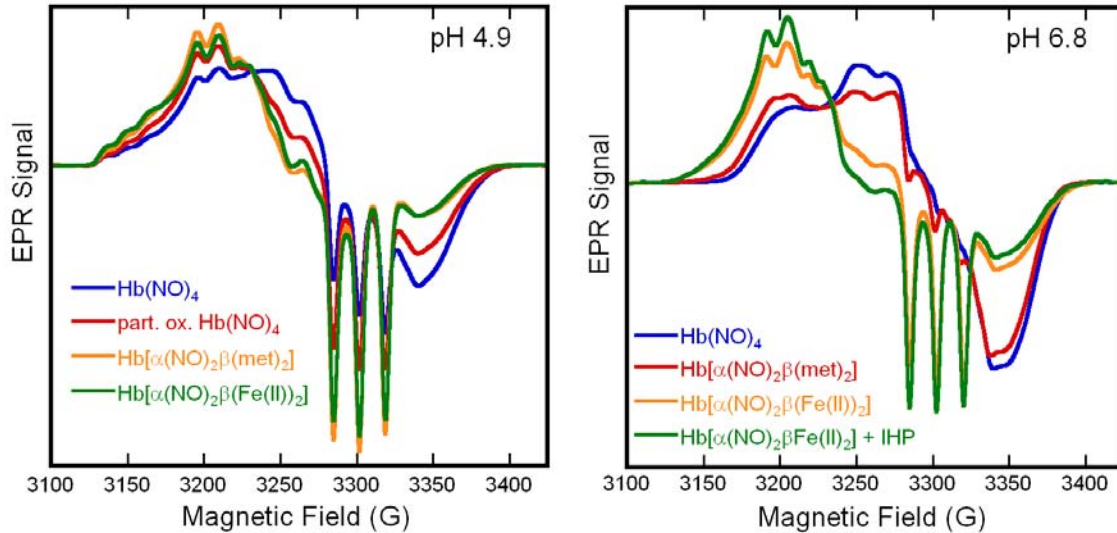


Figure 6-2: EPR spectra of  $\text{Hb}(\text{NO})_4$  and various hybrid derivatives in aqueous buffer at pH 4.9 and 6.8, as labeled.

In Figure 6-2,  $\alpha_5$  heme-Fe(II)NO is observed in all spectra collected at pH 4.9, protons being an allosteric effector of hemoglobin that induces T-state. At pH 6.8, the  $\text{Hb}(\text{NO})_4$  spectrum shows no evidence of pentacoordinate heme-Fe(II)NO, ligands and oxidation (e.g.  $\text{O}_2$ , NO, Fe(III)) being homotropic allosteric effectors of R-state when occupying greater than 50% of a tetramer's heme sites. Oxidation of  $\text{Hb}(\text{NO})_4$  to  $\text{Hb}[\alpha(\text{NO})_2\beta(\text{Met})_2]$  results in the formation of a minor population of  $\alpha_5$  heme-Fe(II)NO, indicating that ligands are not distributed homogeneously across all tetramers. Anaerobic reduction of the oxidized hemes vacates 50% of the heme sites giving  $\text{Hb}[\alpha(\text{NO})_2\beta(\text{Fe}(\text{II}))_2]$  and inducing the conformational change to T-state, evidenced by the spectral changes. Conversion to T-state effected by removal of ligands is

demonstrated by the addition of inositol hexaphosphate (IHP), a T-state inducer, having virtually no effect on the EPR spectrum.

#### Deoxy-Hb + Hb(NO)<sub>4</sub>

Hb(NO)<sub>4</sub> was added to deoxy-Hb with a gas-tight syringe in a 3:1 deoxy-Hb:Hb(NO)<sub>4</sub> ratio. The reaction, carried out at both pH 4.9 and 6.8 in an argon atmosphere, monitors the rearrangement of NO over time.

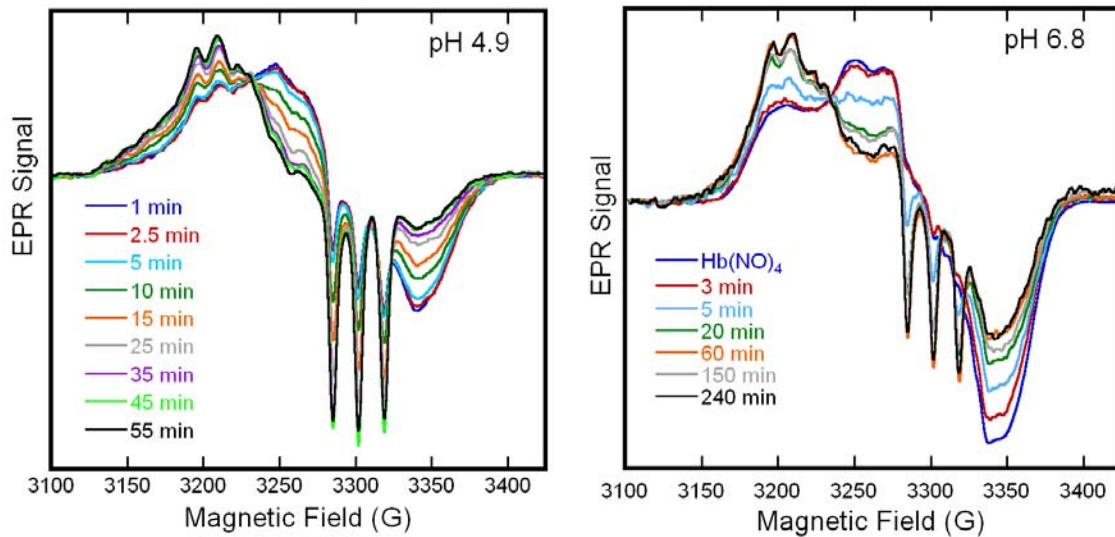


Figure 6-3: EPR spectra of a 3:1 mixture of deoxy-Hb and Hb(NO)<sub>4</sub> at various times after mixing. Samples were prepared in aqueous buffer at pH 4.9 and 6.8, as labeled.

The initial EPR spectra show that at pH 4.9, Hb(NO)<sub>4</sub> is composed of 50%  $\alpha_5$  heme-Fe(II)NO and 50%  $\beta$  heme-Fe(II)NO, whereas at pH 6.8, Hb(NO)<sub>4</sub> is composed of 50%  $\alpha_6$  heme-Fe(II)NO and 50%  $\beta$  heme-Fe(II)NO, as expected. The addition of Hb(NO)<sub>4</sub> to deoxy-Hb results in the net dissociation of NO ligands from  $\beta$  hemes and the migration of NO to vacant  $\alpha$  heme sites. Additionally, at pH 4.9, there is no evidence of hexacoordinate  $\alpha$  heme-Fe(II)NO being formed throughout the reaction. In contrast,

significant amounts of  $\alpha_6$  heme-Fe(II)NO are found to be present when the reaction is carried out at pH 6.8.

#### Deoxy-Hb + DEANO

A ~15  $\mu$ L aliquot of DEANO, a NO-donor, dissolved in 10 mM KOH was added via gas-tight syringe to deoxy-Hb in a 10:1 deoxy-Hb:NO ratio. The reaction was carried out anaerobically at both pH 4.9 and 6.8. The distribution of NO was monitored at various time intervals by EPR spectroscopy.

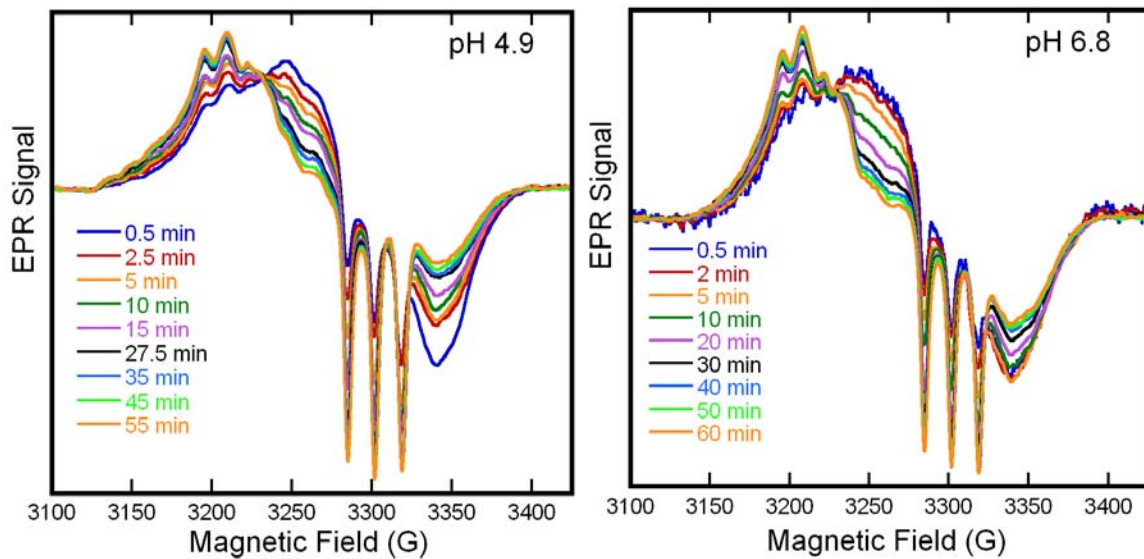


Figure 6-4: EPR spectra of aqueous solutions of deoxy-Hb and DEANO, in a 10:1 heme to NO ratio. Samples were prepared at pH 4.9 and 6.8 with aliquots extracted at various times after DEANO addition, as labeled.

The rate of DEANO decomposition to NO is pH dependent, with a half-life of 16 minutes at pH 7.4 (295 K) and nearly instantaneous at pH 5 [123]. Therefore, at pH 4.9, DEANO addition is comparable to direct NO addition, whereas, at pH 6.8, NO addition is graded over time. This is evidenced by the different noise levels in the 0.5 min spectra, the pH 6.8 spectrum having limited NO signal early in the reaction compared to the pH

4.9 spectrum (spectra are normalized). Despite the rate of NO addition, at both pH 4.9 and 6.8, the initial ratio of  $\alpha$  heme-Fe(II)NO to  $\beta$  heme-Fe(II)NO is roughly 1:1, consistent with the equal rates of NO addition to  $\alpha$  and  $\beta$  subunits determined by others [124].

Essentially, all of the  $\alpha$  heme-Fe(II)NO's are in the pentacoordinate form at pH 4.9 and 6.8. The Hb tetramers remain in the T-state as a result of the increased proton concentration at pH 4.9 sample and, in the pH 6.8 sample, the NO concentration being too limited to achieve >50% ligation per tetramer. As the reactions proceed, there is a net loss of  $\beta$  heme-Fe(II)NO signal and gain of  $\alpha_5$  heme-Fe(II)NO signal per nitrosyl-heme, with a striking absence of  $\alpha_6$  heme-Fe(II)NO signal at either pH. Additionally, the similarity of the EPR spectra in both panels underscores the efficacy of both heme vacancies and low pH as T-state allosteric effectors.

### Discussion

Earlier work by Luchsinger and coworkers demonstrated that the oxidation of Hb(NO)<sub>4</sub> by K<sub>3</sub>Fe(CN)<sub>6</sub> resulted in the preferential oxidation of the  $\beta$  heme-Fe(II)NO over  $\alpha$  heme-Fe(II)NO [30,125]. Herold and Rock [126] determined the first— and rate limiting— step of Hb(NO)<sub>4</sub> oxidation by O<sub>2</sub> to be the dissociation of NO from heme-Fe(II). Using UV-Vis spectroscopy, they determined the dissociation of heme-Fe(II)NO to be biphasic, assigning the faster rate to the  $\alpha$ -subunit and the slower rate to the  $\beta$ -subunit [126]. The assignment of the faster rate to the  $\alpha$ -subunit is in conflict with the EPR spectra presented here. The oxidation of Hb(NO)<sub>4</sub> by O<sub>2</sub> shows clear  $\beta$ -subunit preference (Figure 6-2). Furthermore, while the rate of NO association to each subunit is

similar, as shown in Figure 6-4 and elsewhere [124], the redistribution of NO to vacant heme sites (Figures 6-3 and 6-4) favors the  $\alpha$ -subunit, consistent with  $\alpha$  heme-Fe(II)NO to have a slower rate of dissociation than  $\beta$  heme-Fe(II)NO. This conclusion is in agreement with other studies on the rate of heme-Fe(II)NO dissociation [127-129].

Joshi et al. investigated the effect of the means of NO addition, comparing the direct addition of NO(aq) versus an NO donor on product formation in the reaction of NO with oxy-Hb [130]. They found bolus addition of NO resulted in a different product distribution than NO donor addition, where the delayed release allows for the “pre-mixing” of NO throughout the Hb solution. Interestingly, our results with DEANO, are essentially identical to those of Hille and co-workers [128], who made analogous measurements of the nitrosyl-heme distributions following direct addition of NO(aq) to deoxy-Hb (at 10% NO saturation). Also, similar heme-Fe(II)NO distributions result from the addition of DEANO to deoxy-Hb at pH 6.8 and at pH 4.9, the lower pH effectively producing direct NO addition. Therefore, it appears that direct addition of NO to Hb does not necessarily lead to bolus artifacts.

Prior to ligand binding, the iron-nitrogen bond between the heme-iron and proximal imidazole-nitrogen is intact [131,132]. In T-state, binding ligands such as NO or CO induces the cleavage of proximal histidine-iron bond, changing from a 6-coordinate configuration to 5-coordinate. In the addition of DEANO to deoxy-Hb (Figure 6-4), the absence of  $\alpha_6$  heme-Fe(II)NO at pH 6.8 suggests that the transformation from hexacoordinate to pentacoordinate is rapid and must proceed faster than dissociation of NO from  $\beta$  heme-Fe(II)NO and the subsequent binding of NO to an  $\alpha$  heme. This, however, is not surprising given the sluggish rate of NO dissociation [127-129], as

discussed above. Furthermore, these data also suggest that in the addition of Hb(NO)<sub>4</sub> to deoxy-Hb (Figure 6-3), the  $\alpha_6$  heme-Fe(II)NO measured is the initial, and declining, population of hexacoordinate  $\alpha$  Fe(II)NO in R-state tetramers.

### Conclusions

We have identified synthetic routes for generating Hb[ $\alpha$ (NO)<sub>2</sub> $\beta$ (Met)<sub>2</sub>] hybrids and have converted them to Hb[ $\alpha_5$ (NO)<sub>2</sub> $\beta$ (Met)<sub>2</sub>] with T-state allosteric effectors. Reduction of the  $\beta$  Met-hemes in Hb[ $\alpha$ (NO)<sub>2</sub> $\beta$ (Met)<sub>2</sub>] furnishes Hb[ $\alpha_5$ (NO)<sub>2</sub> $\beta$ (Fe(II))<sub>2</sub>] with pentacoordinate  $\alpha$  heme-Fe(II)NO.

The reaction of Hb(NO)<sub>4</sub> with deoxy-Hb at pH 4.9 and the addition of DEANO to deoxy-Hb at both pH 4.9 and 6.8 show very similar reaction profiles, including the absence of  $\alpha_6$  heme-Fe(II)NO. This result indicates that the conversion from hexacoordinate  $\alpha$  heme-Fe(II)NO species to the pentacoordinate species must proceed at a rate significantly faster than the dissociation of NO from  $\beta$  subunits.

Hexacoordinate  $\alpha$  heme-Fe(II)NO signal is present only in the mixture of Hb(NO)<sub>4</sub> with deoxy-Hb at pH 6.8; evidently these derive only from the Hb(NO)<sub>4</sub> tetramers originally present and are not conserved in the NO migration in these experiments.

In the reaction of DEANO and deoxy-Hb, our results, in conjunction with those of Hille et al. [128], indicate that bolus artifacts should not be considered inevitable with the use of direct NO(aq) addition to Hb solutions. Moreover, the similarity of the reaction of DEANO with deoxy-Hb at pH 6.8 with the reaction at pH 4.9 illustrates the efficacy of vacant heme site in the induction of T-state.

## CHAPTER 7

## CONCLUSION

Electron paramagnetic resonance spectroscopy has been conducted at multiple frequencies and various temperatures to characterize a multiplicity of human hemoglobin adducts.

The spectrum of Met-Hb:NO<sub>2</sub><sup>-</sup> was determined to be the composite of the spectra of two distinct Met-Hb:NO<sub>2</sub><sup>-</sup> species, labeled as Species A and B. The two species appear to be the result of differences in the distal heme pockets of the  $\alpha$ - and  $\beta$ -subunits. Through the creation of [Fe(II)NO/Fe(III)NO<sub>2</sub><sup>-</sup>]-Hb hybrids, it was concluded that the  $\alpha$ -subunit is found only as Species A, while the  $\beta$ -subunit is competent for interconversion between Species A and B. The interconversion of the  $\beta$ -subunit is pH dependent and proposed to be the result of the pH induced rotation of the  $\beta$ His63 histidine residue, which projects into the distal heme pocket. Additional work, such as determination of the pH dependence of Met-Hb:NO<sub>2</sub><sup>-</sup> by ENDOR spectroscopy, is necessary to further elucidate the nature of the interconversion of Species A and B.

The low affinity of Met-Hb for nitrite, as determined by UV-Vis spectroscopy in earlier studies, was confirmed by direct measurement of the Met-Hb:NO<sub>2</sub><sup>-</sup> species by EPR spectroscopy. The low affinity of Met-Hb for nitrite makes a direct role for Met-Hb:NO<sub>2</sub><sup>-</sup> in hypoxic vasodilation implausible. Furthermore, this work illustrates the potential and necessity of detailed spectral simulation and least-squares fitting when quantitating species measured by EPR spectroscopy— especially in systems containing species with different spin states.

Using the  $g$ -values from the EPR spectra of the two Met-Hb:NO<sub>2</sub><sup>-</sup> species, the coefficients of the ground state wavefunction for each species were calculated. In both Met-Hb:NO<sub>2</sub><sup>-</sup> species, the majority of unpaired electron density was found to be localized in the iron 3d<sub>xy</sub> orbital. While the hierarchy of the t<sub>2g</sub> orbitals in both Met-Hb:NO<sub>2</sub><sup>-</sup> species is identical, the splittings between the orbitals are distinct in each species. The slight disparity in the ground state wavefunctions of the two species presumably arises from differences in nitrite orientation.

Multiple species were detected in the EPR spectrum of neat Met-Hb in aqueous solution, consistent with previous studies. The differences observed when using PBS buffer versus HEPES buffer appear to be the result of the pH artifact associated with freezing PBS buffered, aqueous solutions. Furthermore, the temperature dependent interconversion of the major bis-histidine Met-Hb species and aquo-Met-Hb bolsters the proposition that a water molecule resides in the distal heme pocket of the predominate bis-histidine Met-Hb complex.

The W-band EPR spectra of Hb(NO)<sub>4</sub> presented herein provide increased resolution over previous lower frequency EPR spectra. At all temperatures employed in this study, the Hb(NO)<sub>4</sub> spectrum was a composite of rhombic and axial species. At temperatures below 130 K, rhombic contributions dominated the Hb(NO)<sub>4</sub> spectrum. Above 130 K, the Hb(NO)<sub>4</sub> spectrum was predominately axial. The temperature dependent conversion from a rhombic conformation to an axial conformation is gradual, with a continuum of intermediate species between the rhombic and axial limits. While the  $\alpha$ - and  $\beta$ -subunits each have distinct critical temperatures for rhombic to axial conversion, no evidence was found for distinct subunit spectra. Also, though the minor

features which are only observed at low temperatures were best modeled by an axial spectrum, additional work is needed to determine that precise nature of these features.

Finally, methods for the generation of  $[\alpha(\text{NO})_2\beta(\text{Met})_2]\text{-Hb}$  and  $[\alpha(\text{NO})_2\beta(\text{Fe(II)})_2]\text{-Hb}$  hybrids, including T-state tetramers with pentacoordinate  $\alpha$  heme- $\text{Fe(II)NO}$ , have been presented. The similarity between the results observed with direct  $\text{NO(aq)}$  addition and time-release NO donors reveals that bolus artifacts may not be as pervasive as suggested by others. Moreover, the study of these hybrid hemoglobins underscores the efficacy of heme vacancies as modulators of T-state conformation.

REFERENCES CITED

1. Allen, B. W.; Stamler, J. S.; Piantadosi, C. A., Hemoglobin, Nitric Oxide and Molecular Mechanisms of Hypoxic Vasodilation. *Trends Mol Med* 2009, 15, (10), 452-460.
2. Perutz, M. F.; Rossmann, M. G.; Cullis, A. F.; Muirhead, H.; Will, G.; North, A. C. T., Structure of Haemoglobin - 3-Dimensional Fourier Synthesis at 5.5-Å Resolution, Obtained by X-Ray Analysis. *Nature* 1960, 185, (4711), 416-422.
3. Monod, J.; Wyman, J.; Changeaux, J. P., *The Journal of Molecular Biology* 1965, 12, 88-118.
4. Imai, K., *Allosteric Effects in Haemoglobin*. Cambridge University Press: Cambridge, 1982.
5. Chan, N. L.; Kavanaugh, J. S.; Rogers, P. H.; Arnone, A., Crystallographic Analysis of the Interaction of Nitric Oxide with Quaternary-T Human Hemoglobin. *Biochemistry* 2004, 43, (1), 118-132.
6. Chan, N. L.; Rogers, P. H.; Arnone, A., Crystal Structure of the S-Nitroso Form of Liganded Human Hemoglobin. *Biochemistry* 1998, 37, (47), 16459-16464.
7. McMahan, T. J.; Exton Stone, A.; Bonaventura, J.; Singel, D. J.; Solomon Stamler, J., Functional Coupling of Oxygen Binding and Vasoactivity in S-Nitrosohemoglobin. *J Biol Chem* 2000, 275, (22), 16738-16745.
8. McMahan, T. J.; Moon, R. E.; Luchsinger, B. P.; Carraway, M. S.; Stone, A. E.; Stolp, B. W.; Gow, A. J.; Pawloski, J. R.; Watke, P.; Singel, D. J.; Piantadosi, C. A.; Stamler, J. S., Nitric Oxide in the Human Respiratory Cycle. *Nat Med* 2002, 8, (7), 711-717.
9. Gonzalez-Alonso, J.; Richardson, R. S.; Saltin, B., Exercising Skeletal Muscle Blood Flow in Humans Responds to Reduction in Arterial Oxyhaemoglobin, but Not to Altered Free Oxygen. *J Physiol* 2001, 530, (Pt 2), 331-341.
10. Roach, R. C.; Koskolou, M. D.; Calbet, J. A.; Saltin, B., Arterial O<sub>2</sub> Content and Tension in Regulation of Cardiac Output and Leg Blood Flow During Exercise in Humans. *Am J Physiol* 1999, 276, (2 Pt 2), H438-445.
11. Ignarro, L. J.; Buga, G. M.; Wood, K. S.; Byrns, R. E.; Chaudhuri, G., Endothelium-Derived Relaxing Factor Produced and Released from Artery and Vein Is Nitric Oxide. *Proc. Natl. Acad. Sci. USA* 1987, 84, 9265-9269.
12. Palmer, R. M.; Ferrige, A. G.; Moncada, S., Nitric Oxide Release Accounts for the Biological Activity of Endothelium-Derived Relaxing Factor. *Nature* 1987, 327, 524-526.

13. Ingram, D. J. E.; Bennett, J. E., Paramagnetic Resonance in Phthalocyanine, Haemoglobin, and Other Organic Derivatives. *Discussion of the Faraday Society* 1955, 19, 140-146.
14. Antonini, E.; Brunori, M., *Hemoglobin and Myoglobin in Their Reactions with Ligands*. North Holland Publishing Company: 1971; Vol. 21, p 436.
15. Jungersten, L.; Ambring, A.; Wall, B.; Wennmalm, A., Both Physical Fitness and Acute Exercise Regulate Nitric Oxide Formation in Healthy Humans. *J Appl Physiol* 1997, 82, (3), 760-764.
16. Reutov, V. P., Nitric Oxide Cycle in Mammals and the Cyclicity Principle. *Biochemistry (Mosc)* 2002, 67, (3), 293-311.
17. Liao, J. C.; Hein, T. W.; Vaughn, M. W.; Huang, K. T.; Kuo, L., Intravascular Flow Decreases Erythrocyte Consumption of Nitric Oxide. *Proc Natl Acad Sci U S A* 1999, 96, (15), 8757-8761.
18. Liu, X.; Miller, M. J.; Joshi, M. S.; Sadowska-Krowicka, H.; Clark, D. A.; Lancaster, J. R., Jr., Diffusion-Limited Reaction of Free Nitric Oxide with Erythrocytes. *J Biol Chem* 1998, 273, (30), 18709-18713.
19. Liu, X.; Samouilov, A.; Lancaster, J. R., Jr.; Zweier, J. L., Nitric Oxide Uptake by Erythrocytes Is Primarily Limited by Extracellular Diffusion Not Membrane Resistance. *J Biol Chem* 2002, 277, (29), 26194-26199.
20. Tsoukias, N. M.; Popel, A. S., Erythrocyte Consumption of Nitric Oxide in Presence and Absence of Plasma-Based Hemoglobin. *Am J Physiol Heart Circ Physiol* 2002, 282, (6), H2265-2277.
21. Tsoukias, N. M.; Popel, A. S., A Model of Nitric Oxide Capillary Exchange. *Microcirculation* 2003, 10, (6), 479-495.
22. Foster, M. W.; McMahon, T. J.; Stamler, J. S., S-Nitrosylation in Health and Disease. *Trends Mol Med* 2003, 9, (4), 160-168.
23. Gaston, B.; Drazen, J. M.; Jansen, A.; Sugarbaker, D. A.; Loscalzo, J.; Richards, W.; Stamler, J. S., Relaxation of Human Bronchial Smooth Muscle by S-Nitrosothiols in Vitro. *J Pharmacol Exp Ther* 1994, 268, (2), 978-984.
24. Stamler, J. S., S-Nitrosothiols and the Bioregulatory Actions of Nitrogen Oxides through Reactions with Thiol Groups. *Curr Top Microbiol Immunol* 1995, 196, 19-36.

25. Stamler, J. S.; Jaraki, O.; Osborne, J.; Simon, D. I.; Keaney, J.; Vita, J.; Singel, D.; Valeri, C. R.; Loscalzo, J., Nitric Oxide Circulates in Mammalian Plasma Primarily as an S-Nitroso Adduct of Serum Albumin. *Proc Natl Acad Sci U S A* 1992, 89, (16), 7674-7677.
26. Stamler, J. S.; Simon, D. I.; Osborne, J. A.; Mullins, M. E.; Jaraki, O.; Michel, T.; Singel, D. J.; Loscalzo, J., S-Nitrosylation of Proteins with Nitric Oxide: Synthesis and Characterization of Biologically Active Compounds. *Proc Natl Acad Sci U S A* 1992, 89, (1), 444-448.
27. Jia, L.; Bonaventura, C.; Bonaventura, J.; Stamler, J. S., S-Nitrosohaemoglobin: A Dynamic Activity of Blood Involved in Vascular Control [See Comments]. *Nature* 1996, 380, (6571), 221-226.
28. Hess, D. T.; Matsumoto, A.; Kim, S. O.; Marshall, H. E.; Stamler, J. S., Protein S-Nitrosylation: Purview and Parameters. *Nat Rev Mol Cell Biol* 2005, 6, (2), 150-166.
29. Stamler, J. S.; Jia, L.; Eu, J. P.; McMahon, T. J.; Demchenko, I. T.; Bonaventura, J.; Gernert, K.; Piantadosi, C. A., Blood Flow Regulation by S-Nitrosohemoglobin in the Physiological Oxygen Gradient. *Science* 1997, 276, (5321), 2034-2037.
30. Luchsinger, B. P.; Rich, E. N.; Gow, A. J.; Williams, E. M.; Stamler, J. S.; Singel, D. J., Routes to S-Nitroso-Hemoglobin Formation with Heme Redox and Preferential Reactivity in the Beta Subunits. *Proc Natl Acad Sci U S A* 2003, 100, (2), 461-466.
31. Bodansky, O., Methemoglobinemia and Methemoglobin-Producing Compounds. *Pharmacol Rev* 1951, 3, (2), 144-196.
32. Rachmilewitz, E. A.; Peisach, J.; Blumberg, W. E., Studies on the Stability of Oxyhemoglobin a and Its Constituent Chains and Their Derivatives. *J Biol Chem* 1971, 246, (10), 3356-3366.
33. Blumberg, W.; Peisach, J., Low-Spin Compounds of Heme Proteins. *Adv. Chem. Ser.* 1971, 100 271-291.
34. Arnold, E. V.; Bohle, D. S.; Jordan, P. A., Reversible and Irreversible Hemichrome Generation by the Oxygenation of Nitrosylmyoglobin. *Biochemistry* 1999, 38, (15), 4750-4756.
35. Griffith, J. S., Theory of EPR in Low-Spin Ferric Haemoproteins. *Mol Phys* 1971, 21, (1), 135-139.

36. Mellmann, L. Ph.D. Thesis, Montana State University, Bozeman, MT, 2009.
37. Peisach, J.; Blumberg, W. E.; Adler, A., Electron Paramagnetic Resonance Studies of Iron Porphin and Chlorin Systems. *Ann N Y Acad Sci* 1973, 206, 310-327.
38. Walker, F. A., Magnetic Spectroscopic (EPR, ESEEM, Mossbauer, MCD and NMR) Studies of Low-Spin Ferriheme Centers and Their Corresponding Heme Proteins. *Coordin Chem Rev* 1999, 186, 471-534.
39. Weichsel, A.; Maes, E. M.; Andersen, J. F.; Valenzuela, J. G.; Shokhireva, T. K.; Walker, F. A.; Montfort, W. R., Heme-Assisted S-Nitrosation of a Proximal Thiolate in a Nitric Oxide Transport Protein. *Proc Natl Acad Sci U S A* 2005, 102, 594-599.
40. Uchida, H.; Berliner, L. J.; Klapper, M. H., Three New Iron-Ligand Complexes of Human Methemoglobin A. *J Biol Chem* 1970, 245, (18), 4606-4611.
41. Rodkey, F. L., Mechanism for Conversion of Oxyhemoglobin to Methemoglobin by Nitrite. *Clin Chem* 1976, 22, (12), 1986-1990.
42. Smith, R. P., Nitrite Methemoglobin Complex - Its Significance in Methemoglobin Analyses and Its Possible Role in Methemoglobinemia. *Biochem Pharmacol* 1967, 16, (9), 1655-&.
43. Wanat, A.; Gdula-Argasinska, J.; Rutkowska-Zbik, D.; Witko, M.; Stochel, G.; van Eldik, R., Nitrite Binding to Metmyoglobin and Methemoglobin in Comparison to Nitric Oxide Binding. *J Biol Inorg Chem* 2002, 7, (1-2), 165-176.
44. Cosby, K.; Partovi, K. S.; Crawford, J. H.; Patel, R. P.; Reiter, C. D.; Martyr, S.; Yang, B. K.; Waclawiw, M. A.; Zalos, G.; Xu, X.; Huang, K. T.; Shields, H.; Kim-Shapiro, D. B.; Schechter, A. N.; Cannon, R. O.; Gladwin, M. T., Nitrite Reduction to Nitric Oxide by Deoxyhemoglobin Vasodilates the Human Circulation. *Nat Med* 2003, 9, (12), 1498-1505.
45. Reutov, V. P.; Sorokina, E. G., NO-Synthase and Nitrite-Reductase Components of Nitric Oxide Cycle. *Biochemistry (Mosc)* 1998, 63, (7), 874-884.
46. Basu, S.; Grubina, R.; Huang, J.; Conradie, J.; Huang, Z.; Jeffers, A.; Jiang, A.; He, X.; Azarov, I.; Seibert, R.; Mehta, A.; Patel, R.; King, S. B.; Hogg, N.; Ghosh, A.; Gladwin, M. T.; Kim-Shapiro, D. B., Catalytic Generation of N<sub>2</sub>O<sub>3</sub> by the Concerted Nitrite Reductase and Anhydrase Activity of Hemoglobin. *Nat Chem Biol* 2007, 3, (12), 785-794.

47. Huang, K. T.; Keszler, A.; Patel, N.; Patel, R. P.; Gladwin, M. T.; Kim-Shapiro, D. B.; Hogg, N., The Reaction between Nitrite and Deoxyhemoglobin. Reassessment of Reaction Kinetics and Stoichiometry. *J Biol Chem* 2005, 280, (35), 31126-31131.
48. Doyle, M. P.; Pickering, R. A.; DeWeert, T. M.; Hoekstra, J. W.; Pater, D., Kinetics and Mechanism of the Oxidation of Human Deoxyhemoglobin by Nitrites. *J Biol Chem* 1981, 256, (23), 12393-12398.
49. Luchsinger, B. P.; Rich, E. N.; Yan, Y.; Williams, E. M.; Stamler, J. S.; Singel, D. J., Assessments of the Chemistry and Vasodilatory Activity of Nitrite with Hemoglobin under Physiologically Relevant Conditions. *J Inorg Biochem* 2005, 99, (4), 912-921.
50. Huang, Z.; Shiva, S.; Kim-Shapiro, D. B.; Patel, R. P.; Ringwood, L. A.; Irby, C. E.; Huang, K. T.; Ho, C.; Hogg, N.; Schechter, A. N.; Gladwin, M. T., Enzymatic Function of Hemoglobin as a Nitrite Reductase That Produces NO under Allosteric Control. *J Clin Invest* 2005, 115, (8), 2099-2107.
51. Nagababu, E.; Ramasamy, S.; Abernethy, D. R.; Rifkind, J. M., Active Nitric Oxide Produced in the Red Cell under Hypoxic Conditions by Deoxyhemoglobin-Mediated Nitrite Reduction. *J Biol Chem* 2003, 278, (47), 46349-46356.
52. Angelo, R. M.; Singel, D. J.; Stamler, J. S., An S-Nitrosothiol (SNO) Synthase Function of Hemoglobin That Employs Nitrite as a Substrate. *Proc. Natl. Acad. USA* 2006, 103, (22), 8366-8371.
53. Goetz, B. I.; Wang, P.; Shields, H. W.; Basu, S.; Grubina, R.; Huang, J.; Conradie, J.; Huang, Z.; Jeffers, A.; Jiang, A.; He, X.; Azarov, I.; Seibert, R.; Mehta, A.; Patel, R.; King, S. B.; Ghosh, A.; Hogg, N.; Gladwin, M. T.; Kim-Shapiro, D. B., Nitrite-Methemoglobin Inadequate for Hypoxic Vasodilation Reply. *Nat Chem Biol* 2009, 5, (6), 367-367.
54. Schwab, D. E.; Stamler, J. S.; Singel, D. J., Nitrite-Methemoglobin Inadequate for Hypoxic Vasodilation. *Nat Chem Biol* 2009, 5, (6), 366-366.
55. Crawford, J. H.; Isbell, T. S.; Huang, Z.; Shiva, S.; Chacko, B. K.; Schechter, A. N.; Darley-Usmar, V. M.; Kerby, J. D.; Lang, J. D., Jr.; Kraus, D.; Ho, C.; Gladwin, M. T.; Patel, R. P., Hypoxia, Red Blood Cells, and Nitrite Regulate NO-Dependent Hypoxic Vasodilation. *Blood* 2006, 107, (2), 566-574.
56. Hunter, C. J.; Dejam, A.; Blood, A. B.; Shields, H.; Kim-Shapiro, D. B.; Machado, R. F.; Tarekegn, S.; Mulla, N.; Hopper, A. O.; Schechter, A. N.; Power, G. G.; Gladwin, M. T., Inhaled Nebulized Nitrite Is a Hypoxia-Sensitive NO-Dependent Selective Pulmonary Vasodilator. *Nat Med* 2004, 10, (10), 1122-1127.

57. Diesen, D. L.; Hess, D. T.; Stamler, J. S., Hypoxic Vasodilation by Red Blood Cells: Evidence for an S-Nitrosothiol-Based Signal. *Circ Res* 2008, 103, (5), 545-553.
58. Young, L. J.; Siegel, L. M., On the Reaction of Ferric Heme Proteins with Nitrite and Sulfite. *Biochemistry* 1988, 27, (8), 2790-2800.
59. Peisach, J.; Blumberg, W. E.; Ogawa, S.; Rachmilewitz, E. A.; Oltzik, R., The Effects of Protein Conformation on the Heme Symmetry in High Spin Ferric Heme Proteins as Studied by Electron Paramagnetic Resonance. *J Biol Chem* 1971, 246, (10), 3342-3355.
60. Yi, J.; Safo, M. K.; Richter-Addo, G. B., The Nitrite Anion Binds to Human Hemoglobin Via the Uncommon O-Nitrito Mode. *Biochemistry* 2008, 47, (32), 8247-8249.
61. Geraci, G.; Parkhurst, L. J.; Gibson, Q. H., Preparation and Properties of Alpha- and Beta-Chains from Human Hemoglobin. *Journal of Biological Chemistry* 1969, 244, (17), 4664-&.
62. Orii, Y.; Morita, M., Measurement of the pH of Frozen Buffer Solutions by Using pH Indicators. *J. Biochem.* 1977, 812, 163-168.
63. Williams-Smith, D. L.; Bray, R. C.; Barber, M. J.; Tsopanakis, A. D.; Vincent, S. P., Changes in the Apparent pH on Freezing Aqueous Buffer Solutions and Their Relevance to Biochemical Electron-Paramagnetic Resonance Spectroscopy. *Biochem Journ.* 1977, 167, 593-600.
64. Gow, A. J.; Luchsinger, B. P.; Pawloski, J. R.; Singel, D. J.; Stamler, J. S., The Oxyhemoglobin Reaction of Nitric Oxide. *Proc Natl Acad Sci U S A* 1999, 96, (16), 9027-9032.
65. Glasoe, P. K. L., F.A., Use of Glass Electrodes to Measure Acidities in Deuterium Oxide. *The Journal of Physical Chemistry* 1960, 64, (1), 188-190.
66. Stoll, S.; Schweiger, A., Easyspin, a Comprehensive Software Package for Spectral Simulation and Analysis in EPR. *J Magn Reson* 2006, 178, (1), 42-55.
67. Svistunenko, D. A.; Sharpe, M. A.; Nicholls, P.; Blenkinsop, C.; Davies, N. A.; Dunne, J.; Wilson, M. T.; Cooper, C. E., The pH Dependence of Naturally Occurring Low-Spin Forms of Methaemoglobin and Metmyoglobin: An EPR Study. *Biochem J* 2000, 351 Pt 3, 595-605.

68. Flores, M.; Wajnberg, E.; Bemski, G., Temperature Dependence of Q-Band Electron Paramagnetic Resonance Spectra of Nitrosyl Heme Proteins. *Biophys J* 1997, 73, (6), 3225-3229.
69. Huttermann, J.; Burgard, C.; Kappl, R., Proton Endor from Randomly Oriented NO-Ligated Haemoglobin: Approaching the Structural Basis for the R-T Transition. *J. Chem. Soc. Faraday Trans.* 1994, 90, 3077-3087.
70. Morse, R. H.; Chan, S. I., Electron Paramagnetic Resonance Studies of Nitrosyl Ferrous Heme Complexes. Determination of an Equilibrium between Two Conformations. *J Biol Chem* 1980, 255, (16), 7876-7882.
71. Hill, A. V., Proceedings of the Physiological Society: January 22, 1910. *The Journal of Physiology* 40, (Suppl), i-vii.
72. Coryell, C. D. S., F.; Pauling, L., The Magnetic Properties and Structure of Ferrihemoglobin (Methemoglobin) and Some of Its Compounds. *J. Am. Chem. Soc.* 1937, 59, 633-642.
73. Okonjo, K. O.; Vega-Catalan, F. J., The Uptake of Protons by Heme-Linked Ionizable Groups on Azide Binding to Methemoglobin. *Eur J Biochem* 1987, 169, (2), 413-416.
74. Dickinson, L. C.; Chien, J. C. W., Electron-Paramagnetic Resonance of Single-Crystal N-15 Nitrosyl-Fe-57 Myoglobin. *Biochemical and Biophysical Research Communications* 1974, 59, (4), 1292-1297.
75. Doetschman, D. C.; Utterback, S. G., Electron-Paramagnetic Resonance Study of Nitrosylhemoglobin and Its Chemistry in Single-Crystals. *Journal of the American Chemical Society* 1981, 103, (10), 2847-2852.
76. Jenkins, J. D.; Musayev, F. N.; Danso-Danquah, R.; Abraham, D. J.; Safo, M. K., Structure of Relaxed-State Human Hemoglobin: Insight into Ligand Uptake, Transport and Release. *Acta Crystallogr D Biol Crystallogr* 2009, 65, (Pt 1), 41-48.
77. Perutz, M. F., Stereochemistry of Cooperative Effects in Haemoglobin. *Nature* 1970, 228, (5273), 726-739.
78. Perutz, M. F.; Wilkinson, A. J.; Paoli, M.; Dodson, G. G., The Stereochemical Mechanism of the Cooperative Effects in Hemoglobin Revisited. *Annu Rev Biophys Biomol Struct* 1998, 27, 1-34.
79. Akiyama, K.; Fukuda, M.; Kobayashi, N.; Matsuoka, A.; Shikama, K., The pH-Dependent Swinging-out of the Distal Histidine Residue in Ferric Hemoglobin of

- a Midge Larva (Tokunagayusurika Akamusi). *Biochim Biophys Acta* 1994, 1208, (2), 306-309.
80. Geibel, J.; Chang, C. K.; Traylor, T. G., Letter: Coordination of Myoglobin Active Site Models in Aqueous Solution as Studied by Kinetic Methods. *J Am Chem Soc* 1975, 97, (20), 5924-5926.
  81. Tian, W. D.; Sage, J. T.; Champion, P. M., Investigations of Ligand Association and Dissociation Rates in The "Open" And "Closed" States of Myoglobin. *J Mol Biol* 1993, 233, (1), 155-166.
  82. Vallone, B.; Nienhaus, K.; Matthes, A.; Brunori, M.; Nienhaus, G. U., The Structure of Carbonmonoxy Neuroglobin Reveals a Heme-Sliding Mechanism for Control of Ligand Affinity. *Proc Natl Acad Sci U S A* 2004, 101, (50), 17351-17356.
  83. Kamimura, S.; Matsuoka, A.; Imai, K.; Shikama, K., The Swinging Movement of the Distal Histidine Residue and the Autoxidation Reaction for Midge Larval Hemoglobins. *Eur J Biochem* 2003, 270, (7), 1424-1433.
  84. Tsuruga, M.; Matsuoka, A.; Hachimori, A.; Sugawara, Y.; Shikama, K., The Molecular Mechanism of Autoxidation for Human Oxyhemoglobin. Tilting of the Distal Histidine Causes Nonequivalent Oxidation in the Beta Chain. *J Biol Chem* 1998, 273, (15), 8607-8615.
  85. da Silva, G.; Kennedy, E. M.; Dlugogorski, B. Z., Ab Initio Procedure for Aqueous-Phase pKa Calculation: The Acidity of Nitrous Acid. *J Phys Chem A* 2006, 110, (39), 11371-11376.
  86. Hollocher, T. C.; Buckley, L. M., Electron Spin Resonance Studies of Native and Denatured Methemoglobin. pH Effects. *J Biol Chem* 1966, 241, (12), 2976-2980.
  87. Munoz, G.; de Juan, A., pH- and Time-Dependent Hemoglobin Transitions: A Case Study for Process Modelling. *Anal Chim Acta* 2007, 595, (1-2), 198-208.
  88. Haurowitz, F.; Hardin, R. L.; Dicks, M., Denaturation of Hemoglobins by Alkali. *Journal of Physical Chemistry* 1954, 58, (2), 103-105.
  89. Bleaney, B.; O'Brien, M. C. M., Paramagnetic Resonance in Some Complex Cyanides of the Iron Group. *Proc. Phys. Soc., London, Section B* 1956, 69, 1216-1230.
  90. Griffith, J. S., Theory of Electron Resonance in Ferrihaemoglobin Azide. *Nature* 1957, 180, (4575), 30-31.

91. Taylor, C. P. S., The EPR of Low Spin Heme Complexes: Relation of the T<sub>2g</sub> Hole Model to the Directional Properties of the G Tensor, and a New Method for Calculating the Ligand Field Parameters. *Biochimica et Biophysica Acta* 1977, 491, 137-149.
92. Gibson, J. F.; Ingram, D. J., Electron Resonance Studies of Haemoglobin Azide and Hydroxide Derivatives. *Nature* 1957, 180, (4575), 29-30.
93. McGarvey, B. R., Survey of Ligand Field Parameters of Strong Field d<sup>5</sup> Complexes Obtained from the g Matrix. *Coordin Chem Rev* 1998, 170, 75-92.
94. Hori, H., Analysis of the Principle G-Tensors in Single Crystals of Ferrimyoglobin Complexes. *Biochim Biophys Acta* 1971, 251, 227-235.
95. Wallace, W. J.; Houtchens, R. A.; Maxwell, J. C.; Caughey, W. S., Mechanism of Autooxidation for Hemoglobins and Myoglobins. Promotion of Superoxide Production by Protons and Anions. *J Biol Chem* 1982, 257, (9), 4966-4977.
96. Singel, D. J.; Stamler, J. S., Chemical Physiology of Blood Flow Regulation by Red Blood Cells: The Role of Nitric Oxide and S-Nitrosohemoglobin. *Annu Rev Physiol* 2005, 67, 99-145.
97. Rifkind, J. M., Abugo, O., Levy, A., Heim, J., Detection, Formation, and Relevance of Hemichromes and Hemochromes. *Methods in Enzymology* 1994, 231, 449-480.
98. Viola, F.; Aime, S.; Coletta, M.; Desideri, A.; Fasano, M.; Paoletti, S.; Tarricone, C.; Ascenzi, P., Azide, Cyanide, Fluoride, Imidazole and Pyridine Binding to Ferric and Ferrous Native Horse Heart Cytochrome C and to Its Carboxymethylated Derivative: A Comparative Study. *J Inorg Biochem* 1996, 62, (3), 213-222.
99. Henry, Y.; Banerjee, R., Electron Spin Resonance Spectra of Isolated Ferrihemoglobin (Alpha, Beta and Gamma) Chains--an Attempted Correlation with Optical Absorption Spectra. *J. Mol. Biol.* 1970, 50, (1), 99-110.
100. Shiga, T.; Hwang, K. J.; Tyuma, I., Electron Paramagnetic Resonance Studies of Nitric Oxide Hemoglobin Derivatives. I. Human Hemoglobin Subunits. *Biochemistry* 1969, 8, (1), 378-383.
101. Wajnberg, E.; Bemski, G.; el-Jaick, L. J.; Alves, O. C., Nitrosyl Hemoglobins: EPR above 80 K. *Int J Biol Macromol* 1996, 18, (3), 231-235.
102. Wajnberg, E.; Linhares, M. P.; el-Jaick, L. J.; Bemski, G., Nitrosyl Hemoglobin: EPR Components at Low Temperatures. *Eur Biophys J* 1992, 21, (1), 57-61.

103. Schmidt, P. P.; Kappl, R.; Huttermann, J., On the Mode of Hexacoordinated NO-Binding to Myo- and Hemoglobin: Variable-Temperature EPR Studies at Multiple Microwave Frequencies. *Applied Magnetic Resonance* 2001, 21, 423-440.
104. Peisach, J.; Blumberg, W. E.; Wittenberg, B. A.; Wittenberg, J. B., The Electronic Structure of Protoheme Proteins. 3. Configuration of the Heme and Its Ligands. *J Biol Chem* 1968, 243, (8), 1871-1880.
105. Vergara, A.; Vitagliano, L.; Verde, C.; di Prisco, G.; Mazzarella, L., Spectroscopic and Crystallographic Characterization of Bis-Histidyl Adducts in Tetrameric Hemoglobins. *Methods Enzymol* 2008, 436, 425-444.
106. Yonetani, T.; Iizuka, T.; Waterman, M. R., Studies on Modified Hemoglobins. 3. Spin States of Ferric Hemoglobin, Semi-Hemoglobin, and Isolated Subunit Chains. *J Biol Chem* 1971, 246, (24), 7683-7689.
107. Levy, A.; Kuppusamy, P.; Rifkind, J. M., Multiple Heme Pocket Subconformations of Methemoglobin Associated with Distal Histidine Interactions. *Biochemistry* 1990, 29, (40), 9311-9316.
108. Levy, A.; Sharma, V. S.; Zhang, L.; Rifkind, J. M., A New Mode for Heme-Heme Interactions in Hemoglobin Associated with Distal Perturbations. *Biophys J* 1992, 61, (3), 750-755.
109. Brunori, M.; Amiconi, G.; Antonin, E.; Wyman, J.; Zito, R.; Fanelli, A. R., The Transition between 'Acid' and 'Alkaline' Ferric Heme Proteins. *Biochim Biophys Acta* 1968, 154, (2), 315-322.
110. Culotta, E.; Koshland, D.E., NO News Is Good News. *Science* 1992, 258, (5090), 1862-1865.
111. Allen, B. W.; Piantadosi, C. A., How Do Red Blood Cells Cause Hypoxic Vasodilation? The SNO-Hemoglobin Paradigm. *Am J Physiol Heart Circ Physiol* 2006, 291, (4), H1507-1512.
112. Nagai, K.; Hori, H.; Yoshida, S.; Sakamoto, H.; Morimoto, H., The Effect of Quaternary Structure on the State of the Alpha and Beta Subunits within Nitrosyl Haemoglobin. Low Temperature Photodissociation and the ESR Spectra. *Biochim Biophys Acta* 1978, 532, (1), 17-28.
113. Kon, H., Paramagnetic Resonance Study of Nitric Oxide Hemoglobin. *J. Biol. Chem.* 1968, 243, (16), 4350-4357.

114. Wayland, B. B.; Olson, L. W., Spectroscopic Studies and Bonding Model for Nitric Oxide Complexes of Iron Porphyrins. *J Am Chem Soc* 1974, 96, (19), 6037-6041.
115. Szabo, A.; Perutz, M. F., Equilibrium between Six- and Five-Coordinated Hemes in Nitrosylhemoglobin: Interpretation of Electron Spin Resonance Spectra. *Biochemistry* 1976, 15, (20), 4427-4428.
116. Bemski, G., Contribution of Electron Paramagnetic Resonance to the Studies of Hemoglobin: The Nitrosylhemoglobin System. *Mol Biol Rep* 1997, 24, (4), 263-269.
117. Henry, Y.; Banerjee, R., Electron Paramagnetic Studies of Nitric Oxide Haemoglobin Derivatives: Isolated Subunits and Nitric Oxide Hybrids. *J. Mol. Biol.* 1973, 73, (4), 469-482.
118. Yonetani, T.; Yamamoto, H.; Erman, J. E.; Leigh, J. S., Jr.; Reed, G. H., Electromagnetic Properties of Hemoproteins. V. Optical and Electron Paramagnetic Resonance Characteristics of Nitric Oxide Derivatives of Metalloporphyrin-Apohemoprotein Complexes. *J Biol Chem* 1972, 247, (8), 2447-2455.
119. Trandafir, F.; Van Doorslaer, S.; Dewilde, S.; Moens, L., Temperature Dependence of NO Binding Modes in Human Neuroglobin. *Biochim Biophys Acta* 2004, 1702, (2), 153-161.
120. Tyryshkin, A. M.; Dikanov, S. A.; Reijerse, E. J.; Burgard, C.; Huttermann, J., Characterization of Bimodal Coordination Structure in Nitrosyl Heme Complexes through Hyperfine Couplings with Pyrrole and Protein Nitrogens. *Journal of the American Chemical Society* 1999, 121, 3396-3406.
121. Schwab, D. E. S., D.J.; Stamler, J.S., *Inorganic Chemistry* 2009, In Press.
122. Praneeth, V. K.; Nather, C.; Peters, G.; Lehnert, N., Spectroscopic Properties and Electronic Structure of Five- and Six-Coordinate Iron(II) Porphyrin NO Complexes: Effect of the Axial N-Donor Ligand. *Inorg Chem* 2006, 45, (7), 2795-2811.
123. Maragos, C. M.; Morley, D.; Wink, D. A.; Dunams, T. M.; Saavedra, J. E.; Hoffman, A.; Bove, A. A.; Isaac, L.; Hrabie, J. A.; Keefer, L. K., Complexes Of NO with Nucleophiles as Agents for the Controlled Biological Release of Nitric Oxide. Vasorelaxant Effects. *J Med Chem* 1991, 34, (11), 3242-3247.
124. Hille, R.; Palmer, G.; Olson, J. S., Chain Equivalence in Reaction of Nitric Oxide with Hemoglobin. *J. Biol. Chem.* 1977, 252, 403-405.

125. Williams, E. M. Oxidation of Human Nitrosyl Hemoglobin Monitored by Uv-Vis and EPR Spectroscopies: Detection of Products and Intermediates. M.S. Thesis, Montana State University Bozeman, MT, 2005.
126. Herold, S.; Rock, G., Mechanistic Studies of the Oxygen-Mediated Oxidation of Nitrosylhemoglobin. *Biochemistry* 2005, 44, (16), 6223-6231.
127. Azizi, F.; Kielbasa, J. E.; Adeyiga, A. M.; Maree, R. D.; Frazier, M.; Yakubu, M.; Shields, H.; King, S. B.; Kim-Shapiro, D. B., Rates of Nitric Oxide Dissociation from Hemoglobin. *Free Radic Biol Med* 2005, 39, (2), 145-151.
128. Hille, R.; Olson, J. S.; Palmer, G., Spectral Transitions of Nitrosyl Hemes During Ligand Binding to Hemoglobin. *J Biol Chem* 1979, 254, (23), 12110-12120.
129. Moore, E. G.; Gibson, Q. H., Cooperativity in the Dissociation of Nitric Oxide from Hemoglobin. *J Biol Chem* 1976, 251, (9), 2788-2794.
130. Joshi, M. S.; Ferguson, T. B., Jr.; Han, T. H.; Hyduke, D. R.; Liao, J. C.; Rassaf, T.; Bryan, N.; Feelisch, M.; Lancaster, J. R., Jr., Nitric Oxide Is Consumed, Rather Than Conserved, by Reaction with Oxyhemoglobin under Physiological Conditions. *Proc Natl Acad Sci U S A* 2002, 99, (16), 10341-10346.
131. Fujii, M.; Hori, H.; Miyazaki, G.; Morimoto, H.; Yonetani, T., The Porphyrin-Iron Hybrid Hemoglobins. Absence of the Fe-His Bonds in One Type of Subunits Favors a Deoxy-Like Structure with Low Oxygen Affinity. *J Biol Chem* 1993, 268, (21), 15386-15393.
132. Yonetani, T.; Tsuneshige, A.; Zhou, Y.; Chen, X., Electron Paramagnetic Resonance and Oxygen Binding Studies of Alpha- Nitrosyl Hemoglobin. A Novel Oxygen Carrier Having NO-Assisted Allosteric Functions. *J Biol Chem* 1998, 273, (32), 20323-20333.

APPENDICES

APPENDIX A

SULFUR K-EDGE X-RAY ABSORPTION SPECTROSCOPY AS AN  
EXPERIMENTAL PROBE FOR S-NITROSO PROTEINS



## Sulfur K-edge X-ray absorption spectroscopy as an experimental probe for *S*-nitroso proteins

Robert K. Szilagyi\*, David E. Schwab

*Department of Chemistry and Biochemistry, Montana State University, Bozeman, MT 59717, USA*

Received 25 January 2005

### Abstract

X-ray absorption spectroscopy at the sulfur K-edge (2.4–2.6 keV) provides a sensitive and specific technique to identify *S*-nitroso compounds, which have significance in nitric oxide-based cell signaling. Unique spectral features clearly distinguish the *S*-nitroso-form of a cysteine residue from the sulfhydryl-form or from a methionine thioether. Comparison of the sulfur K-edge spectra of thiolate, thiol, thioether, and *S*-nitroso thiolate compounds indicates high sensitivity of energy positions and intensities of XAS pre-edge features as determined by the electronic environment of the sulfur absorber. A new experimental setup is being developed for reaching the in vivo concentration range of *S*-nitroso thiol levels in biological samples.

© 2005 Elsevier Inc. All rights reserved.

**Keywords:** Nitric oxide; *S*-Nitroso proteins; Hemoglobin; X-ray absorption spectroscopy; Electronic structure

Nitric oxide (NO) is a free radical that is implicated in the regulation of blood circulation [1,2], cell death [3,4], and neural functions [5,6]. The proposed mechanism for NO bioactivity involves post-translational modifications, where NO can oxidize proteins or attach NO<sub>2</sub> (nitrate) or NO (nitrosate) to amino acid residues [1–7]. The *S*-nitrosation of specific cysteines is emerging as an important mechanism for regulation of signal transduction in cells [8]. Despite the progress in understanding the details of NO-based cell signaling, research is hindered by a lack of a sensitive and specific method to identify *S*-nitrosated (SNO) proteins [9,10]. This is partially due to the low concentration of nitrosated intracellular proteins as well as the great sensitivity of the ON–S bond to sample aging, manipulation, and redox conditions [11,12].

In red blood cells, release of NO from a specific cysteine (SNO-βC93) induced by hypoxic conditions (low

tissue *p*O<sub>2</sub>) triggers vasodilation [2]. At physiological conditions [13,14], the hemoglobin concentration is in the millimolar range. It is proposed, however, that only 1 in 5000 hemoglobin possess a molecule of NO (micromolar range) [15].

The current chemical [11,16–19], electrochemical [20], biochemical techniques [10,21–23], and standards [24] employed in detecting and quantitating protein SNO levels at an uncomfortable low analyte concentration utilize the *unique chemical reactivity* of NO. Among the spectroscopic methods, the EPR technique can determine the metal (heme) bound NO at nanomolar level [25–27]; however, it is transparent to SNO due to its diamagnetic electronic ground state.

The *unique electronic structure* of *S*-nitroso thiols can provide a specific experimental handle for detecting and characterizing SNO formation and release. Molecular orbital theory defines  $\sigma$  and  $\pi$  bonding interactions between the sulfur 3p and the NO  $\pi^*$  orbitals that render the SNO electronic structure unique with respect to cysteine and methionine. Fig. 1 illustrates the three lowest

\* Corresponding author. Fax: +1 406 994 5407.

E-mail address: [Szilagyi@Montana.EDU](mailto:Szilagyi@Montana.EDU) (R.K. Szilagyi).

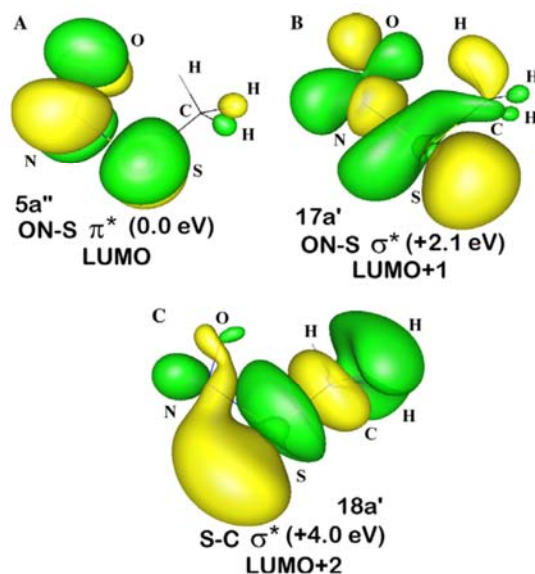


Fig. 1. Frontier unoccupied orbitals (LUMO through LUMO + 2) of S-nitroso methylthiolate ( $\text{H}_3\text{C-SNO}$ ).

lying, unoccupied orbitals in the order of increasing energy with significant sulfur character. The sensitivity of SNO toward reduction can be rationalized by the antibonding nature of these valence orbitals along the N–S bond vectors.

The sulfur 3p-based bonding interactions of SNO can be directly probed by X-ray absorption spectroscopy [28]. The sulfur K-edge XAS in the energy range of 2.4–2.6 keV corresponds to excitation of sulfur core 1s electrons to unoccupied orbitals, giving various bound states and, at higher energies, excitation to the continuum giving rise to an intense edge jump. The bound states appear as pre-edge or rising-edge features before the edge jump. Analysis of these near-edge spectral features (NEXAS [29]) provides electronic structural information about the absorber atom, while the energy region beyond the edge jump (EXAFS [30]) gives geometric information by defining the radial distribution of atoms (as scatterers) around the absorber. Since the bound state transitions are localized on sulfur and electric dipole allowed, the intensity of the pre-edge features is proportional to the sulfur 3p character in the unoccupied, acceptor orbitals.

Sulfur K-edge XAS has already been successfully applied in analytical determination of chemical speciation [31–38] and in electronic structure studies of transition metal thiolates [39,40], Fe–S clusters [41,42], and various bioinorganic active sites [28,43–45]. This study introduces a novel experimental way of detecting SNO in proteins using a comparison of sulfur K-edge XAS

spectra of S-nitroso compounds to cysteine and methionine, and various thiolate salts. Using the data obtained for the solid models, the spectrum of the crystallographically characterized S-nitroso human hemoglobin [46] is predicted.

## Materials and methods

**XAS data collection.** SNO compounds (Fig. S1) were purchased from Cayman Chemicals and other sulfur compounds from Sigma–Aldrich. Sulfur K-edge XAS measurements were carried out at BL9.3.1 of Advanced Light Source under ultrahigh vacuum ( $10^{-7}$  torr) with a liquid nitrogen-cooled sample rod. The solid samples were ground and pasted onto a sulfur-free Mylar dot (Shercon). Preparation of SNO samples was carried out in a liquid nitrogen boil-off cooled, portable glovebox with continuous dry nitrogen purge (atmosphere temperature was maintained at  $0 \pm 5$  °C) to minimize SNO decomposition. Due to the low temperature data collection setup, no photoreduction, radiation damage or change in the color of the samples was observed over a lengthy exposure to the beam. The sample cell was positioned at approximately  $45^\circ$  relative to the incident beam. Fluorescence signal was collected using a Si-photodiode aligned parallel with the sample cell. The incident photon energy was scanned in 0.5 eV steps outside the rising-edge region, where the stepsize was 0.1 eV. The resting time of the Si(111) double crystal monochromator and the dwell time for data collection were set to 400 ms and 1s, respectively. At least five scans were averaged to obtain a good signal-to-noise ratio. The incident photon energy was calibrated to the first transition (2472.02 eV) of the sodium thiosulfate pentahydrate spectrum with reproducibility within 0.1 eV. A smooth background (second order polynomial) was subtracted from the spectra and normalized at 2490 eV of the spline (second order polynomial). Rough data processing was carried out at the beamline immediately after data collection, while final data processing of calibration, background subtraction, spline, and fitting was performed using PeakFit 4.12 (SeaSolve).

**Electronic structure calculations.** Electronic structure calculations were carried out using the Gaussian03 suite [47]. The geometry of S-nitroso methylthiolate was optimized using GGA Becke exchange [48] and Perdew correlation [49] functionals with 6-31G(d) basis set for all atoms [50,51]. The electronic wave function at the equilibrium geometry (no imaginary vibrational frequency) was analyzed by Natural Population Analysis [52–54].

## Results and discussion

### Unique spectral features of SNO

The sulfur K-edge spectra (Fig. 2) of sodium salt, sulfhydryl, and S-nitroso thiolates show dramatic XAS spectral differences. The thiolate salt has a characteristic transition at 2472.1 eV, which is well resolved from the rising-edge features. The former transition corresponds to a sulfur 1s  $\rightarrow$  S–C  $\sigma^*$  excitation, while the latter to  $\rightarrow$ sulfur 4p excitations superimposed with atomic scattering. In cysteine, the protonation of sulfur increases the sulfur effective nuclear charge and thus shifts the  $\rightarrow$ C–S  $\sigma^*$  excitation to higher energy (2474.2 eV). The corresponding feature in S-nitroso glutathione (GSNO, Fig. S1) appears at even higher energy (2474.9 eV), due

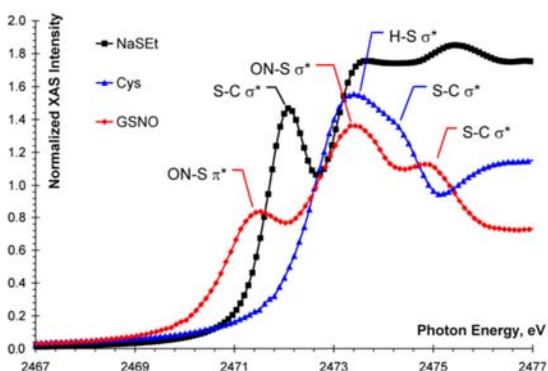


Fig. 2. Normalized sulfur K-edge spectra of sodium ethylthiolate (black ■), cysteine (blue ▲), and GSNO (red ◆) with spectral assignments. (For interpretation of the references to color in this figure legend, the reader is referred to the web version of this paper.)

to electron donation from the sulfur 3p orbital to a vacant  $\pi^*$  orbital of the formally  $\text{NO}^+$  moiety. As anticipated from Fig. 1,  $\text{NO}^+$  binding to the thiolate gives rise to features corresponding to  $\rightarrow\text{ON-S } \pi^*$  and  $\sigma^*$  excitations, at 2471.4 and 2473.3 eV, respectively (Fig. 2). The energy splitting of the three resolved features (1.9 and 1.5 eV for  $\text{ON-S } \pi^*/\sigma^*$  and  $\text{ON-S/S-C } \sigma^*$ , respectively) of the GSNO spectrum correlates well with the calculated splitting of the unoccupied orbitals (2.1 and 1.9 eV, respectively) in the ground electronic state of *S*-nitroso methylthiolate shown in Fig. 1.

#### Sensitivity of sulfur K-edge XAS

In addition to detecting SNO, sulfur K-edge XAS shows sensitivity to changes in the electronic environment of the sulfur absorber. Perturbation in the electron donating ability of the organic moiety changes the energy positions of pre-edge features by affecting the sulfur effective nuclear charge. For example, the  $\text{S-C } \sigma^*$  transition is shifted up in energy by approximately 0.8 eV in

the sodium salt of phenylthiolate (Table 1) due to the electron withdrawing effect of the aromatic ring, relative to the alkyl groups in ethylthiolate (Fig. S2). In methionine, two  $\text{C-S } \sigma^*$  transitions are observed, which are only slightly higher in energy (0.1–0.2 eV) relative to cysteine (Fig. S3). Most importantly in SNO, the perturbation of the organic moiety influences the  $\text{ON-S}$  bonding, as indicated by the change in energy positions of corresponding features (Table 1, Fig. S4) in *N*-acetyloxy-3-nitrosothiovaline (Fig. S1, SNAP) relative to GSNO. In SNAP, the sulfur is attached to a tertiary carbon, which has a greater electron donating ability than the primary carbon in GSNO (or SNO-Cys). This results in increased electron donation to the sulfur (decreasing effective nuclear charge) and thus shifts the transitions corresponding to the  $\text{C-S } \sigma^*$  excitation down in energy by about 0.7 eV (Table 1). It is important to note that the  $\text{ON-S } \sigma$  bonding interaction is also perturbed, while the perpendicular  $\text{ON-S } \pi$  bonding does not seem to be affected significantly, as indicated by the energy positions of corresponding transitions in Table 1.

#### Predicted spectrum for *S*-nitroso human hemoglobin

Using the normalized sulfur K-edge spectra of GSNO, cysteine, and methionine, the XAS spectra of *S*-nitroso proteins can be predicted. The tetrameric, *S*-nitroso hemoglobin [46] contains 12 sulfur atoms that are potential absorbers in sulfur XAS. Subunits A and C contribute Met32, Met76, and Cys104, while subunits B and D give rise to features due to Met55, Cys112, and SNO-Cys93. The heme bound NO will not contribute to the XAS spectrum in this energy region.

The predicted sulfur K-edge spectrum of the *S*-nitroso hemoglobin is shown in Fig. 3. Due to the overlapping features, only the sulfur  $1s \rightarrow \text{ON-S } \pi^*$  transition is expected to be resolved in the protein spectra. The minimum at  $2471.4 \pm 0.1$  eV of the second derivative spectrum (dotted lines) allows for the quantitation of the

Table 1  
Assignments of sulfur 1s core electron excitations for selected model compounds

Compounds	Excitation ( $\text{S } 1s \rightarrow$ )	Transition energy (eV)
NaSEt	$\text{S-C } \sigma^*$	2472.1
NaSPh	$\text{S-C } \sigma^*$	2472.9
Cysteine	$\text{H-S } \sigma^*$	2473.4
	$\text{S-C } \sigma^*$	2474.2
Methionine	$\text{S-C } \sigma^*$	2473.5
		2474.4
GSNO	$\text{ON-S } \pi^*$	2471.4
	$\text{ON-S } \sigma^*$	2473.3
	$\text{S-C } \sigma^*$	2474.9
SNAP	$\text{ON-S } \pi^*$	2471.3
	$\text{ON-S } \sigma^*$	2472.9
	$\text{S-C } \sigma^*$	2474.2

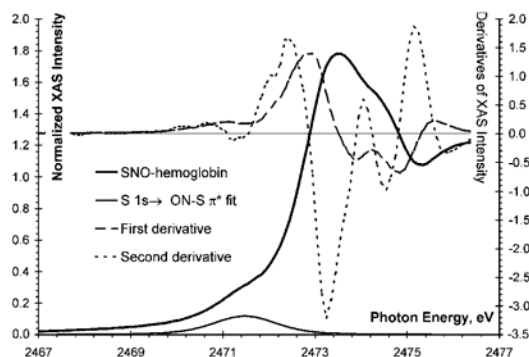


Fig. 3. Predicted sulfur K-edge spectrum of the *S*-nitrosated-form of human hemoglobin.

*ON–S*  $\pi^*$  transition, which can be directly correlated with the *S*-nitroso thiol concentration. Alternatively, subtraction of protein spectra with and without bound SNO can give resolved features corresponding to the ON–S  $\pi^*$  and  $\sigma^*$  transitions, thus providing two points for analytical quantitation.

The potential of XAS has been demonstrated for detecting *S*-nitroso compounds. The high sensitivity of sulfur K-edge XAS provides insights into the electronic, electrostatic, and steric environments around the SNO moiety. These can be derived from pre-edge energy positions, intensities and from EXAFS analysis, respectively. Experiments carried out at Advanced Light Source BL9.3.1 employ fluorescence detection in an ultrahigh vacuum chamber. In order to approach the concentration range of in vivo samples, a new beamline end-station is being designed with detectors for simultaneous data collection in transmission, electron-yield, and fluorescence modes from windowless, frozen biological samples.

#### Acknowledgments

Authors are thankful for financial support from NSF EPSCoR (Infrastructure: Cross-Sectional Partnership Building for the Future) and NIH BRIN P20 RR-16455-01, for stimulating discussions with Profs. D.A. Singel and E.A. Dratz, and for assistance from ALS staff. D.E.S. acknowledges the graduate student fellowship from NIH BRIN. We also thank A.S. Schlachter (ALS, LBNL) for his assistance with data collection and arrangement of the beam time. The Advanced Light Source is supported by the Director, Office of Energy Research, Office of Basic Energy Sciences, Materials Sciences Division of the US Department of Energy under contract No. DE-AC03-76SF00098.

#### Appendix A. Supplementary data

Supplementary data associated with this article can be found, in the online version, at doi:10.1016/j.bbrc.2005.02.127.

#### References

- [1] J.S. Stamler, D.I. Simon, O. Jaraki, J.A. Osborne, S. Francis, M. Mullins, D. Singel, J. Loscalzo, *S*-nitrosylation of tissue-type plasminogen-activator confers vasodilatory and antiplatelet properties on the enzyme, *Proc. Natl. Acad. Sci. USA* 89 (1992) 8087–8091.
- [2] J.S. Stamler, G. Meissner, Physiology of nitric oxide in skeletal muscle, *Phys. Rev.* 81 (2001) 209–237.
- [3] C.M. Schonhoff, B. Gaston, J.B. Mannick, Nitrosylation of cytochrome *c* during apoptosis, *J. Biol. Chem.* 278 (2003) 18265–18270.
- [4] J.Y. Heo, S.L. Campbell, Mechanism of p21(Ras) *S*-nitrosylation and kinetics of nitric oxide-mediated guanine nucleotide exchange, *Biochemistry* 43 (2004) 2314–2322.
- [5] S.A. Lipton, J.S. Stamler, Actions of redox-related congeners of nitric-oxide at the NMDA receptor, *Neuropharm* 33 (1994) 1229–1233.
- [6] S.A. Lipton, Y.B. Choi, H. Takahashi, D.X. Zhang, W.Z. Li, A. Godzik, L.A. Bankston, Cysteine regulation of protein function—as exemplified by NMDA-receptor modulation, *Trends Neurosci.* 25 (2002) 474–480.
- [7] J.S. Stamler, A. Hauslade, Oxidative modifications in nitrosative stress, *Nat. Struct. Biol.* 5 (1998) 247–249.
- [8] P. Lane, S.S. Gross, Cell signaling by nitric oxide, *Semin. Nephrol.* 19 (1999) 215–229.
- [9] J.B. Mannick, C.M. Schonhoff, NO means no and yes: regulation of cell signaling by protein nitrosylation, *Free Rad. Res.* 38 (2004) 1–7.
- [10] S.R. Jaffrey, M. Fang, S.H. Snyder, Nitrosopeptide mapping: a novel methodology reveals *S*-nitrosylation of Dexas1 on a single cysteine residue, *Chem. Biol.* 9 (2002) 1329–1335.
- [11] E. Nagababu, S. Ramasamy, D.R. Abernethy, J.M. Rifkind, Active nitric oxide produced in the red cell under hypoxic conditions by deoxyhemoglobin-mediated nitrite reduction, *J. Biol. Chem.* 278 (2003) 46349–46356.
- [12] T. Rassaf, N.S. Bryan, R.E. Maloney, V. Specian, M. Kelm, NO adducts in mammalian red blood cells: too much or too little?, *Nat. Med.* 9 (2003) 481–482.
- [13] R.J. Gorczynski, B.R. Duling, Role of oxygen in arteriolar functional vasodilation in hamster striated muscle, *Am. J. Physiol.* 235 (1978) H505–H515.
- [14] C.R. Honig, T.E. Gayeski, Resistance to O<sub>2</sub> diffusion in anemic red muscle: roles of flux density to cell  $\rho$ O<sub>2</sub>, *Am. J. Physiol.* 265 (1993) H868–H875.
- [15] D.J. Singel, J.S. Stamler, Chemical physiology of blood flow regulation by red blood cells: role of nitric oxide and sno-hemoglobin, *Annu. Rev. Physiol.* 67 (2005) 99–145.
- [16] J.B. Mannick, A. Hausladen, L.M. Liu, D.T. Hess, M. Zeng, Q.X. Miao, L.S. Kane, A.J. Gow, J.S. Stamler, Fas-induced caspase denitrosylation, *Science* 284 (1999) 651–654.
- [17] J.P. Eu, J.H. Sun, L. Xu, J.S. Stamler, G. Meissner, The skeletal muscle calcium release channel: coupled O<sub>2</sub> sensor and NO signaling functions, *Cell* 102 (2000) 499–509.
- [18] R. Marley, M. Feelisch, S. Holt, K. Moore, A chemiluminescence-based assay for *S*-nitrosoalbumin and other plasma *S*-nitrosothiols, *Free Rad. Res.* 32 (2000) 1–9.
- [19] T.J. McMahon, R.E. Moon, B.P. Luchsinger, M.S. Carraway, A.E. Stone, B.W. Stolp, A.J. Gow, J.R. Pawloski, P. Watke, D.J. Singel, C.A. Piantadosi, J.S. Stamler, Nitric oxide in the human respiratory cycle, *Nat. Med.* 8 (2002) 711–717.
- [20] B. Datta, T. Tufnell-Barrett, R.A. Bleasdale, C.J. Jones, I. Becton, Red blood cell nitric oxide as an endocrine vasoregulator: a potential role in congestive heart failure, *Circulation* 109 (2004) 1339–1342.
- [21] J.S. Stamler, D.T. Hess, D.J. Singel, Reply to “NO adducts in mammalian red blood cells: too much or too little?”, *Nat. Med.* 9 (2003) 483–484.
- [22] B. Gaston, S. Sears, J. Woods, J. Hunt, M. Ponaman, T. McMahon, J.S. Stamler, Bronchodilator *S*-nitrosothiol deficiency in asthmatic respiratory failure, *Lancet* 351 (1998) 1317–1319.
- [23] B. Gaston, J. Reilly, J.M. Drazen, J. Fackler, P. Ramdev, D. Arnelle, M.E. Mullins, D.J. Sugarbaker, C. Chee, D.J. Singel, J. Loscalzo, J.S. Stamler, Endogenous nitrogen oxides and bronchodilator *S*-nitrosothiols in human airways, *Proc. Natl. Acad. Sci. USA* 90 (1993) 10957–10961.
- [24] J.S. Stamler, *S*-Nitrosothiols in the blood: roles, amounts and methods of analysis, *Circ. Res.* 94 (2004) 414–417.

- [25] A.B. Milsom, C.J. Jones, J. Goodfellow, M.P. Frenneaux, J.R. Peters, P.E. James, Abnormal metabolic fate of nitric oxide in type I diabetes mellitus, *Diabetologia* 45 (2002) 1515–1522.
- [26] K. Kirima, K. Tsuchiya, H. Sei, T. Hasegawa, M. Shikishima, Evaluation of systemic blood NO dynamics by EPR spectroscopy: HbNO as an endogenous index of NO, *Am. J. Physiol. Heart Circ. Physiol.* 285 (2003) H589–H596.
- [27] G. Aldini, M. Orioli, R. Maffei Facino, M. Giovanna Clement, M. Albertini, Nitrosohemoglobin formation after infusion of NO solutions: ESR studies in pigs, *Biochem. Biophys. Res. Commun.* 318 (2004) 405–414.
- [28] S.E. Shadle, J.E. Penner-Hahn, H.J. Schugar, B. Hedman, K.O. Hodgson, E.I. Solomon, X-ray absorption spectroscopic studies of the blue copper site: metal and ligand K-edge studies to probe the origin of the EPR hyperfine splitting in plastocyanin, *J. Am. Chem. Soc.* 115 (1993) 767–776.
- [29] E.I. Solomon, B. Hedman, K.O. Hodgson, A. Dey, R.K. Szilagyi, Ligand K-edge X-ray absorption spectroscopy: covalency of ligand–metal bonds, *Coord. Chem. Rev.* 249 (2004) 97–129.
- [30] H.H. Zhang, B. Hedman, K.E. Hodgson, in: E.I. Solomon, A.B.P. Lever (Eds.), *Inorganic Electronic Structure and Spectroscopy*, Wiley, New York, 1999, pp. 513–554.
- [31] A. Rompel, R.M. Cinco, M.J. Latimer, A.E. McDermott, R.D. Guiles, A. Quintanilha, R.M. Krauss, K. Sauer, V.K. Yachandra, M.P. Klein, Sulfur K-edge X-ray absorption spectroscopy: a spectroscopic tool to examine the redox state of S-containing metabolites in vivo, *Proc. Natl. Acad. Sci. USA* 95 (1998) 6122–6127.
- [32] E. Paris, G. Giuli, M.R. Carroll, I. Davoli, The valence and speciation of sulfur in glasses by X-ray absorption spectroscopy, *Can. Mineral.* 39 (2001) 331–339.
- [33] D.A. McKeown, I.S. Muller, H. Gan, I.L. Pegg, W.C. Stolte, Determination of sulfur environments in borosilicate waste glasses using X-ray absorption near-edge spectroscopy, *J. Non-Cryst. Solids* 333 (2004) 74–84.
- [34] I.J. Pickering, G.N. George, E.Y. Yu, D.C. Brune, C. Tuschak, J. Overmann, J.T. Beatty, R.C. Prince, Analysis of sulfur biochemistry of sulfur bacteria using X-ray absorption spectroscopy, *Biochemistry* 40 (2001) 8138–8145.
- [35] A. Prange, R. Chauvistre, H. Modrow, J. Hormes, H.G. Truper, C. Dahl, Quantitative speciation of sulfur in bacterial sulfur globules: X-ray absorption spectroscopy reveals at least three different species of sulfur, *Microbiology-Sgm* 148 (2002) 267–276.
- [36] M. Sandstrom, F. Jalilehvand, I. Persson, U. Gelius, P. Frank, I. Hall-Roth, Deterioration of the seventeenth-century warship Vasa by internal formation of sulphuric acid, *Nature* 415 (2002) 893–897.
- [37] E.Y. Snedden, H.H. Harris, I.J. Pickering, R.C. Prince, S. Johnson, X.J. Li, E. Block, G.N. George, The sulfur chemistry of shiitake mushroom, *J. Am. Chem. Soc.* 126 (2004) 458–459.
- [38] D. Solomon, J. Lehmann, C.E. Martinez, Sulfur K-edge XANES spectroscopy as a tool for understanding sulfur dynamics in soil organic matter, *Soil Sci. Soc. Am. J.* 67 (2003) 1721–1731.
- [39] S.E. Shadle, B. Hedman, K.O. Hodgson, E.I. Solomon, Ligand K-edge X-Ray-absorption spectroscopic studies: metal–ligand covalency in a series of transition-metal tetrachlorides, *J. Am. Chem. Soc.* 117 (1995) 2259–2272.
- [40] K.R. Williams, B. Hedman, K.O. Hodgson, E.I. Solomon, Ligand K-edge X-ray absorption spectroscopic studies: metal–ligand covalency in transition metal tetrathiolates, *Inorg. Chim. Acta* 263 (1997) 315–321.
- [41] T. Glaser, B. Hedman, K.O. Hodgson, E.I. Solomon, Ligand K-Edge X-ray absorption spectroscopy: a direct probe of ligand–metal covalency, *Acc. Chem. Res.* 33 (2000) 859–868.
- [42] A. Dey, T. Glaser, M.M.J. Couture, L.D. Eltis, R.H. Holm, B. Hedman, K.O. Hodgson, E.I. Solomon, Ligand K-edge X-ray absorption spectroscopy of  $[\text{Fe}_4\text{S}_4]^{(1+2+,3+)}$  clusters: changes in bonding and electronic relaxation upon redox, *J. Am. Chem. Soc.* 126 (2004) 8320–8328.
- [43] K. Rose, S.E. Shadle, M.K. Eidsness, D.M. Kurtz, R.A. Scott, B. Hedman, K.O. Hodgson, E.I. Solomon, Investigation of iron–sulfur covalency in rubredoxins and a model system using sulfur K-edge X-ray absorption spectroscopy, *J. Am. Chem. Soc.* 120 (1998) 10743–10747.
- [44] S. DeBeer George, M. Metz, R.K. Szilagyi, H. Wang, S.P. Cramer, Y. Lu, W.B. Tolman, B. Hedman, K.O. Hodgson, E.I. Solomon, A quantitative description of the ground-state wave function of  $\text{Cu}_A$  by X-ray absorption spectroscopy: comparison to plastocyanin and relevance to electron transfer, *J. Am. Chem. Soc.* 123 (2001) 5757–5767.
- [45] S. DeBeer George, L. Basumallick, R.K. Szilagyi, D.W. Randall, M.G. Hill, A.M. Nersissian, J.S. Valentine, B. Hedman, K.O. Hodgson, E.I. Solomon, Spectroscopic investigation of stellacyanin mutants: axial ligand interactions at the blue copper site, *J. Am. Chem. Soc.* 125 (2003) 11314–11328.
- [46] N.L. Chan, P.H. Rogers, A. Arnore, Crystal structure of the S-nitroso form of liganded human hemoglobin, *Biochemistry* 37 (1998) 16459–16464.
- [47] M.J. Frisch, G.W. Trucks, H.B. Schlegel, G.E. Scuseria, M.A. Robb, J.R. Cheeseman, J.A. Montgomery, Jr., T. Vreven, K.N. Kudin, J.C. Burant, J.M. Millam, S.S. Iyengar, J. Tomasi, V. Barone, B. Mennucci, M. Cossi, G. Scalmani, N. Rega, G.A. Petersson, H. Nakatsuji, M. Hada, M. Ehara, K. Toyota, R. Fukuda, J. Hasegawa, M. Ishida, T. Nakajima, Y. Honda, O. Kitao, H. Nakai, M. Klene, X. Li, J.E. Knox, H.P. Hratchian, J.B. Cross, C. Adamo, J. Jaramillo, R. Gomperts, R.E. Stratmann, O. Yazyev, A.J. Austin, R. Cammi, C. Pomelli, J.W. Ochterski, P.Y. Ayala, K. Morokuma, G.A. Voth, P. Salvador, J.J. Dannenberg, V.G. Zakrzewski, S. Dapprich, A.D. Daniels, M.C. Strain, O. Farkas, D.K. Malick, A.D. Rabuck, K. Raghavachari, J.B. Foresman, J.V. Ortiz, Q. Cui, A.G. Baboul, S. Clifford, J. Cioslowski, B.B. Stefanov, G. Liu, A. Liashenko, P. Piskorz, I. Komaromi, R.L. Martin, D.J. Fox, T. Keith, M.A. Al-Laham, C.Y. Peng, A. Nanayakkara, M. Challacombe, P.M.W. Gill, B. Johnson, W. Chen, M.W. Wong, C. Gonzalez, J.A. Pople, *Gaussian03 Rev. C 02*, Gaussian, Inc., Pittsburgh, PA, 2004.
- [48] A.D. Becke, Density-functional exchange-energy approximation with correct asymptotic behavior, *Phys. Rev. A* 38 (1988) 3098–3100.
- [49] J.P. Perdew, Density-functional approximation for the correlation energy of the inhomogeneous electron gas, *Phys. Rev. B* 33 (1986) 8822–8824.
- [50] M.M. Francl, W.J. Pietro, W.J. Hehre, J.S. Binkley, M.S. Gordon, D.J. DeFrees, J.A. Pople, Self-consistent molecular orbital methods. XXIII. A polarization-type basis set for second-row elements, *J. Chem. Phys.* 77 (1982) 3654–3665.
- [51] V.A. Rassolov, J.A. Pople, M.A. Ratner, T.L. Windus, 6-31G\* basis set for atoms K through Zn, *J. Chem. Phys.* 109 (1998) 1223–1229.
- [52] J.P. Foster, F. Weinhold, Natural hybrid orbitals, *J. Am. Chem. Soc.* 102 (1980) 7211–7218.
- [53] J.E. Carpenter, F. Weinhold, Analysis of the geometry of the hydroxymethyl radical by the “different hybrids for different spins” natural bond orbital procedure, *J. Mol. Struct. (THEO-CHEM)* 46 (1988) 41–62.
- [54] A.E. Reed, L.A. Curtiss, F. Weinhold, Intermolecular interactions from a natural bond orbital, donor–acceptor viewpoint, *Chem. Rev.* 88 (1988) 899–926.

APPENDIX B

SUPPLEMENTARY MET-HB:NO<sub>2</sub><sup>-</sup> PLOTS

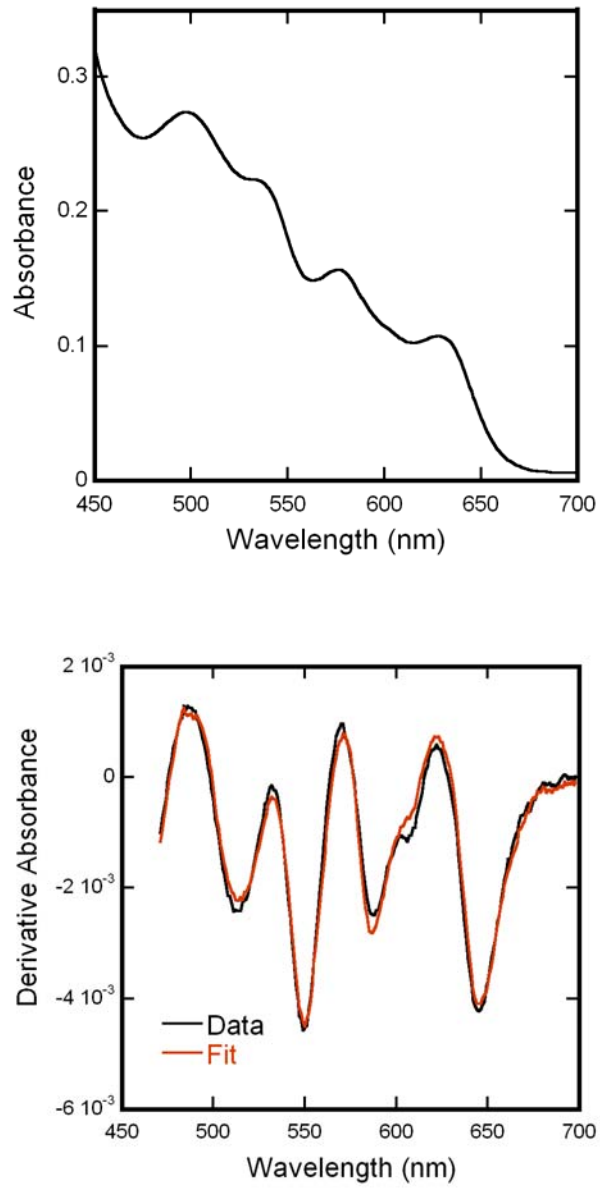


Figure B-1: UV-Vis absorbance spectrum of Met-Hb in pH 7.4 PBS buffer (upper) and its derivative spectrum with best fit (lower).

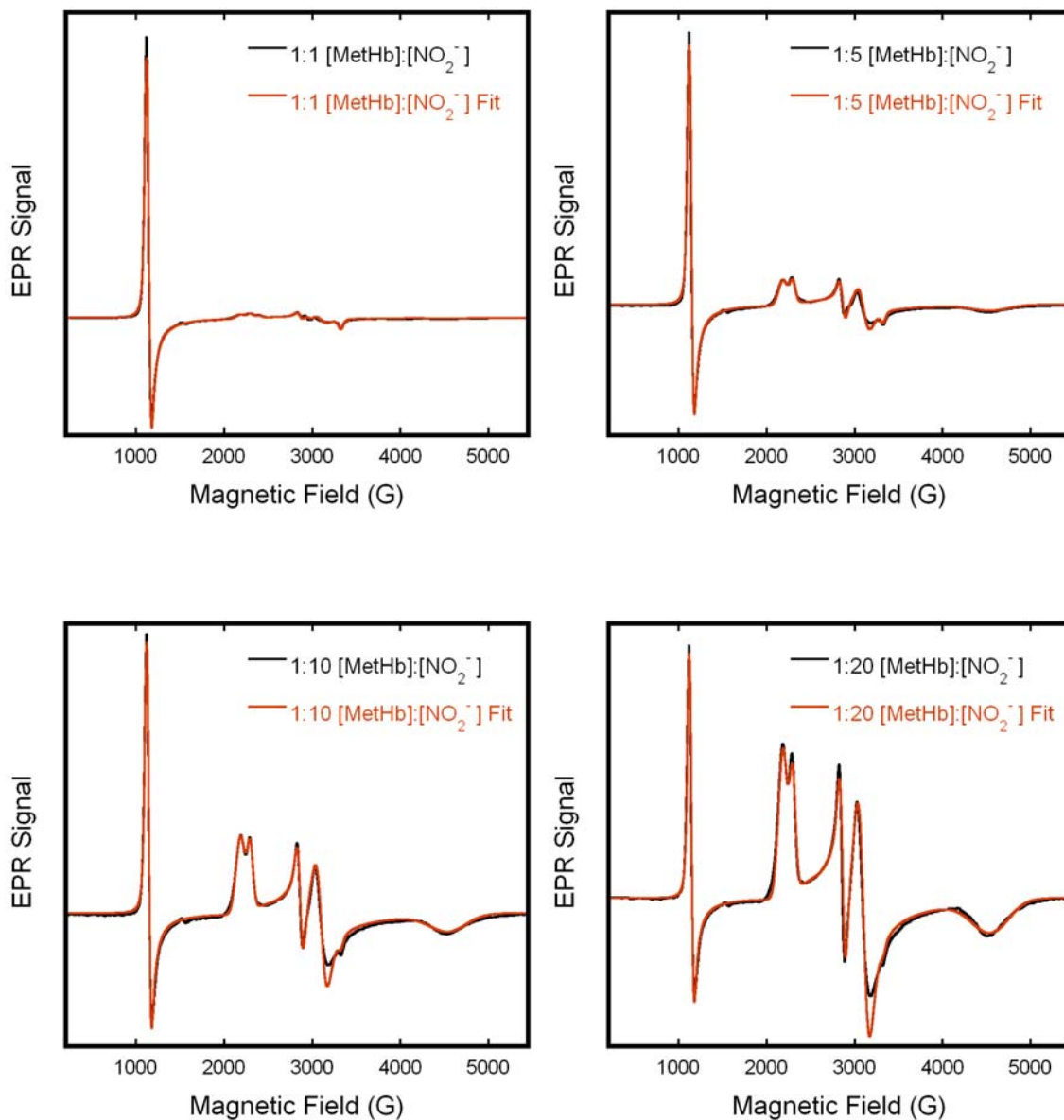


Figure B-2: Exemplary experimental EPR spectra with best fits of Met-Hb: $\text{NO}_2^-$  with heme to  $\text{NO}_2^-$  ratios of 1:1, 1:5, 1:10, and 1:20. Protein concentration in all samples was 0.5 M in 0.1 M PBS buffer, pH 7.4. EPR spectra were obtained at 20 K with the following spectrometer parameter values: 0.5 s time constant, 5 G modulation amplitude, 16.67 G/s sweep rate, 5 mW microwave power, and 9.24 GHz microwave frequency.

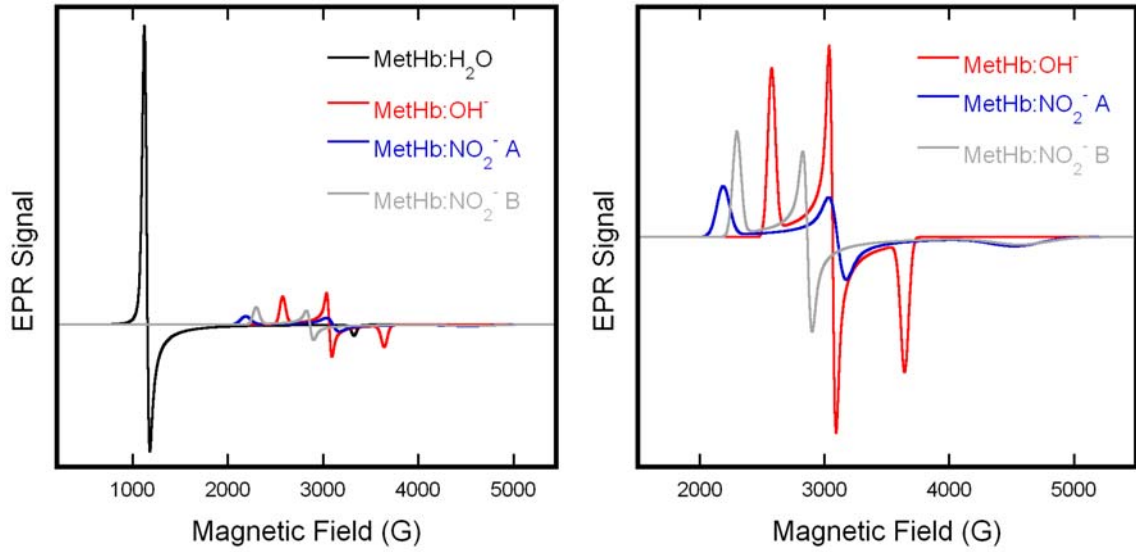


Figure B-3: Exemplary EPR basis spectra employed in fitting Met-Hb: $\text{NO}_2^-$  experimental spectra in PBS buffer, pH 7.4.

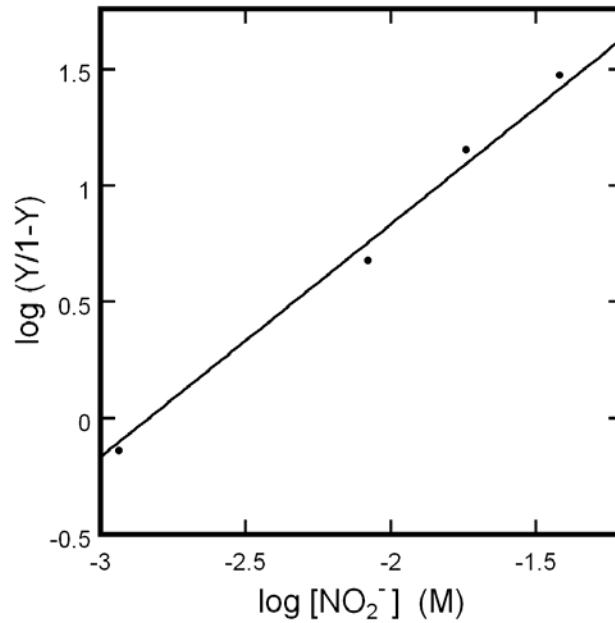


Figure B-4: Exemplary Hill plot generated from data obtain from best fits displayed in Figure B-2.

APPENDIX C

SUPPLEMENTARY VARIABLE TEMPERATURE MET-HB PLOTS

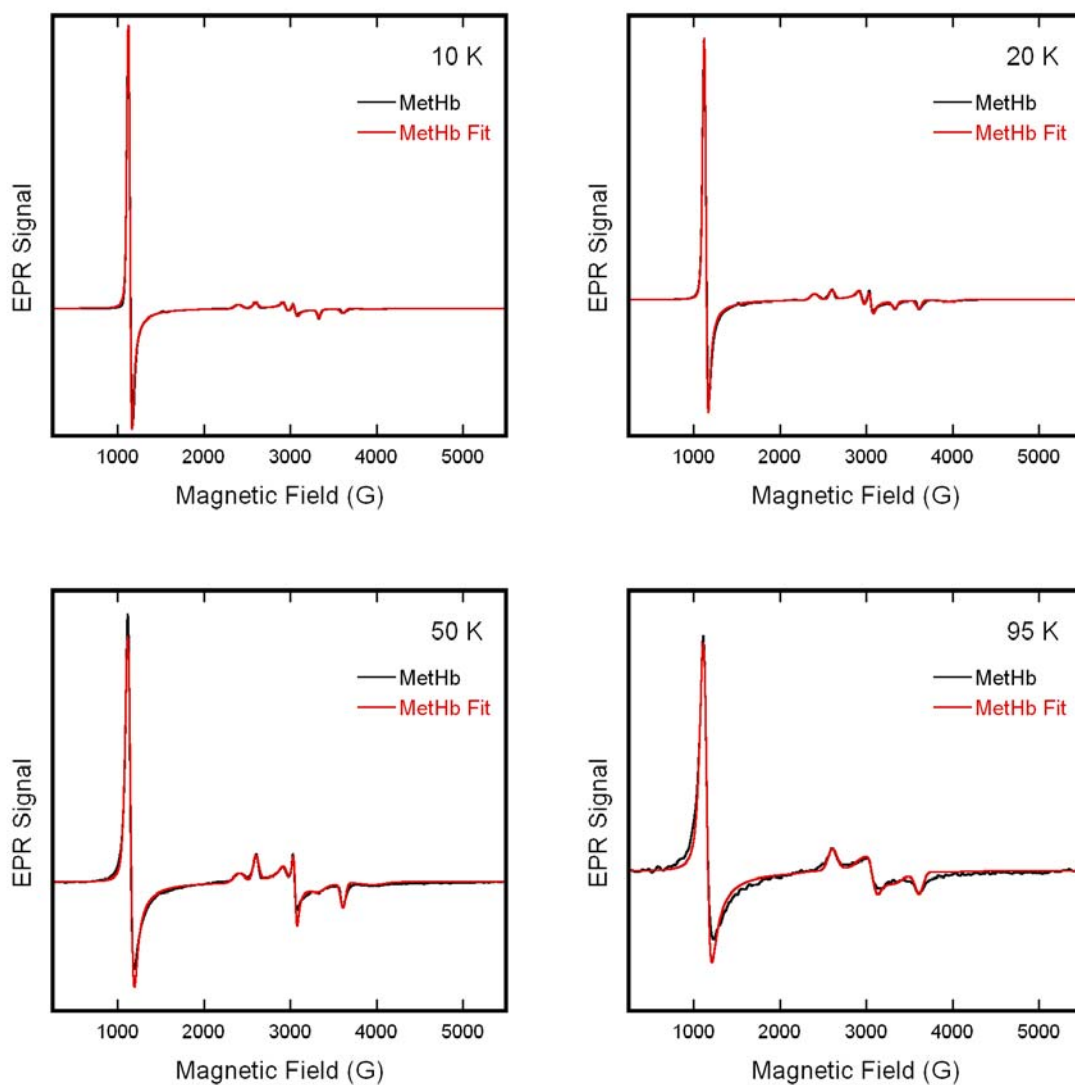


Figure C-1: Exemplary EPR spectra of neat Met-Hb in aqueous HEPES buffer, pH 7.4, at 10, 20, 50 and 95 K, as labeled. Each spectrum is displayed with its best fit spectrum. Spectra were collected with the following spectrometer settings: microwave frequency of 9.24 GHz, 5 mW of microwave power, 0.5 s time constant, modulation amplitude of 5 G and a sweep rate of 16.67 G/s.

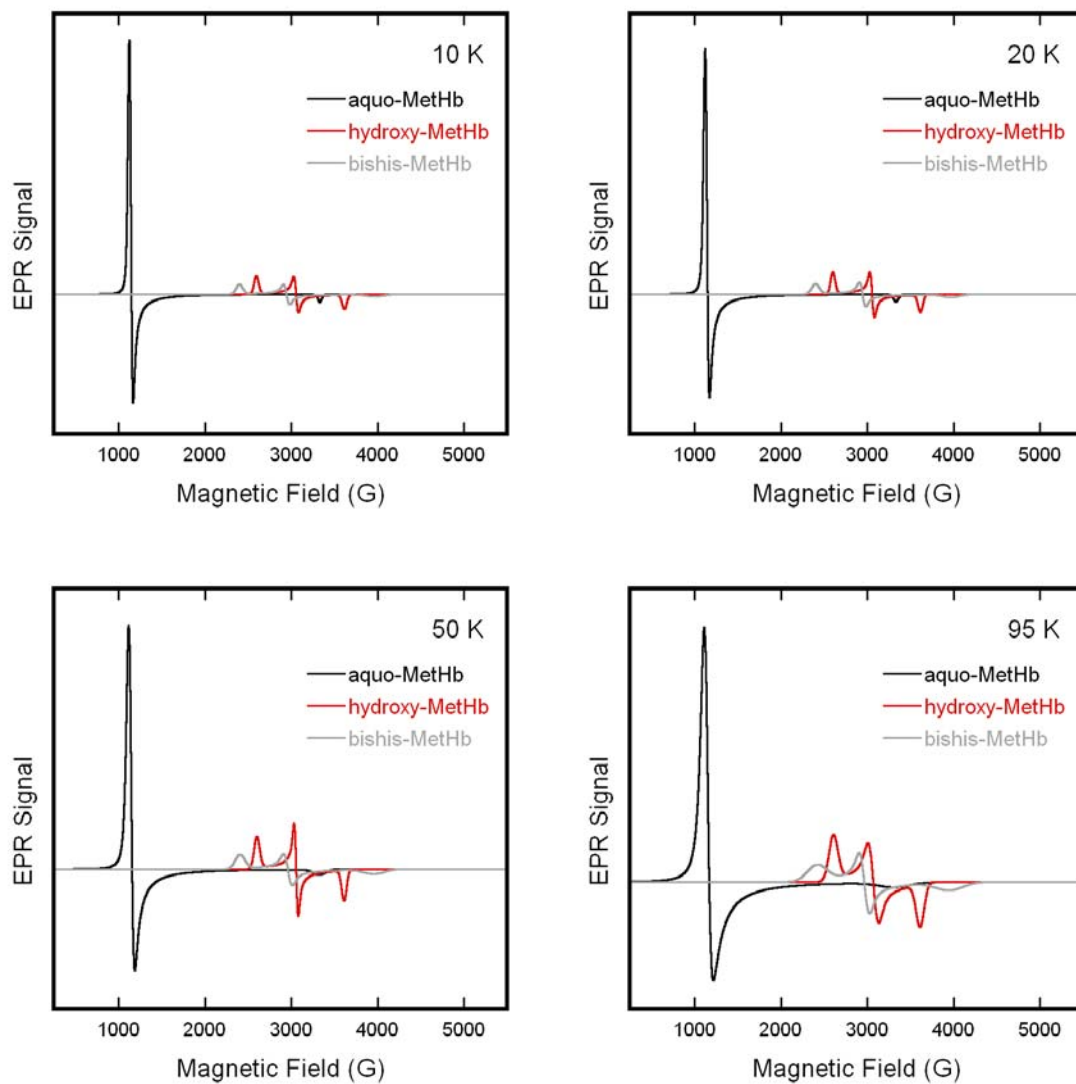


Figure C-2: Exemplary EPR basis spectra employed in fitting neat Met-Hb experimental spectra in HEPES buffer, pH 7.4, at 10, 20, 50 and 95 K, as labeled.

APPENDIX D

SUPPLEMENTARY VARIABLE TEMPERATURE HB(NO)<sub>4</sub> PLOTS

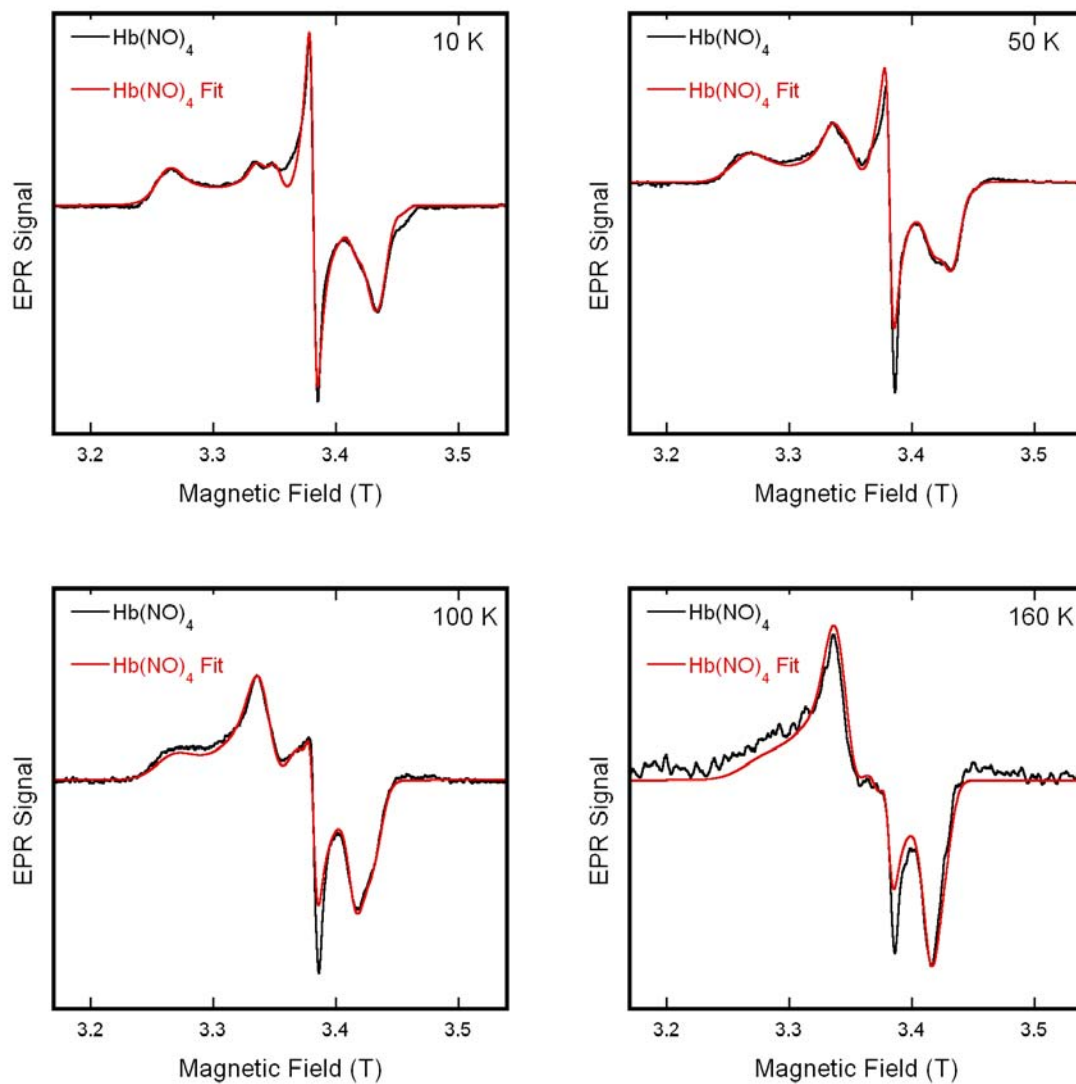


Figure D-1: W-band EPR experimental and best fit spectra of  $\text{Hb}(\text{NO})_4$  in aqueous solution at temperatures at 10, 50, 100 and 160 K, as labeled. Spectra were collected with 94.9 GHz microwave frequency, microwave power ranging from 2.2-16.8  $\mu\text{W}$ , 0.1 s time constant, modulation amplitude of 10 G, and a 0.2 T/min sweep rate.

APPENDIX E

SUPPLEMENTARY HYBRID NITROSYL-HB PLOTS

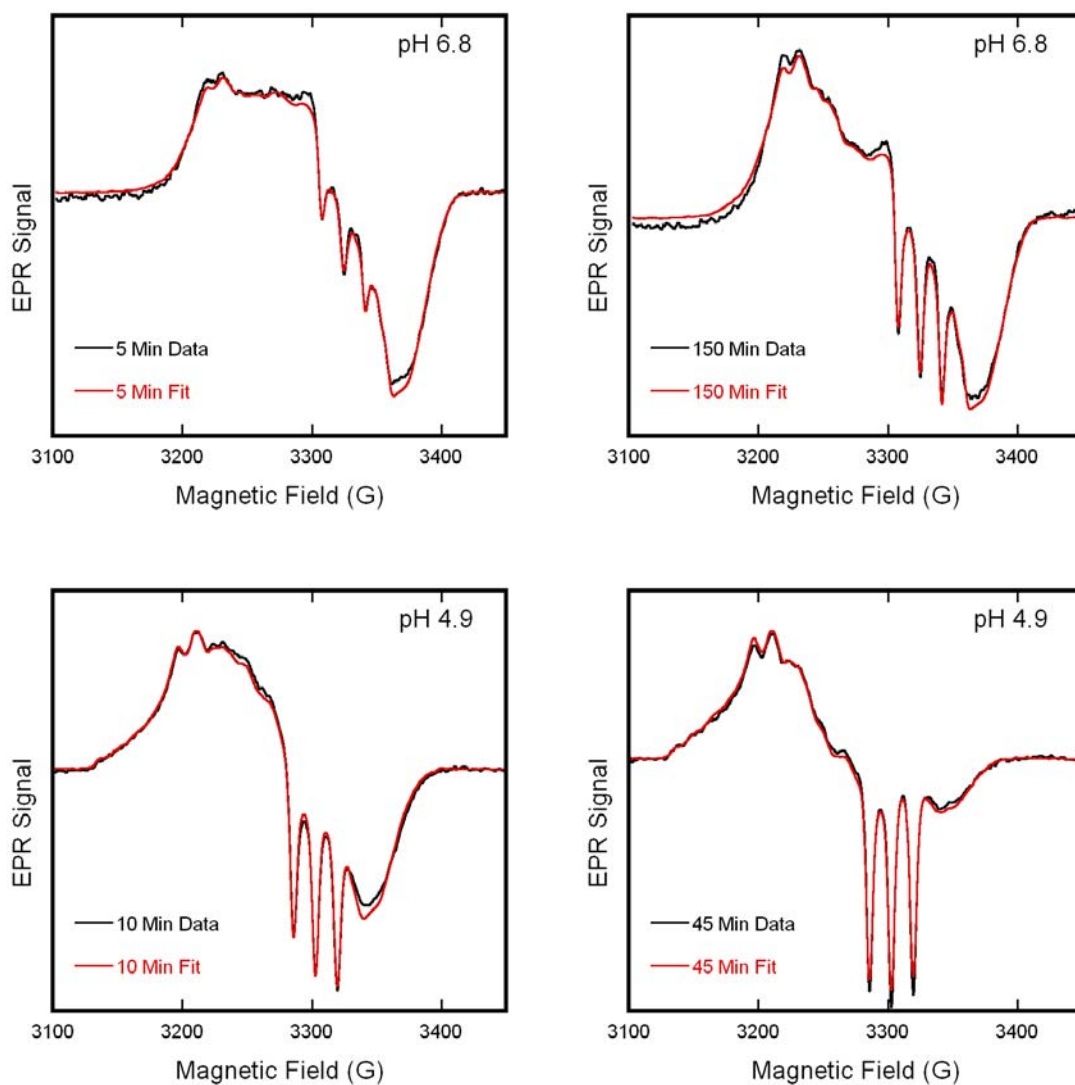


Figure E-1: Exemplary experimental and best fit EPR spectra of a 3:1 mixture of deoxy-Hb and Hb(NO)<sub>4</sub> at various times after mixing. Samples were prepared in aqueous buffer at pH 4.9 and 6.8, as labeled. Data was collected at a microwave frequency of 9.14 GHz, with 10 mW microwave power, modulation amplitude of 2 G, a time constant of 0.128 s, and a sweep rate of 3.33 G/s.

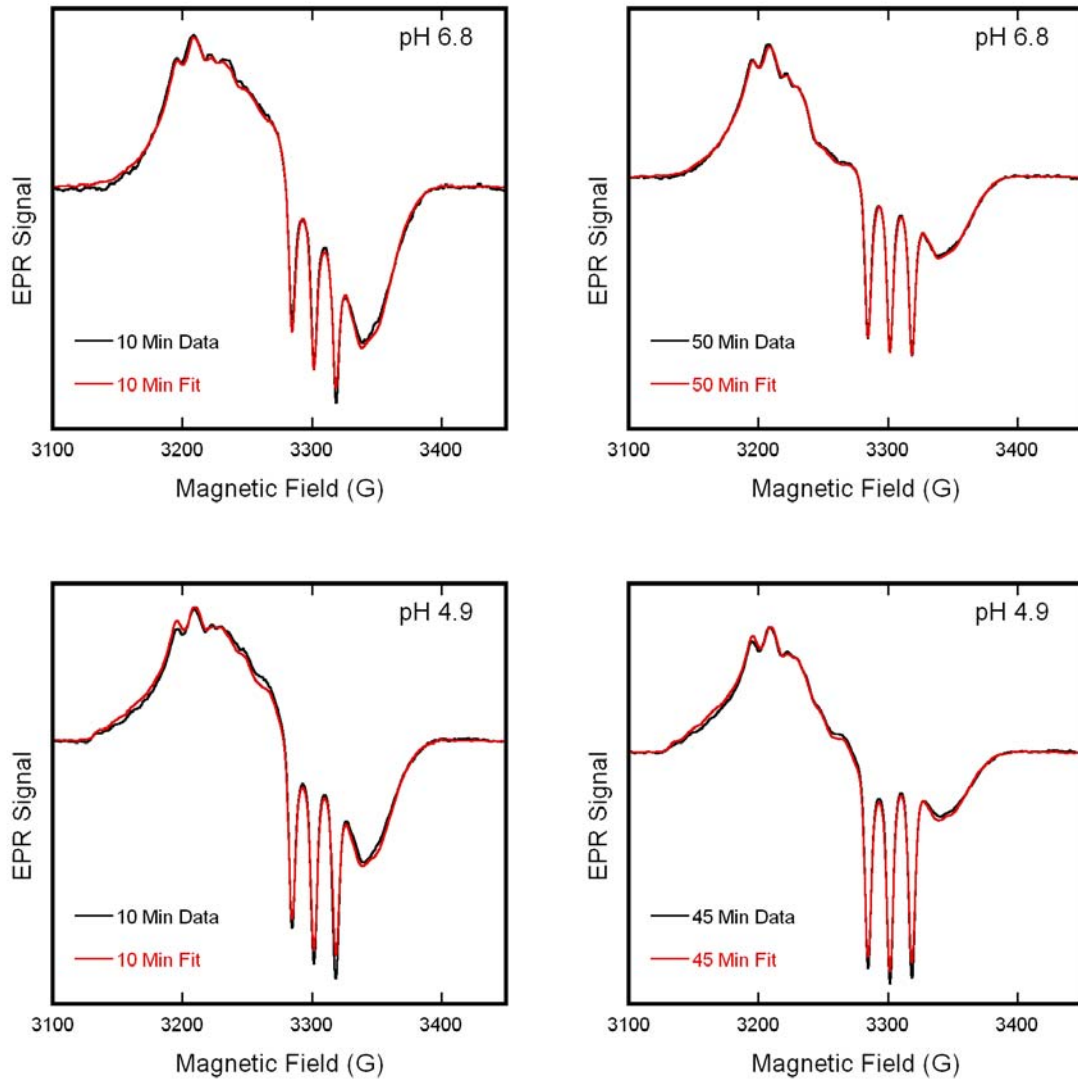


Figure E-2: Exemplary experimental and best fit EPR spectra of deoxy-Hb and DEANO, in a 10:1 NO:heme ratio. Samples were prepared at pH 4.9 and 6.8 with aliquots extracted at various times after DEANO addition, as labeled. Data was collected at a microwave frequency of 9.14 GHz, with 10 mW microwave power, modulation amplitude of 2 G, a time constant of 0.128 s, and a sweep rate of 3.33 G/s.

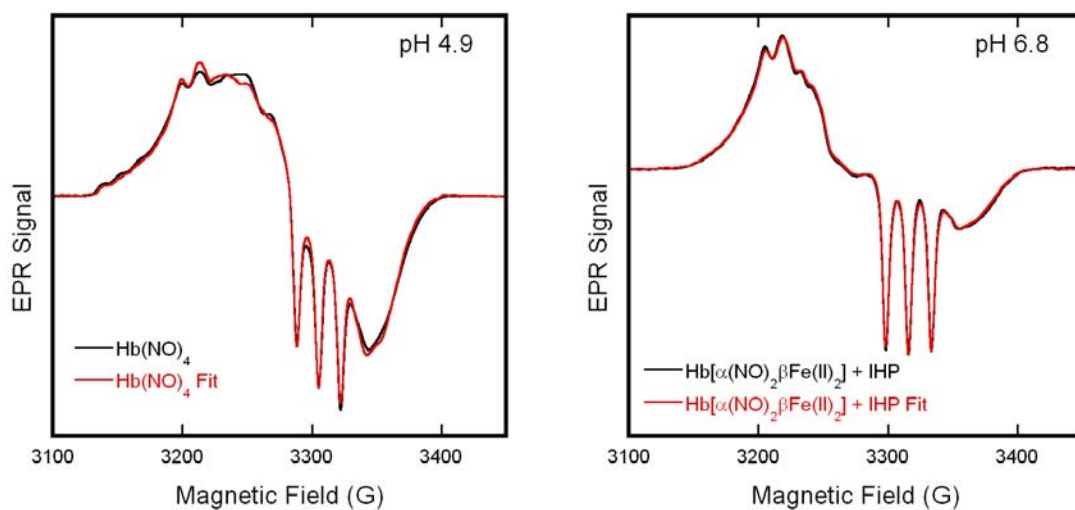


Figure E-3: Exemplary experimental and best fit EPR spectra of Hb(NO)<sub>4</sub> in pH 4.9 aqueous solution (left) and a deoxy/nitrosyl-hybrid Hb with inositol hexaphosphate in pH 6.8 aqueous solution (right). Data was collected at a microwave frequency of 9.14 GHz, with 10 mW microwave power, modulation amplitude of 2 G, a time constant of 0.128 s, and a sweep rate of 3.33 G/s.